Ag-exchanged Zeolite Membranes for Olefin Separation from Gaseous Mixtures

気体混合物からのオレフィン分離用銀カチオン交換型ゼオライト膜

February, 2022

Motomu SAKAI
酒井　求

Ag-exchanged Zeolite Membranes for Olefin Separation from Gaseous Mixtures

気体混合物からのオレフィン分離用銀カチオン交換型ゼオライト膜

2022年2月

Waseda University
Graduate School of Advanced Science and Engineering

Motomu SAKAI
酒井　求

This thesis is reproduced in part with permissions from following books and articles.

1. Sakai, M. et al., "Advanced Materials for Membrane Fabrication and Modification; chapter 7 Zeolite Membrane for Gas Separation". *CRC Press Taylor & Francis* **2019**, 213-230. Copyright [2019] Taylor & Francis Group.
2. Sakai, M. et al., "Zeolites and Metal-Organic Frameworks – From lab to industry; chapter 8. Membranes with zeolites and MOFs: how, where, and why". *Atlantis Press-Amsterdam University Press* **2018**, 209-233. Copyright [2018] Atlantis Press-Amsterdam University Press.
3. Sakai, M. *et al.,* Self-defect-healing of silicalite-1 membrane in alkaline aqueous solution with surfactant. *Mater. Adv.* **2021**, 2, 3892. Copyright [2021] Authors.
4. Sakai, M. *et al.,* Olefin Selective Ag-Exchanged X-Type Zeolite Membrane for Propylene/Propane and Ethylene/Ethane Separation. *ACS Appl. Mater. Interfaces* **2019**, 11, 4145. Copyright [2019] American Chemical Society.
5. Sakai, M. *et al.,* Preferential Adsorption of Propylene over Propane on a Ag-Exchanged X-Type Zeolite Membrane. *ACS Appl. Mater. Interfaces* **2020**, 12, 24086. Copyright [2020] American Chemical Society.
6. Sakai, M. *et al.,* Formation process of *BEA-type zeolite membrane under OSDA-free conditions and its separation property. *Micropor. Mesopor. Mater.* **2019**, 284, 360. Copyright [2019] Authors.
7. Sakai, M. *et al.,* Olefin Recovery by *BEA-Type Zeolite Membrane: Affinity-Based Separation with Olefin-Ag^+ Interaction. *Chem. Asian J.* **2021**, 16, 1101. Copyright [2021] Authors.

Contents

Chapter 1 General introduction

In Chapter 1, I preface the preparation methods, separation principles and applications of zeolite membranes. In addition, respectable previous studies about olefin recovery by using membrane and membrane-based separation are introduced. From the results of these studies, I discuss the concept of zeolite membrane and the preparation and separation property of membrane required for olefin recovery.

1.1. Membrane separation and other separation processes

Kinds of separation processes have been utilized for purification of chemicals, such as distillation, crystallization, adsorption and membrane separation. Each separation process has different principles and unique features. Table 1.1 shows the characters of each separation process.

Table 1.1 The separation principles and features of separation processes

	Principle	Additive	Initial phase	Final phase	Operation
Distillation	Phase creation	Heat	Liquid and/or vapor	Liquid and/or vapor	Continuous
Crystallization	Phase creation	Heat	Liquid	Solid (and liquid, vapor)	Discontinuous
Adsorption	Solid agent	Adsorbent	Liquid, gas or vapor	Liquid, gas or vapor	Discontinuous or quasi-continuous
Membrane separation	Barrier	Membrane	Liquid, gas or vapor	Liquid, gas or vapor	Continuous

Distillation is a kind of separation techniques based on phase creation by heat. A feed mixture of two or more components is separated into two or more products. The feed is liquid or vapor. Bottom product is liquid and distillates are liquid or vapor or both. When the feed components have different volatilities, they will partition between two phase. Then, the two phase can be separated by gravity.

Distillation is preferred purification process in chemical separation because of high throughput and continuous operation. Although distillation is energy-efficient for the mixture with large difference of volatility, is ineffective for the mixture with close volatility or azeotropic point.

Crystallization is also a kind of separation process founded on phase creation. Feed phase is liquid and created phase is solid (and vapor). Crystalline particles are formed from a homogeneous fluid phase. Crystallization has the strong advantages that morphology and particle size of crystalline particle can be controlled. In contrast, small capacity and discontinuous operation are disadvantages.

Adsorption is separation operation based on a solid agent. The components in feed are separated by the difference of affinity with adsorbent. Initial phase and product phase are liquid or gas. In principle, phase change is not necessary in adsorption process. Thus, adsorption requires small energy consumption if appropriate adsorbent is used for each separation process. In other words, the design of separation process strongly depends on the property of adsorbent.

Membrane separation is a kind of separation technique on the basis of a barrier. Liquid or vapor feed components are separated whether they can penetrate through a membrane or not. Further detail of membrane process is described in following sections.

1.2. How to prepare zeolite membranes

1.2.1 Inorganic membranes; Zeolite, metal-organic framework, carbon, silica

Thin films of inorganic porous crystals, zeolites and metal-organic frameworks (MOFs), have been developed for use as sensors [1-5], electronic materials [6-9], micro-reactors [10-13], and separation membranes. In particular, zeolite membranes have been attracting intense research interest as separation materials in the past decades.

Membrane separations using polymeric membranes have become widespread worldwide for seawater desalination [14-16], wastewater treatment [17,18], and clarification [19,20]. These membrane separation processes have considerably contributed to reduce energy consumption. For example, reverse osmosis (RO) for seawater desalination consumes energy less than about 20 % of that required in thermal desalination processes [14,15]. Consequently, seawater RO has exponentially expanded its throughput in recent decades. More than 40 million cubic meters of desalinated water were produced in 2008, and more than 100 million cubic meters desalinated water production were projected for 2016 [16]. The polymeric membranes used in water treatment, however, are difficult to be applied into energy production and chemical industry processes because of their insufficient thermal, chemical, and pressure resistance. Accordingly, the development of inorganic materials-based membranes usable under such conditions, for example elevated temperature and pressure, is greatly expected.

Separation and purification processes account for as much as 40% of the energy consumption in the chemical industry. In other words, innovation in separation process is almost as significant as innovation in the chemical industry or in large scale energy-production. It is

expected that inorganic materials-based membranes mentioned above can contribute to reduce drastically the current energy consumption. Moreover, a downsizing of equipment is expected upon introduction of novel membrane separation units instead of conventional separation processes. Such economic advantages based on energy-savings and downsizing are strong motivations to pursue their practical realisation in the chemical industry.

There are several kinds of inorganic membranes competitive with zeolites. Other types of inorganic-based membrane materials, like metal [21-23], carbon [24,25], silica [26,27] organosilica [28] and MOF have been studied. Figure 1.1 shows the typical characteristics and uses of these membranes. Although Pd and Pd-Ag alloy membranes exhibit superior permeability and extremely high selectivity, they can only be applied for hydrogen separation. While having good chemical and thermal stability, carbon membranes are better suited for separation of small gas molecules, such as hydrogen, because of their small pore sizes. Separation properties and stabilities of silica and organosilica membranes can be controlled by synthesis methods. Silica-based membranes have been widely studied for gas separation, not only hydrogen, but also gas mixtures of light hydrocarbon [26-28].

The greatest features of zeolite as membrane materials are their rigid uniform micropore channels and their unique adsorption properties. By selecting an appropriate framework topology and chemical composition, zeolite membranes can be applied to diverse separations, hydrocarbon, water, CO_2 and hydrocarbon separations.

Zeolites are composed of tetrahedral SiO_4 units. Part of Si^{4+} can be replaced by Al^{3+} and the skeleton shows anionic property. Aluminosilicate zeolites have anionic framework and thus cation exchange property to compensate electronic balance. Aluminophosphate ($AlPO_4$-n) and silicoalminophosphate (SAPO-n) zeolites are also used for gas separation. $AlPO_4$-n is made by alternately ordered tetrahedral AlO_4 and PO_4 units. $AlPO_4$-n framework does not has cation exchange property unlike aluminosilicate because their frameworks hold electric neutrality based on AlO_4^- and PO_4^+ units. When a part of P and Al in $AlPO_4$-n are replaced by Si, it is called SAPO-n. Counter cations are occluded in their framework of SAPO-n like aluminosilicate zeolites as well. In this Chapter, I collectively refer such aluminosilicate, aluminophosphate, and silicoaluminophosphate as zeolite. In addition, zeolites have ordered micropore channels in their crystalline structure and exhibited unique adsorption and molecular sieving properties based on their micropore systems. Such distinct characters contribute to their unique permselectivities of zeolite membranes.

Although over 230 zeolite frameworks have been synthesized, few have been successfully prepared as membranes, namely AEI [29,30], CHA [31-34], LTA [35,36], DDR [37,38], MFI [39-42], FAU [43-45], and MOR [46,47]. To develop membranes with good separation

properties, avoiding the formation of inter-crystalline pathways by controlling the nucleation and crystal growth is absolutely imperative. Particularly, crystal size and morphology control is one of the preferred ways to prepare high quality membranes having few defects. The knowledge of basic synthesis studies are extremely important for membrane synthesis. Preparing zeolite membranes having a novel topology is a really hard challenge and, therefore, the development of zeolite membrane requires the knowledge of synthesis procedures and crystallisation behaviours, which has so far been generated mostly in research as adsorbents and catalysts.

Similarly, the flexibility available for designing the pore size, pore-shape, and adsorption properties is the strongest point of MOFs as membrane materials thanks to the number and diversity of MOF structures, which far exceeds the number of zeolite frameworks available. More than 20,000 types of MOFs, a hundred times more than zeolite topologies, have been reported [48]. However, most of them are unstable in the presence of water or humidity [49,50]. Some MOFs, namely ZIF and MIL series, which have sufficient water and thermal stability, are often chosen as membrane materials. For examples, ZIF-7 [51,52], ZIF-8 [53-55], ZIF-90 [56,57], MIL-53 [58,59] and HKUST-1 [60,61] membranes have been developed for H_2, CO_2 and propylene separations. MOFs offer great possibilities for designing their pore size, adsorption properties, and stability. For this reason, MOF membranes can be used in various applications by optimizing the MOF species for each separation. As in the case with zeolites, the studies on MOF membranes cannot develop without the advancement in basic studies about design and synthesis. Although many studies on MOF synthesis are reported in the literature and therefore the research on MOF membranes has grown much over the past decade, this field is still immature and the performance of MOF membranes is still low.

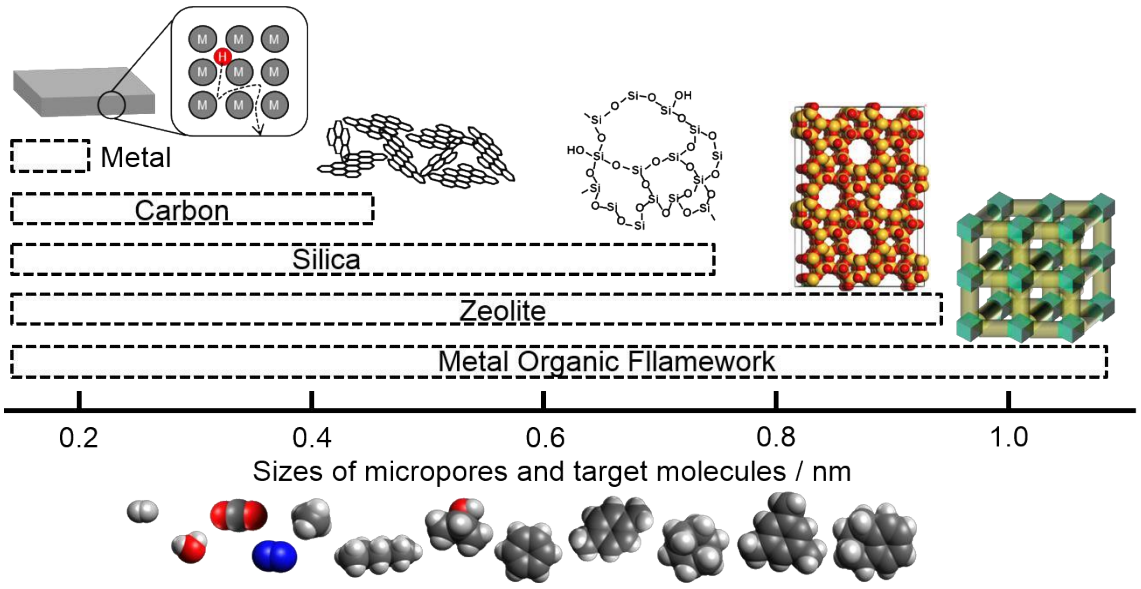

Figure 1.1. The variety of inorganic porous membranes.

1.2.2. Materials and shapes of membrane supports

Since self-supporting membranes are thick and lack mechanical strength, almost all zeolite and MOF membranes are prepared on or in a porous support. Porous silica, alumina, mullite, titania, zirconia, and stainless steel are used as inorganic supports of membranes. Polymers are also occasionally used as supports. Polymeric membrane in which zeolite and/or MOF crystals are dispersed are called mixed matrix membranes, MMM. Polymeric supports have the advantage of their high membrane surface area and moldability common to general polymeric membranes. For MMMs, the compatibility between dispersion phase and polymer phase is important [62,63] because microgaps between these phases reduce the separation selectivity. Since using polymeric supports may limit the chemical and thermal resistance of the membrane, inorganic porous supports are preferred for relatively stable zeolites and MOFs.

In addition to sufficient mechanical strength, inorganic porous supports require high stability, high permeability, and appropriate surface properties such as roughness and pore size. Permeability of porous support depends on pore size, thickness, and tortuosity. Highly permeable supports need large pore size, small thickness and low tortuosity. However, these factors pose a trade-off with the mechanical strength and suitability for membrane preparation. Thus, some of porous supports have asymmetric structures, *e.g.* a surface layer with small pores on top of large pore support [64].

The shape of the porous support is a main factor not only for membrane preparation but also for membrane module design. Plate-like [39,41], tubular [29-31], hollow fiber [65-67], and monolith-type [68,69] supports have been proposed so far. Tubular supports have a strong advantage on mechanical strength, which favours their use in high pressure conditions. Most zeolite membranes used commercially are tubular-type membranes [70,71] and the module can be designed with almost the same concept as a multitubular heat exchanger. Plate-like and hollow fiber supports have high packing density (*i.e.* membrane area/module volume). For example, hollow fiber supports with a diameter of 4 mm yield packing densities as large as 1000 m^2 m^{-3}, more than 10 times larger than those of tubular supports [65]. However, hollow fiber membranes have some problems for their use in a module, such as low mechanical strength, high pressure loss, and sealing method. Monolith-type supports show both high mechanical strength and packing density, whereas suitability for membrane preparation is enormously poor [68].

1.2.3. Procedure of membrane preparation

Zeolite membranes are prepared by in situ or seed-assisted hydrothermal or solvothermal synthesis methods. In situ synthesis, just heating the support in a synthesis solution in which nucleation and crystal growth occur, is the simplest way to obtain membranes. This method was employed in the early stage of membrane synthesis studies because of its ease. However, it is difficult to control where nucleation and crystal growth occur by the in situ synthesis method. As a result, the membranes obtained by this method tended to be thick and uncompact, and therefore in situ synthesis is hardly used in recent years. In order to solve the problems of the in situ method, the seed-assisted synthesis, usually called 'secondary growth', was developed.

Figure 1.2 shows a typical procedure of membrane preparation by a seed-assisted method. Seed crystals are supported on a support prior to a growth step, mainly a hydro- or solvothermal treatment. A thin and compact membrane can be obtained by the seed-assisted method because nucleation and/or crystal growth are led to occur nearby the seed crystals on the surface of a support. At present, seed-assisted syntheses are commonly used for zeolite and MOF membranes. The details of the seed-assisted method are described in the following section.

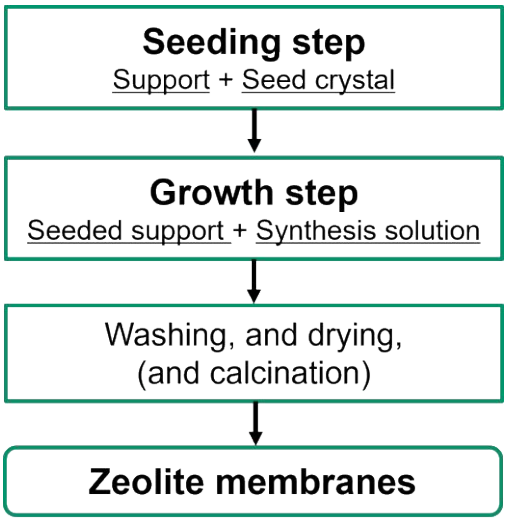

Figure 1.2. Typical preparation procedure of zeolite membrane.

In addition, some synthesis methods have been reported besides the hydrothermal synthesis mentioned above. Zeolite membranes can be synthesized by the vapour phase transport (VPT) method [72-75]. A general procedure of membrane preparation by the VPT method is as follows. Porous support is soaked in a parent aluminosilicate gel and dried. The support coated with dry gel is treated by heating in the presence of water and organic structure-directing agent vapour for crystallisation of the dry gel layer. It is noted that membrane can be prepared on a support having intricate shapes by the VPT method. On the other hand, this method has the disadvantage that the thickness of obtained membrane is relatively large.

MOF membranes can be obtained by the counter diffusion method [76,77] or by the interfacial reaction method [66,78]. The metal ion solution and the organic ligand solution are separated by a porous support and, then, MOF crystals are generated at the interface at which metal ions and ligands encounter and react. Alternatively, the support is soaked in the metal ion solution and then it is immersed into the organic ligand solution. In both two methods thin MOF membranes can be prepared without overgrowth because the reaction stops by the formation of a compact crystal layer.

1.2.4. Seeding techniques

The role of seed crystals in the seed-assisted method is quite important and the obtained membrane performances are strongly influenced by the seeding conditions before the growth step. Various techniques have been developed extensively to control seeding, including the amount, size, location, and orientation of the seed crystals. Rubbing [29-31,79], dip-coating [34,36,41], hot dip-coating [80-83], spin-coating [84], Langmuir-Blodgett [85], filtration seeding [86], vacuum seeding [87], spray-coating [88,89], electrophoresis [90], *etc.* have been used to prepare seed layers on supports. Figure 1.3 gives a schematic diagram of different seeding techniques.

One of the simplest ways of seeding is the rubbing method. Seed crystals with or without a small amount of dispersion media are rubbed on the surface of the support, in many cases by fingers or hands. The rubbing method is widely employed at the laboratory scale. However, the quality of the seeded layer prepared depends on the experimenter's skill and the quality of the seed layer is difficult to control among membranes. In addition, it is also a severe problem how to scale up the membrane area by the rubbing method.

The dip-coating method is one of the easiest ways and it is easy to scale up. The general procedure of the dip-coating method is as follows. The support is immersed into a slurry in which seed crystals are dispersed. After drawing up the support from the slurry and drying, the seeded support is obtained. In this method, the formation of a seeding layer is governed by the capillary and gravitation forces. This method is suitable for commercialisation because the quality of the seeded layer is not influenced by hand skills and, in addition, it is economically efficient because of the reusability of the seed slurry and the use of simple equipment. However, the seed crystal distribution is often ununiform because of the negative influence of gravitation force during drawing up and drying steps. A larger amount of seed crystals tend to attach on the lower side of support than that on the upper side. Additionally, a combination method of rubbing and dip-coating was reported [91]. It has been reported that rubbing and dip-coating are suitable for rough and flat surfaces, respectively, and then the combined approach can produce high

performance membranes with high reproducibility.

In the filtration seeding and vacuum seeding methods, a seed crystal slurry is also used. In these methods, seed crystals larger than the pore size of the porous support are dispersed into a slurry. After removing the dispersion media by filtration, strained seed crystals remain on the surface of the support. Although the seeding behaviour is influenced by the capillary and gravitation forces in the vacuum seeding as well, the negative effect of gravitation force can be reduced by the assistance of vacuum compared with the dip-coating method [87]. Furthermore, hot dip-coating, a combination of dip-coating and vacuum seeding has also been reported [80-83]. In this method, the porous support is preheated prior to dip-coating. Capillary and vacuum forces work at the same time by the immersion of the preheated support into the seed slurry. As a result, a uniform seed layer can be obtained as in the case of filtration and vacuum seeding.

Electrostatic interactions can contribute to the seeding behavior. In the case of the preparation of a thin MFI-type zeolite membrane, seed crystals electrostatically adsorbed on the surface support were coated with cationic polymer molecules [92]. Seed crystals can be deposited on a conductive support such as stainless steel by electrophoresis under an electric field. In addition, spin-coating and spray-coating methods are applied to seeding in lab-scale. The spin-coating method can only be applied to the seeding on relatively small plate-like support having a smooth surface.

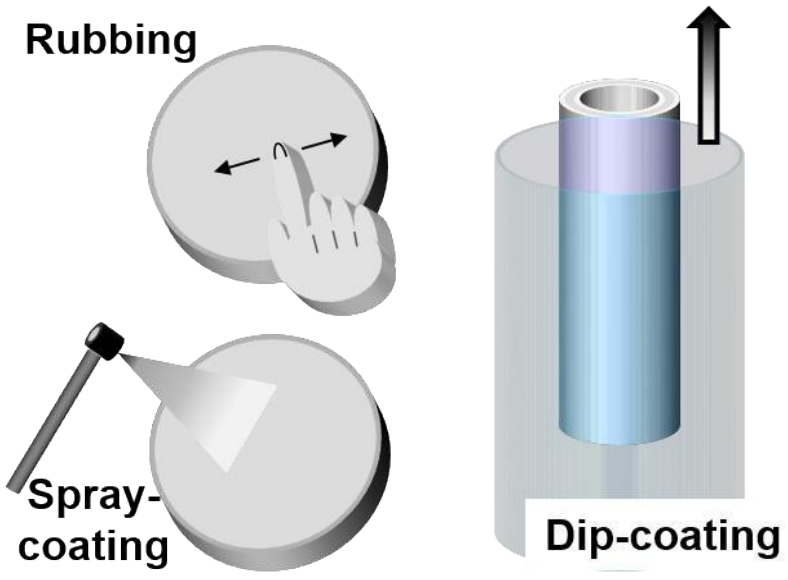

Figure 1.3. Schematic diagrams of seeding techniques.

Physically supported seed crystals often detach from support surface and are unlikely to contribute to the formation of membrane in the growth step. When the grown layer weakly

adheres to the support, the crystal layer readily peels off by frictions. Thus, preventing the detachment of seed crystals from the support surface is also of great importance.

For zeolite membrane preparation, chemical bonding between seed and support can be formed by dehydration condensation of hydroxyl groups [93]. Dehydration condensation between hydroxyl groups on the surface of zeolite and on a support such as alumina or titania occur upon heating, leading to strong adhesion. In addition, steam-assisted conversion seeding was reported as another way of immobilisation of the seed layer [94]. Seeds-containing synthesis paste was rubbed on the support and then steam-assisted conversion (heat treatment in the presence of steam) was carried out. By this steam-assisted conversion seeding, a well interlocked seed layer was generated on the support surface.

On the other hand, chemical modification was reported to improve the interaction between MOF and support in MOF membrane preparation [95]. Some functional groups produced by modification, such as amino and carboxyl groups, combine with MOF linkers. These functional group can contribute to heterogeneous nucleation on the support surface as well.

1.2.5. Roles of seed crystals in the course of membrane formation

In the seed-assisted synthesis, a hydrothermal or solvothermal treatment of the seeded support is carried out to grow the zeolite layer. The roles of the crystal seeds in synthesis solution on the crystal growth has been studied energetically. In fact, it has been one of the most interesting topics in not only membrane but also in the whole zeolite synthesis for years. A portion of it is has been clarified and some of it is still unclear.

Some roles of seed crystals contributing to form compact zeolite membranes have been reported. For example, seed crystals work as an origin of crystal growth [39,96], origin of heterogeneous nucleation [41,97,98], structure-directing agents [99], and directing crystal orientation [39,96]. Figure 1.4 shows examples of seed roles in synthesis solution through growth step. In this part, some examples will be introduced with a focus on the role in formation of thin crystal layer.

The seed crystals sometimes act as the origin of crystal growth, particularly in silicalite-1 (pure silica MFI-type zeolite) membrane synthesis. The seed crystals play a role in the dilute synthesis solution such that secondary growth of seed occurs without homogeneous and heterogeneous nucleation. It is noted that the silicalite-1 membrane formed without nucleation sometimes retains the crystal orientation of seed layer [39]. In particular, the *b*-oriented silicalite-1 membrane had been obtained by secondary growth of *b*-oriented seed layer in dilute solutions. As another specific example of secondary growth, the heteroepitaxial growth of zeolite membrane has been reported [100]. ETS-10, a kind of titanosilicate zeolite, was grown

from ETS-4 which is a structurally related material with ETS-10. In this case, ETS-10 crystals were grown epitaxially on the (*h00*) face of ETS-4.

In many cases, homo- and heterogeneous nucleation and crystal growth often occur at the same time during the growth step in the seed-assisted method. In such a case, the grown crystal layer is difficult to uniformly cover whole surface by a combination of nucleation and secondary growth if the seed crystals did not cover all the support surface. Some crystals are newly generated from by homogeneous nucleation in the bulk synthesis solution and/or by heterogeneous nucleation on the support. Then, both the beforehand supported seed and the fresh crystals formed in situ grow in the solution. Both growth of seed crystal and heterogeneous nucleation on the support contribute to the formation of compact membrane layer.

Controlling the zeolite topology formed from a synthesis solution by using seed crystals has been widely reported for powder synthesis. Seed crystals often act as a substrate to determine the topology of the zeolite formed in the membrane preparation as well as in the cases of powder synthesis. For example, both MOR and ZSM-5 zeolite membranes can be synthesized under the same synthesis conditions by only using different seed crystals [99]. Pure MOR and ZSM-5 zeolite membranes can be obtained by using MOR seed and ZSM-5 seed crystals, respectively. *BEA zeolite membrane can be obtained by using *BEA seed in the synthesis solution, whereas nucleation and growth of MOR zeolite occurs without the seed crystals [101]. In this report, *BEA membrane was prepared by a seed-assisted method in the absence of organic structure-directing agent as an example.

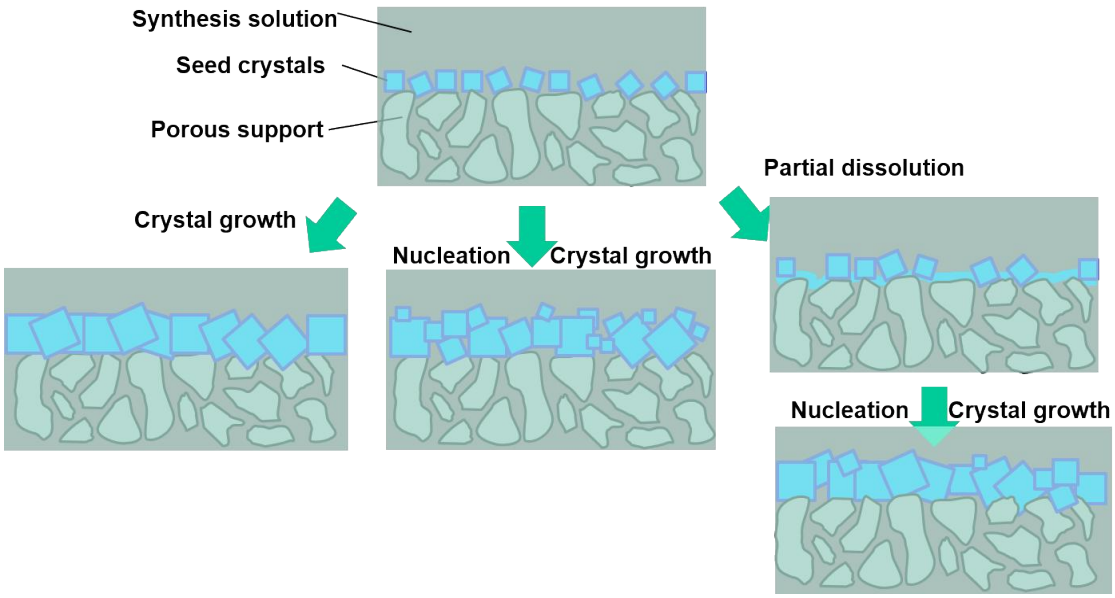

Figure 1.4. Roles of seed crystals during growth step of membrane formation.

1.2.6. Scale-up of the membrane preparation

A reproducibility is one of the important issues for the development of commercial membranes. Tubular type of zeolite membranes have so far been commercialized by several companies since 1998 [102-105]. The lengths of the membranes are one meter or so with diameters of 10-16 mm. This is about ten times longer than the membranes synthesized in laboratories. For scaling-up zeolite and MOF membranes on such long tubular supports, uniformity of seed crystals applied on the tube surface and distributions of temperature and concentration in synthesis solution throughout the growth step are often problems. In addition, the qualities of porous supports are quite important as well.

In general, at least hundreds of membranes are bundled in a module, and the separation performance of the module can be easily spoiled by a single poor-quality membrane. The simplest but burdensome solution in this case is checking the separation performance of all the membranes. The total inspection can be applied for up to a few hundred membranes in relatively small process. However, it is naturally an unsuitable control method for a larger process which requires over tens of thousands of tubes. Therefore, inexpensive and effective approaches of quality check are required in the future.

1.3. The principles of separation by porous crystal membranes

Permeability, selectivity, and life-time are a set of important factors for permselective membrane, and thus most of membrane developments focus on improvement of these factors. Zeolite membrane has structures in which zeolite crystals are accumulated unlike other amorphous inorganic membranes such as silica and carbon membranes. Hence, it is easily assumed that there are two kinds of pathways across a membrane, intracrystalline and intercrystalline pathways [106]. Figure 1.5 shows the schematic diagram of intra- and intercrystalline pathways, being the pathways through zeolite micropores in crystals and defects among crystals, respectively. The permeation through a few intercrystalline pathways easily spoils separation performance. Thus, reducing the intercrystalline pathways would help zeolite membranes to improve permselectivity. On the other hand, people should focus on improving permeability through the intracrystalline pathways to increase permeation properties.

The principles of separation with nanoporous crystal membranes are described in this part. Although a perfectly compact porous crystal membrane with no defects should have only intra-crystalline pathways, actual membranes generally have both inter- and intra-crystalline pathways. Thus, it is necessary to consider the effects of both pathways on the permeation properties. In general, selective permeation occurs through intra-crystalline pathways and non-selective permeation occurs through inter-crystalline voids and generally reduces the

separation selectivity. Selective permeation through inter-crystalline pathways only occurs exceptionally.

Permeation phenomena through intra-crystalline pathway can be divided into three steps as follows. The first step is the adsorption of molecule from the gas or liquid phase on the micropores of zeolite in the feed side. The second step is the diffusion along the micropores through the membrane. The last step is the desorption from the membrane to gas or liquid phase in the permeate side. A mixture is separated through zeolite membranes when specific molecules in the mixture preferentially proceed across the membrane through these three steps. In many cases, mixtures are separated by preferentially adsorption and/or faster diffusion in the first and second step. Details are shown in the following part with some examples.

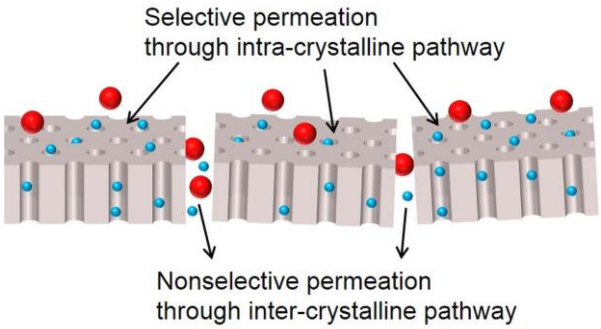

Figure 1.5. The schematic diagram of intra- and intercrystalline pathways

1.3.1. Molecular sieving

Separation by molecular sieving is based on the difference of molecular sizes as the term suggests. In other words, the molecules are separated by the difference in their diffusion rates along the membrane micropores. Because diffusivity in micropores tends to decrease with increasing molecular size, smaller molecules permeate preferentially through the membrane. When the molecular size is obviously larger than pore size and not able to enter the micropore, separation selectivity could theoretically be infinite. It is noted that molecular sieving membranes certainly exhibit selectivity to smaller molecules.

Propylene/propane separation by ZIF-8 membrane and xylene isomer separation by MFI zeolite membrane are typical examples of separation based on the molecular sieving effect. In the case of propylene/propane separation by ZIF-8 membrane, it was reported that the diffusivity of propylene through ZIF-8 membrane was 9-23 times larger than that of propane [55]. I will deal the separation of propylene/propane by ZIF-8 membrane in following section, 1.5.3.

Similarly, because the diffusion coefficient of *p*-xylene in MFI zeolite is *ca*. 100 and 1000 times higher than those of *o*- and *m*-xylene, MFI zeolite has been used as *p*-xylene selective

membrane from a xylene isomer mixture [107].

To separate mixtures by the molecular sieving effect, the selection of the type of zeolite with an appropriate size of pore for a specific separation target is very important. In addition, methods for pore size control by ion exchange and post-treatment have been studied to obtain a membrane with an optimum pore size. Ion exchange of SAPO-34 membrane from H^+ to larger cations for CO_2/CH_4 separation was reported [108]. The ion exchange decreased the permeance of both CO_2 and CH_4, and with larger cations exchanged their permeances were further reduced because of steric hindrance. CO_2 selectivity increased in all cases by cation exchange from H^+ to Li^+, Na^+, Cu^{2+}, and NH_4^+. Control of pore size with pyrolytic carbon was also reported [109].

1.3.2. Affinity-based separation

Not only the difference of molecular sizes but that of affinity between molecules and membrane material is utilized for separation. Molecules that have strong interaction with membrane material preferentially adsorb in the micropores of membranes and penetrate through the membrane. Adsorption properties due to heteroatoms and cations in zeolites and metal sites in MOFs can play important roles in such separation depending on the affinity.

It should be noted that larger molecule selective membranes can be obtained in the case of affinity-based separations. For example, it was reported that Na-MFI membrane exhibited a high methanol selectivity for methanol/H_2 mixture, indicating that larger methanol molecules strongly adsorbed on Na cation occluded in the micropores of zeolite blocked the permeation of H_2 in the system [110]. The selectivity for larger molecules by affinity-based separation is called “reverse selectivity”.

Selective permeations by both molecular sieving effect and affinity described above occur through intra-crystalline pores. On the other hand, selective permeation can occur even through inter-crystalline pathways when there is great intermolecularly interaction in addition to affinity with membrane. In the dehydration of organic solvents, there are cases like that capillary condensation of water molecules in the inter-crystalline pathways such as defects and voids in a membrane occurs, and then condensed water blocks permeation of organic molecule [34]. As a result, water selectively penetrated through both intra- and inter-crystalline pathways.

1.3.3. Intra-crystalline and inter-crystalline pathways

Since both zeolite and MOF are crystals, these membranes have structures in which crystals are accumulated. Thus, there are two kinds of pathways across the membrane, that is, intra-crystalline and inter-crystalline pathways as mentioned above [106]. The intra-crystalline

and inter-crystalline pathways are micropores in crystals and defects in membranes, such as cracks and void between crystals.

A very small amount of inter-crystalline pathway can easily spoil the separation properties. Thus, improving the separation properties of zeolite membranes critically depends on how much the inter-crystalline pathways, or more specifically the defects between crystals, are reduced. On the other hand, the way of improving the permeation property should focus on improving the permeability through intra-crystalline pathways.

Reducing inter-crystalline pathways, voids and cracks is the first step to obtain a membrane exhibiting excellent separation properties because non-selective permeation through a very small amount of inter-crystalline readily disables selectivity. For example, it was reported that only 0.19 % defect area of the total membrane area is enough to depress selectivity for CO_2/H_2 through MFI membrane [111]. Therefore, characterisation for inter-crystalline pathway is essentially important for membrane development, and various evaluation methods for pore size distribution and position of defects have been reported [112-118].

Pore size distribution are often evaluated by using nano-permporometry [112-114]. In this method, a mixture of gas with a given partial pressure of condensable vapour is fed to a membrane and gas permeance is measured. Usually, He or N_2 is used for gas, and steam or hexane is used as condensable vapour. The partial pressure of vapour is raised in a stepwise manner during measurement. Pores in a membrane are plugged with condensed vapour in order from small to large, and then gas permeance decreases with increasing vapour partial pressure. Because there is relationship between vapor partial pressure and pore size plugged with condensed vapour at a given partial pressure, pore size distribution can be evaluated from gas permeation at each vapour partial pressure. The pore size distribution in the range of 0.5-30 nm is evaluated based on the Kelvin equation [114].

To locate nano-sized defects, permeation tests using a capillary assembly were proposed [115,116]. Feed and permeate areas were limited by using probe needles and then permeances could be measured with the resolution of ca. 1 mm. The locations of defects in TS-1 and SAPO-34 membrane were visually mapped by this method. As another way to visualize inter-crystalline pathways, a fluorescence confocal optical microscopy was developed [117,118]. Inter-crystalline pathways in MFI membrane were filled with a fluorescent dye by impregnation and the dye was not able to enter intra-crystalline pathways because of its bulky size. As a result, it is possible to observe the three-dimensional network of inter-crystalline pathways.

1.3.4. Post-treatment for the healing of inter-crystalline defect

Well-prepared zeolite membranes showed high separation performances based on the

molecular sieving property. However, inter-crystalline defects such as pinholes and cracks in zeolite membrane often spoiled the separation performance. Improvement of productivity of membrane by a simple post-treatment could contribute to the reduction of membrane cost. For this reason, some post-treatment methods for inter-crystalline defects-healing have been reported [111,119-123].

Silica deposition techniques have been proposed for defect-healing in zeolite membrane. Amorphous silica was deposited by the hydrolysis of silicate or by the chemical vapor deposition (CVD) method [111,119,120]. In these methods, amorphous silica was formed in membrane defects and plugged them, resulting in the improvement of separation performance. However, chemicals used in these methods such as tetraethyl orthosilicate (TEOS) and triethoxyfluorosilane (TEFS) are expensive. Moreover, the equipment for CVD treatment would not be cost-effective.

Defect-healing in zeolite membrane by carbon deposition was also reported. The separation performance of ZSM-5 membrane increased by coking of 1,3,5-triisopropylbenzene immersed in membrane defects [121]. Hong *et al.* reported a method for blocking defects using water-soluble dye molecules [122]. The molecular size of the dye is ~1 nm, which is too large to diffuse into the zeolitic pores but enough to selectively block microdefects.

Although previous methods described above successfully improved separation performance, permeation property seriously decreased owing to plugging of the zeolite pore by deposited silica, cokes and dyes. Then, it is still a big challenge to develop a defect-healing technique by a simple method without a decrease in permeability.

Sakai *et al.* have reported the alkaline-treatment with surfactant for defect-healing [123]. By immersion of silicalite-1 membrane into an aqueous solution of sodium hydroxide and cetyltrimethylammonium bromide (CTAB), defects among crystals are plugged with amorphous silica leached from the membrane itself. During the treatment, zeolite pores in the membrane were protected by CTAB from excess alkaline-etching. As a result, the separation performance of silicalite-1 membrane successfully improved by this post-treatment without a decrease in the permeability owing to collaborative effect of NaOH and CTAB. The separation factor for *n*-hexane/2,3-dimethylbutane mixture increased from 86.5 to 559 after just 15-min treatment. In addition, separation performances of other zeolite membranes (Na-*BEA, Na-ZSM-5, Na-MOR) were also improved by the treatment. The novel defect-healing technique breaks the trade-off line of permeation and separation performance observed in previous post-treatments.

1.3.5. Improvement of permeability through intra-crystalline pathways

It is well-known that the permeation performance of the zeolite membrane is strongly

affected by the membrane structure, such as the thickness and orientation of crystals. Previously, some strategies for flux improvement have been invented.

Controlling crystal orientation and reducing membrane thickness have been at-tempted to improve the permeability of the MFI-type zeolite membrane. To prepare highly permeable membranes, signature methods for orientational seeding and morphology control were developed. Lai *et al.* reported a preparation method of oriented silicalite-1 membranes [39,96,124]. In their study, the *b*-oriented silicalite-1 membrane, in which through-pores are formed in the direction of molecular permeation, showed high *p*-xylene permeability for xylene isomer separation. Hedlund *et al.* prepared an ultra-thin MFI-type zeolite membrane by using a masking technique [92,125]. Pores of porous support were plugged with polymethyl methacrylate (PMMA) prior to crystallization to avoid the formation of amorphous and crystalline materials inside the support. After the crystallization, PMMA was removed by calcination. Their ultra-thin membrane exhibited high permeabilities for C_4-C_8 hydrocarbon separation. Recently, a 2-dimensional nano-sheet MFI-type zeolite membrane was developed by Tsapatsis and his co-workers [126]. The nano-sheet had an *a*-*c* plane, and the thickness along the *b*-axis was below 100 nm. Their *b*-oriented nano-sheet membrane had a superior *p*-xylene permselectivity. Ueno *et al.* re-ported the *b*-oriented tubular silicalite-1 membrane by a gel-free, steam-assisted conversion method. In this method, the membrane layers that retain the orientation of seed crystals can be obtained [127].

The grain boundary is also an important factor for the zeolite membrane. There is some literature that reported the effect of the grain boundary on the permeation and separation performances of the zeolite membranes. The transport barrier at the inter-crystalline regions in the A-type zeolite membrane has been proposed by Kärger *et al.* for the first time in experimental research [128]. Takaba *et al.* also reported the effect of the sub-nanometer grain boundary in all-silica chabazite (CHA) zeolite membranes on their permeation properties through a calculational study [129]. In addition, the direct observation method for the grain boundary, through using fluorescene confocal optical microscopy, was re-ported by Tsapatsis *et al.* [117]. Falconer et al. reported that the grain boundary in the MFI-type zeolite membrane played an important role in hydrocarbon permeation [130]. The grain boundary in their membrane, called the “nano-valve”, opened and closed with and without the adsorption of *n*-hexane. The importance of the grain boundary for zeolite membranes has been pointed out, as mentioned above; however, the role of the grain boundary is still an open question.

Sakai *et al.* have reported that two types of silicalite-1 membranes were prepared and their pore-connectivities were investigated [131]. In their study, a membrane with many grain boundaries in the direction across the molecular permea-tion resulted in lower pore-connectivity,

smaller effective pore size and lower permeation performance. In contrast, a membrane with fewer grain boundaries exhibited relatively better pore-connectivity and permeation performance, indicating that the narrowness and obstruction of micropores occurred at the grain boundaries of the silicalite-1 crystals. As a results of permeation measurements, they have concluded that it is important to reduce grain boundaries and improve pore-connectivity to obtain a highly permeable membrane.

1.4. Applications for membrane separation and membrane reactor

As referred above, zeolite membranes have great advantages on mechanical strength, thermal and chemical resistance compared with polymeric membranes currently used. Thus, they are expected to be applied to processes running under more severe conditions. This section describes four kinds of applications: gas separation, dehydration of organic solvents, hydrocarbon separation, and food manufacturing. Typical applications drawing attention as a target of zeolite membrane will be introduced. Figure 1.6 shows typical applications of nanoporous membranes.

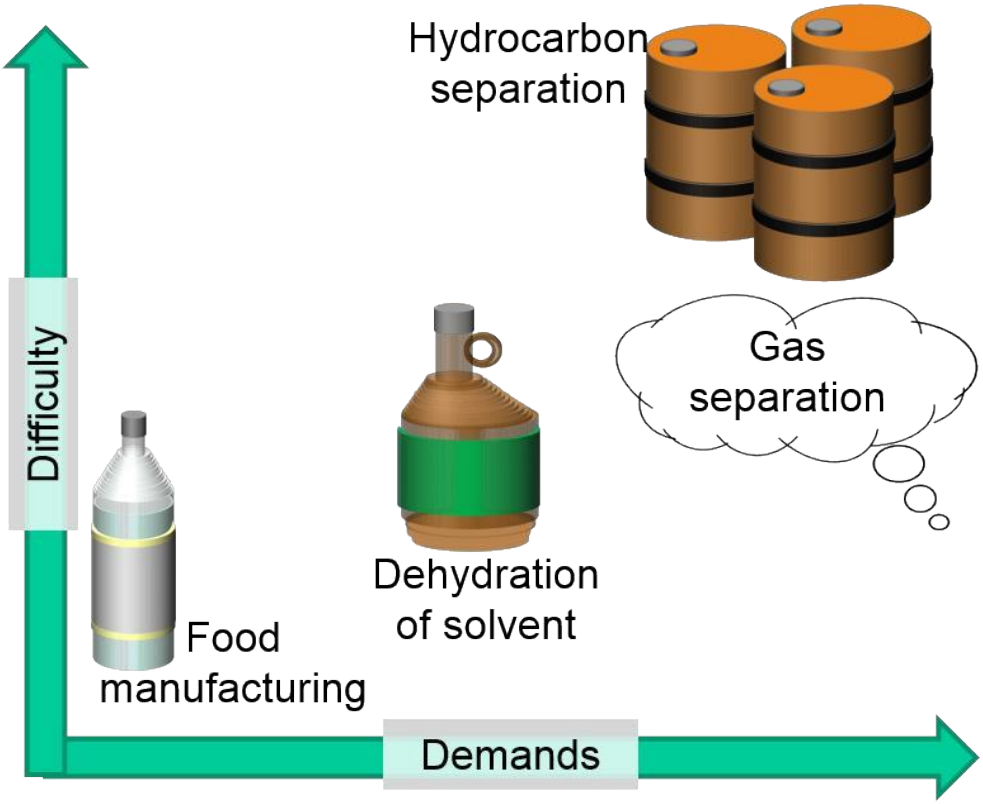

Figure 1.6. Typical applications of nanoporous membranes.

1.4.1. Dehydration of organic solvents

Dehydration of organic solvents for recycle use through zeolite membranes is relatively straightforward. The process size is generally small and thus the recycle system does not generally cause critical problems. Therefore, zeolite membranes for dehydration and dehydration systems using zeolite membranes have been commercialized. For the dehydration of organic solvents, hydrophilic zeolites such as LTA, CHA, and FAU are used.

The first large-scale plant using 16 modules with 125 pieces of LTA tubular membrane has been operated for the dehydration of ethanol since 1999 [70]. 531 L h^{-1} of 99.8 wt.% ethanol is successfully produced from 605 L h^{-1} of 90 wt.% ethanol solution by the membrane separation system. In addition, a commercial plant of isopropyl alcohol (IPA) purification for lenses cleaning by using LTA membrane has been operating since 1999 as well [132]. In this operation, 8.6 L h^{-1} of 99.65 wt.% IPA is successfully obtained from 10.5 L h^{-1} of 88.8 wt.% IPA solution by using 24 pieces of membrane. Recently, there are some reports about dehydration from acidic or basic solutions using MOR or MFI-type zeolite membrane [46,133].

1.4.2. Liquid and vapor of hydrocarbon separations

Hydrocarbon separation is one of the largest and most promising targets for zeolite membranes. Hydrocarbon separation falls roughly into two categories, isomer separation and saturated/unsaturated hydrocarbon separation.

As typical isomer separation, separations of butane isomers [40-42,92], hexane isomers [40,92], and xylene isomers separations have been attempted for decades [39,40,92,134]. The general principle is the molecular sieving effect that enables us to separate mixtures of molecules by their sizes.

Xylene isomers are one of the most important basic chemicals produced from petroleum. *o*-xylene is the feedstock of phthalic anhydride and *m*-xylene is used as a raw material for plasticizing agents and colorants. The demand of *p*-xylene as the feedstock of polyesters is particularly larger than that of the other isomers. *p*-Xylene is produced by isomerisation of xylene isomers, by disproportionation of toluene or by transalkylation. However, *p*-xylene selectivity in these reactions is limited by thermodynamic equilibria. For example, *p*-xylene selectivity in isomerisation reaction is about 20% under common reaction conditions. This is the reason why *p*-xylene has to be separated from large amounts of other xylene isomers. MFI-type zeolite has been studied as a *p*-xylene selective membrane as it is also used as a *p*-xylene selective catalyst based on its shape selectivity for xylene isomerisation and toluene disproportionation. Although excellent MFI membranes and preparation methods were previously reported [39,92], the permeabilities of *p*-xylene through these membranes were still insufficient for practical use.

Issues such as a relatively elevated operation temperature, the existence of impurities, and the large throughput required make it difficult to use membrane separations in petroleum refinery and petrochemistry. Nevertheless, one can expect great profits for hydrocarbon separation using membranes because enormous amounts of power consumption is inevitable in current separations processes.

1.4.3. Food manufacturing

Zeolite membrane have been started to be applied in food manufacturing. A novel Japanese sake (a kind of rice wine) is produced by the dehydration of conventional Japanese sake using CHA-type zeolite membrane [135]. The alcohol content in Sake is increased from the conventional 20 % to 30 % by membrane dehydration. With the help of membranes sake can be concentrated without losing molecules such as flavors and tastes in contrast to fermentation and distillation processes. The new Japanese Sake was served at the 42nd G7 summit held at Mie prefecture in Japan in 2016. Membrane separation processes are expected to continue to create high added value products in food manufacturing in the future.

1.4.4. Gas separations

Gas separations are one of the most attractive targets for membrane separation technologies as well as water treatment. There are much demands of gas separations in industrial field and a great number of report about gas separation using zeolite membranes such as CO_2 recovery, H_2 purification, natural gas upgrading and air separation. Gas mixture has currently been separated by using cryogenic distillation, absorption, and/or adsorption. However, cooling step in cryogenic distillation and regeneration steps in absorption and adsorption require large energy consumption. To save the energy consumption for gas separation, many kinds of membrane materials, such as polymeric, molecular sieving carbon, amorphous silica, organosilica, zeolite, metal organic framework, and mixed matrix membranes, were developed for past decades. Inorganic membranes including zeolite membranes generally have strong advantages for operations at high temperature and pressure because of their good thermal and mechanical stability. Figure 1.7 shows the sorts of zeolite widely used for gas separation.

The principle of gas separation using zeolite membranes is mainly based on molecular sieving effect. Zeolite membranes are able to separate molecules smaller than the micropore of zeolite and large molecules which cannot enter the micropore. In this case, selectivity of zeolite membrane without defects ideally reaches infinity. Zeolite membranes can also separate molecules by the difference of diffusivities in the micropore on the basis of their difference of molecular size even though both sorts of them can enter the micropore. Small pore zeolites

having 8-membered ring openings are often used for gas separations because these pore sizes (ca. 0.36-0.42 nm) are suitable for the appearance of molecular sieving effect in such applications.

In addition, differences in the affinities between gas molecules and zeolite membrane can be utilized for separation. Molecules having strong affinity with zeolite preferentially penetrate through membrane. In this case, zeolite membranes can exhibit selectivity for larger molecules, being different from separation by molecular sieving effects [136,110].

There are numerous reports about gas separation by zeolite and MOF membranes such as CO_2 recovery, H_2 purification, natural gas purification, air separation, noble gas recovery. In addition, demonstration tests of CO_2 recovery from natural gas using zeolite membrane have been started [137].

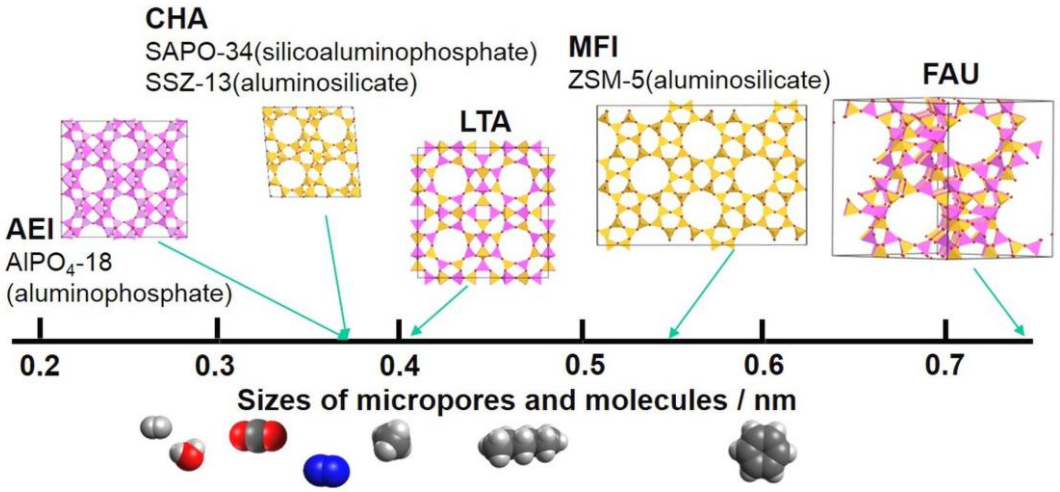

Figure 1.7. The sorts of zeolite widely used for gas separation.

1.4.4.1. Carbon dioxide separation

CO_2 recovery from gas mixtures with N_2, O_2, H_2, H_2O, and CH_4, *etc.* is one of the hottest topics of zeolite and MOF membranes as a measure against global warming [29-33,37,38,59,62,68]. CO_2 recovery from air and light hydrocarbon gas mixtures is required in the treatment of exhaust gases from thermal power plants, and CO_2 separation from CH_4 is a step of natural gas upgrading. Such CO_2 recoveries from exhaust gas and natural gas treatments are carried out at relatively high pressure (~7 MPa) and/or temperature (~473 K). In addition, a high CO_2 concentration causes the plasticisation of polymeric membranes and thus inorganic membranes are required for such applications.

Low CO_2 purity in the permeation side of membrane is so far allowed because recovered CO_2 is not always utilized as a feedstock. On the other hand, since the amount of mixture gas to treat is huge in both processes, an important property of CO_2 separation membrane has been

permeability rather than selectivity.

Carbon capture and storage (CCS) is a technology expected for CO_2 emission reduction. Cost reduction in CO_2 recovery step is the urgent need to proceed social implementation of CCS because it is estimated that the cost for CO_2 recovery occupies above 50% of the total cost of CCS, above \$60 per t-CO_2. CO_2 recovery from gas mixture is carried out by physical absorption, chemical absorption, adsorption, and membrane separation. The costs for CO_2 recovery is expected to depress down to \$25 and \$15 per t-CO_2 by the improvement of absorption and membrane separation processes, respectively. Regeneration steps in absorption and adsorption require large energy consumption. Hence, membrane separation draws attention as an ace in the hole.

Table 1.2 lists typical applications that CO_2 separation using membrane separation is expected to be introduced. CO_2 separation is required in natural gas purification, treatment of flue gas from power plant, and syngas purification before and after water gas shift reaction. The CO_2 concentration in natural gas depends on gas field, and at most reach 70%. Although the CO_2 separation using polymeric membranes from methane has been commercialized in natural-gas purification processes, plasticization of polymeric membranes occurs in high CO_2 concentration atmosphere exceeding 10%. For this reason, development of chemically stable inorganic membrane contribute to expand applicability of membrane separation, and to reduce the consumption energy for CO_2 removal at CO_2 rich gas field. In addition, separation performance of membrane is a very important factor to determine the yields of products in the cases of purification like CO_2/CH_4 separation in natural gas upgrading. Improvement of selectivity by developing inorganic membrane goes directly to improvement of product yield even under low CO_2 concentration conditions in which polymeric membranes are able to be used currently. On the other hand, an important property for CO_2 capture such as CO_2/N_2 separation in the treatment of flue gas is not so much selectivity as permeability. Necessary CO_2 purity to reduce CO_2 emission is limited to ca. 95%. Extremely high separation performance is not required for membrane. Since a huge amount of mixture gas should be treated in both natural gas purification and CO_2 capture processes, improvement of permeability is essential.

For these applications, membranes have been developed with a focus on small pore zeolites and MOFs, such as CHA, AEI, DDR and ZIF-8, which have a strong interaction with CO_2 molecules. Mitsubishi Chemical Corp. is conducting a demonstration test for natural gas upgrading by CHA-type zeolite membrane at Kurosaki, a northern part of Fukuoka prefecture in Japan, since 2016 [137].

SAPO-34, a silicoaluminophosphate CHA-type zeolite, membrane for gas separation was first reported in 1997 by Enze and his coworkers [138]. They reported the single gas permeances

of H_2, CO_2, N_2, and *n*-C_4H_{10} at 323 K. The permeances decreased with increasing molecular size and finally *n*-C_4H_{10} permeance was hard to be observed. Noble and co-workers have been developed SAPO-34 membrane for gas separation for the last dozen years [139-141]. They prepared SAPO-34 membrane on an alumina tubular support [142]. The membrane exhibited molecular sieving properties. The permeances through the membrane were in the order of CO_2 > N_2 > CH_4 > *n*-C_4H_{10} and the membrane showed CO_2 selectivity of 30 from CO_2/CH_4 equimolar mixture at 300 K. They investigated permeation and separation performances of SAPO-34 membrane under highly pressurized conditions up to 3.1 MPa [143]. The CO_2 permeance through SAPO-34 membrane was 2.4 x 10^{-7} mol m^{-2} s^{-1} Pa^{-1} with the separation factor of 95 at 295 K with a low pressure drop of 0.14 MPa. Even under the high pressure drop condition of 3 MPa, the membrane kept the high CO_2 permeance of 1.0 x 10^{-7} mol m^{-2} s^{-1} Pa^{-1} and the separation factor of 60. In addition, effect of cation species in SAPO-34 membrane on permselectivity for CO_2/CH_4 was also studied [108]. Ion-exchange from H^+ to Li^+, Na^+, K^+, and NH_4^+ in SAPO-34 membrane increased separation factor up to 60% for CO_2/CH_4 mixture. The permeance, in particular CH_4, depressed by the ion-exchange, apparently due to steric hindrance occluded in the micropores of SAPO-34.

SSZ-13, an aluminosilicate CHA-type zeolite, is also a promising material for CO_2 separation [144,145]. Falconer and co-workers prepared SSZ-13 membrane inside of a porous stainless tube and investigated its permeation properties [146]. SSZ-13 membrane showed the CO_2/CH_4 and H_2/CH_4 ideal selectivities of 11 and 9.0, respectively. Hensen and co-workers prepared SSZ-13 membrane on an α-alumina hollow fiber support [144,147]. The membrane exhibited the CO_2 separation factors of 42 and 12 for CO_2/CH_4 and CO_2/N_2 mixture, respectively, with the CO_2 permeance of 3.0 x 10^{-7} mol m^{-2} s^{-1} Pa^{-1}.

Figure 1.8 shows relative permeances of small gas molecules through $AlPO_4$-18 membrane, small pore aluminophosphate, at 313 K [148]. The permeances are divided by that of CO_2 for normalization. The permeances decrease in order of molecular size increases, besides CO_2. The order of permeances is CO_2 > H_2 > N_2 > CH_4 ≈ C_2 > C_3 ≈ *n*-C_4 ≈ *i*-C_4. Not only $AlPO_4$-18 but also various small pore zeolites exhibit this order of permeances [144-146]. This result suggests the permeances through small pore zeolite are mainly dominated by molecular size, in other words diffusivities in micropore. The CO_2 permeance is generally larger than that of H_2. As in the case of CO_2, when a sort of molecule has strong affinity with membrane material, its permeance would overwhelm that assumed from a molecular size. By contrast, the CO_2 permeance can be smaller than that of H_2 under conditions in which the interaction between CO_2 and membrane is weak.

Table 1.2 Typical applications of CO_2 separation

Application	Gas mixture	Temperature (K)	Pressure (MPa)	CO_2 conc. in feed (%)
Natural gas purification	$CO_2/CH_4/(H_2O)$	< 373	< 7	~ 70
Flue gas from power plant	CO_2/N_2	< 473	< 1	12~15
Syngas from natural gas	$H_2/CO/CO_2$	200~400	2~4	ca. 3
Syngas from coal				ca. 10
WGS syngas from natural gas	H_2/CO_2	323~423	2~4	ca. 30
WGS syngas from coal				ca. 40

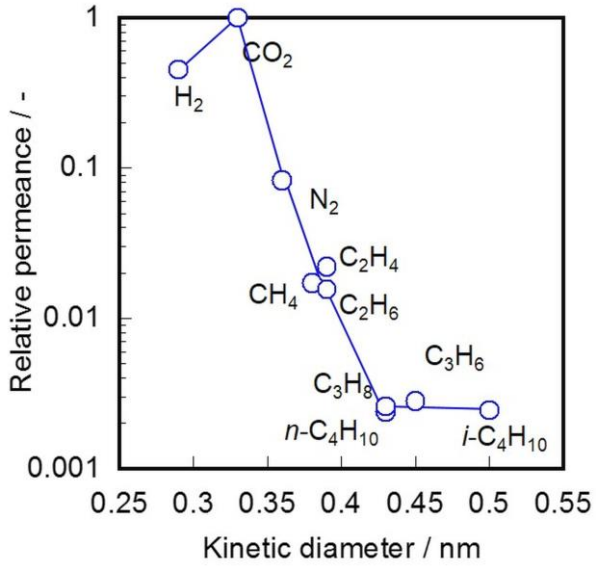

Figure 1.8. Relative permeances of small gas molecules through $AlPO_4$-18 membrane, small pore aluminophosphate, at 313 K [148].

MFI-type zeolite having ca. 0.55 nm micropore is also studied for CO_2 selective membrane material [149-152]. Hedlund's group reported the preparation of uniformly oriented MFI membrane and its permeation property [153]. This sort of MFI membrane exhibits high CO_2/H_2 separation performance at relatively low temperatures around 273 K. The separation factor reached 109 at 238 K with a high CO_2 permeance of 5.1 x 10^{-6} mol m^{-2} s^{-1} Pa^{-1}. Competitive adsorption contributed to such CO_2 selective permeation in CO_2/H_2 mixtures.

Some post-treatment and modification methods were developed to improve CO_2 permselectivity of zeolite membranes [111,149,154]. Kita and co-workers prepared SSZ-13 membrane modified by ionic liquid which had strong interaction with CO_2 [155]. The separation

factor to CO_2 for a CO_2/CH_4 mixture through SSZ-13 membrane increased from 13 to 81 by such modification. It might be due to that strongly adsorbed CO_2 inhibited CH_4 permeation.

The effects of impurities such as water vapor and light hydrocarbons on CO_2 permselectivity are also investigated. In many reports, CO_2 permeance was depressed by water because it strongly adsorbs on micropore of zeolite and inhibits CO_2 permeation. Falconer and co-workers further studied the effect of impurities in feed stream on CO_2 permeance through SAPO-34 membrane [156]. The permselectivity for CO_2/CH_4 mixtures with some impurities such as H_2O, C_2, C_3, and C_4 were evaluated. The CO_2 permeance decreased by 12 % after 12 days of exposure to 170 ppm of water vapor. Adding 1 % of hydrocarbons depressed both permeance and selectivity, indicating that such impurities adsorbed on membrane and inhibited CO_2 permeation. Hensen and co-workers also studied the effect of humidity on CO_2/CH_4 permselectivity through SSZ-13 membrane [144]. The permeances of both CO_2 and CH_4 decreased in the presence of 2.2 kPa of water vapor. At higher temperature, the permeances increased close to the values under dry condition because the water coverage on a membrane decreased.

Tables 1.3–1.5 summarize typical results of CO_2 separation with various zeolite membranes. Zeolites having 8-membered ring opening tended to show high permeability and selectivity compared with those having larger pores. Small pore zeolites are suitable materials for CO_2 selective membrane. In particular, CHA-type zeolites, SAPO-34 and SSZ-13 of small pore zeolites exhibited superior permselectivity.

Figure 1.9 shows Robeson plots of CO_2/CH_4 separation. Permselectivities of polymeric and zeolite membranes are compared in Figure 1.9(a). As a result, zeolite membranes clearly overwhelm the upper bound of polymeric membranes. The results of zeolite membranes were classified by age in Figure 1.9(b). One can see the change of research trends from this figure. Main objectives of zeolite membrane development shifted from improvement of permselectivity to durability. In the early stage of development, permselectivity improved year by year. In contrast, the upper bound of membrane performance hardly changed in recent years although the number of reports does not decrease. Membrane durability has been focused on in recent reports. The permselectivities of zeolite membranes for CO_2/CH_4 separation reached nearly sufficient in laboratory scale. In fact, Mitsubishi Chemical Corp. has started the demonstration test for natural gas upgrading by CHA-type zeolite membrane at Kurosaki, a northern part of Fukuoka prefecture in Japan, since 2016 [137].

Table 1.3 Typical results of CO_2/CH_4 separation by using zeolite membranes.

Membrane	Partial pressure (kPa)	Temp. (K)	CO_2 selectivity	CO_2 permeance (10^{-7} mol m^{-2} s^{-1} Pa^{-1})	Ref

			(-)		
SAPO-34	CO_2/CH_4 = 112/112	295	290	4.1	[157]
SAPO-34	CO_2/CH_4 = 100/100	298	160	12	[158]
Ba-SAPO-34	CO_2/CH_4 = 50/50	303	103	3.8	[159]
Li-SAPO-34	CO_2/CH_4 = 111/111	295	87	0.80	[108]
CrAPSO-34	CO_2/CH_4 = 111/111	302	156	7.9	[160]
SSZ-13	CO_2/CH_4 = 100/100	303	300	2.0	[145]
$AlPO_4$-18	CO_2/CH_4 = 152/152	298	240	5.9	[161]
DDR	CO_2/CH_4 = 100/100	298	500	0.35	[162]
T-type	CO_2/CH_4 = 50/50	308	400	0.46	[163]
Silicalite-1	CO_2/CH_4 = 50/50	200	15	0.75	[164]
Na-Y	CO_2/CH_4 = 50/50	303	20	1.0	[79]

Table 1.4 Typical results of CO_2/H_2 separation by using zeolite membranes.

Membrane	Partial pressure (kPa)	Temp. (K)	CO_2 or H_2 selectivity (-)	CO_2 or H_2 permeance (10^{-7} mol m^{-2} s^{-1} Pa^{-1})	Ref
LTA	CO_2/H_2 = 50/50	373	12.5 (H_2)	1.4 (H_2)	[165]
SAPO-34	CO_2/H_2 = 688/912	253	140 (CO_2)	0.26 (CO_2)	[166]
$AlPO_4$-5/$AlPO_4$-34	CO_2/H_2 = 50/50	308	9.7 (H_2)	2.0 (H_2)	[167]
MFI	CO_2/H_2 = 450/450	238	109 (CO_2)	51 (CO_2)	[153]
H-ZSM-5	CO_2/H_2 = 450/450	235	210 (CO_2)	62 (CO_2)	[168]
B-ZSM-5	CO_2/H_2 = 111/111	773	60 (H_2)	1.3 (H_2)	[169]

Table 1.5 Typical results of CO_2/N_2 separation by using zeolite membranes.

Membrane	Partial pressure (kPa)	Temp. (K)	CO_2 selectivity (-)	CO_2 permeance (10^{-7} mol m^{-2} s^{-1} Pa^{-1})	Ref
SAPO-34	CO_2/N_2 = 120/120	295	32	12	[170]
T	CO_2/N_2 = 50/50	308	104	0.38	[163]
Silicalite-1	CO_2/N_2 = 50/50	293	69	7.1	[171]
ZSM-5	CO_2/N_2 = 50/50	298	54.3	0.36	[172]
ETS-10	CO_2/N_2 = 55/55	298	10	0.28	[173]
K-Y	CO_2/N_2 = 50/50	308	67	13	[174]

Na-Y	CO_2/N_2 = 50/50	303	100	0.5	[79]
Na-X	CO_2/N_2 = 50/50	296	8.4	0.5	[175]

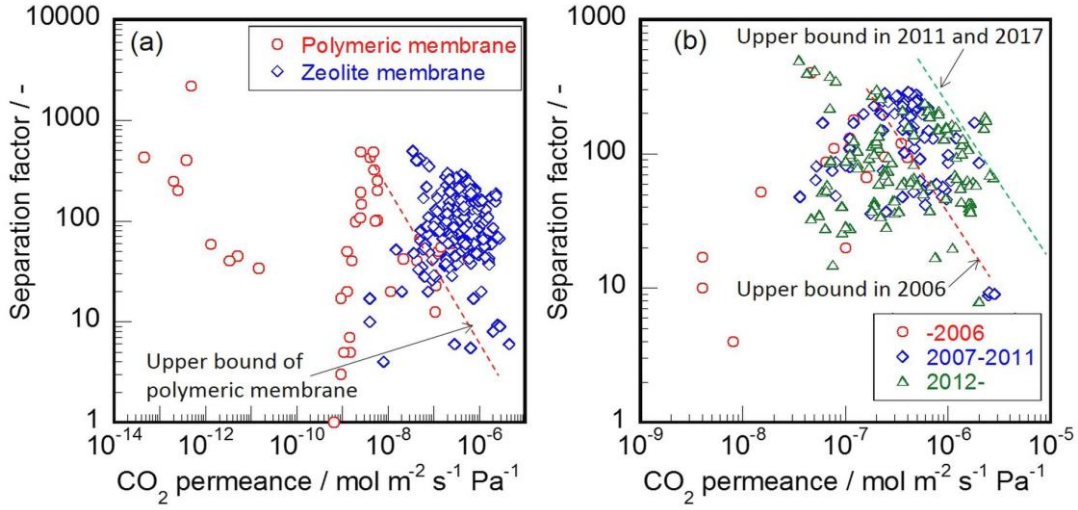

Figure 1.9 Robeson plots of CO_2/CH_4 separations. (a) Comparison of polymeric and zeolite membranes. (b) The results of zeolite membranes classified by age.

1.4.4.2. Nitrogen separation for natural gas upgrading

N_2 separation from CH_4 for natural gas upgrading comes under the spotlight in common with CO_2/CH_4 separation. Most of research about N_2/CH_4 separation are carried out along with CO_2/CH_4 separation. In general, the permeance and selectivity of N_2 from N_2/CH_4 mixture are less than those of CO_2 from CO_2/CH_4 mixture. N_2 does not have interaction between membrane materials as strong as CO_2 and its diffusivity in micropore is smaller than that of CO_2 due to its molecular size. This is the reason why the N_2 permselectivity tends to be low. Noble's group reported N_2/CH_4 separation results through SSZ-13 membrane [176]. The membrane which had a CO_2 separation factor of 280 for CO_2/CH_4 mixture at 293 K, exhibited only 13 of the separation factor to N_2 for N_2/CH_4 mixture at the same temperature. Table 1.6 gives typical results of N_2/CH_4 separation by using various zeolite membranes.

Table 1.6 Typical results of N_2/CH_4 separation by using zeolite membranes.

Membrane	Partial pressure (kPa)	Temp. (K)	N_2 selectivity (-)	N_2 permeance (10^{-7} mol m^{-2} s^{-1} Pa^{-1})	Ref
SAPO-34	N_2/CH_4 = 111/111	298	8.6	7.2	[177]

$AlPO_4$-18	N_2/CH_4 = 111/111	298	4.6	10	[178]
SSZ-13	N_2/CH_4 = 135/135	293	13	0.18	[176]
ETS-4	N_2/CH_4 = 50/50	308	5.1	0.50	[179]

1.4.4.3. Hydrogen separations

Membrane separation for H_2 purification has also been focused on in recent years. H_2 is an important feedstock in petroleum and petrochemical industries and a novel energy carrier. Research about H_2 membrane separation is mainly classified into H_2 generation process, H_2 carrier system, and dehydrogenation reaction. H_2 is often generated by steam reforming and water gas shift reaction (WGSR), as shown in following equations, and thus H_2 is recovered from mixtures of CO, CO_2, H_2O, and hydrocarbons:

steam reforming,

$$C_nH_m + nH_2O \rightleftarrows nCO + (m/2 + n)H_2 \quad \text{(eq. 9.1)}$$

and water gas shift reaction,

$$CO + H_2O \rightleftarrows CO_2 + H_2 \quad \text{(eq. 9.2).}$$

There have been reports on CO_2 selective membranes for CO_2/H_2 mixture separation by using affinity described in the above section. In contrast, some reports about H_2 selective zeolite membrane for CO_2/H_2 mixture separation on the basis of molecular sieving effect. Silylated ZSM-5 membranes prepared by catalytic cracking of methyldietoxysilane (MDES) were proposed for H_2 separation from H_2/CO_2 and H_2/CH_4 mixtures [169]. They prepared boron-substituted ZSM-5 membrane on which MDES reacted in the micropores of B-ZSM-5 and reduced its effective pore diameter. The silylation at 623 K for 10 h increased the H_2 separation factor from 1.4 and 1.6 to 37 and 33 for H_2/CO_2 and H_2/CH_4 mixtures, respectively. MFI membrane silylated by the catalytic cracking of MDES was also reported by Xu and his coworkers [180]. In this case, the separation factor of H_2/CO_2 at 773 K increased from 3.4 to 45.6 by this treatment. Huang and Caro [181] reported the preparation and permeation property of $AlPO_4$ membrane having the LTA topology. Their membrane exhibited separation performance by a molecular sieving effect. The separation factors for H_2/CO_2, H_2/N_2, H_2/CH_4, and H_2/C_3H_8 mixtures were 10.9, 8.6, 8.3, and 142, respectively with the H_2 permeance of ca. 1.9×10^{-7} mol m^{-2} s^{-1} Pa^{-1}.

Organic hydride is one of the materials proposed as H_2 carrier in energy use. Toluene/cyclohexane system has often been chosen for H_2 transfer due to the ease of operation because both saturated and unsaturated hydrocarbons keep liquid phase. Then, H_2/toluene

separation has widely studied by various inorganic membranes.

H_2 separation from organic hydrides has been investigated by using small pore zeolite as in the case of CO_2 separation. Since the polymer electrolyte fuel cell needs H_2 with a high purity (> 99.97 %), the membrane should possess an excellent separation property. However, the selectivity to H_2 through the zeolite and MOF membrane is a magnitude lower than those of carbon and metal membranes mentioned above. The relatively wide working window of temperature is a strong positive point of zeolite and MOF membranes.

Kita and co-workers prepared MFI membrane on the outer surface of tubular mullite support [182]. Their membrane showed the H_2 permeance of 1.6 x 10^{-7} mol m^{-2} s^{-1} Pa^{-1} with the separation factor (H_2/toluene) of 4.1 from the mixture of H_2/toluene = 98/2. As a result, the hydrogen purity in the permeate reached 99.5%. Table 1.7 shows typical results of H_2/CH_4 separation by various zeolite membranes.

Table 1.7 Typical results of H_2/CH_4 separation by using zeolite membranes.

Membrane	Partial pressure (kPa)	Temp. (K)	H_2 selectivity (-)	H_2 permeance (10^{-7} mol m^{-2} s^{-1} Pa^{-1})	Ref
LTA	H_2/CH_4 = 50/50	293	4.5	5.9	[183]
SAPO-34	H_2/CH_4 = 102/87	293	29	0.21	[166]
Li-SAPO-34	H_2/CH_4 = 111/111	295	16	0.33	[108]
SSZ-13	H_2/CH_4 = 300/300	293	22	2.0	[147]
B-ZSM-5	H_2/CH_4 = 111/111	523	1.6	1.4	[169]
FAU	H_2/CH_4 = 50/50	323	9.9	1.9	[184]

1.4.4.4. Noble gas separation

Zeolite membranes for noble gas separation have recently been reported. Helium is an important and scarce resource. There is a large and increasing market of He for industrial and medical use all over the world. The main He resource is natural gas fields containing small concentrations of He. In addition, a small number of natural gas fields can produce the gas mixture with economically feasible concentrations of He, higher than 0.4%. At present, He recovery from natural gas fields has been carried out via a combined process of cryogenic distillation, adsorption and membrane separation. Although polymeric membranes are used in these process, a highly permeable membrane is required for efficiency increase. Development of separation technology for He from N_2 and CH_4 would contribute to not only price decline but also improving recoverable reserves. Noble and co-workers reported the permselectivity of

SAPO-34 membrane for He/CH_4 mixture [185]. The He permeance was about 4.5 x 10^{-7} mol m^{-2} s^{-1} Pa^{-1} with the separation factor > 20 at 293 K. Their membrane shows He selective permeation by a molecular sieving effect. In addition, the separation factor increased with decreasing He molar fraction in feed gas mixture, and reached 30 at 0.3 of the He molar fraction. Hedlund and co-workers investigated separation performance of MFI membrane for N_2/He mixture under very low temperature conditions [186]. Although the He permeance in the single gas system was greater than that of N_2, it drastically decreased in binary separation experiments and dropped below the N_2 permeance. Strong adsorption of N_2 inhibited the permeation of He in the binary system. Their membrane shows the N_2 permeance of 3.9 x 10^{-6} mol m^{-2} s^{-1} Pa^{-1} with the separation factor of 75.7 at 124 K.

Xe/Kr separation with zeolite membrane has been reported from several groups. Both ^{136}Xe and ^{85}Kr are released as off-gas with other species such as ^{129}I, $^{3}H_2O$, NO, NO_2 and CO_2 from used nuclear fuel recycling process. While ^{136}Xe is a stable isotope, ^{85}Kr has to be captured because of the long decay half-lives. Thus Xe/Kr separation is required to reduce a volume of radiation waste. Carreon and co-workers prepared SAPO-34 membrane on tubular alumina support and reported that their SAPO-34 membrane exhibited Kr selectivity with the Kr permeance of 1.0 x 10^{-7} mol m^{-2} s^{-1} Pa^{-1} the mixture of Kr/Xe = 9/1 [187]. The separation factor was reported to be 35. In addition, their membrane showed the Kr permeance of 1.2 x 10^{-7} mol m^{-2} s^{-1} Pa^{-1} with 45 of the separation factor under Kr lean conditions, Kr/Xe = 9/91. Nair and co-workers also reported Kr selective SAPO-34 membrane showing the Kr permeance of 3.8 x 10^{-9} mol m^{-2} s^{-1} Pa^{-1} with 30 of separation factor at 255 K for the mixture of Kr/Xe = 1/9 [188]. They reported that the membrane showed Kr selective permeation whereas the amount of Xe adsorbed on SAPO-34 is larger than that of Kr, strongly indicating that Kr has a larger diffusivity in the micropore of SAPO-34 in comparison with Xe. This is a good example to show that the difference in diffusivity contributes to preferential permeation.

1.4.5. Membrane reactors

In recent years, membrane reactors have received much attention from the view point of saving energy, saving space, and highly efficient production. When the membrane reactors could be applied into practice, drastic and innovative change would occur in chemical processes.

Membrane reactors are categorized into three types, namely, extractor, distributor and active contactor, as shown in Figure 1.10 Membrane reactors using nanoporous membranes often refer to the extractor-type. Researchers have extensively studied the extractor-type membrane reactors applied to reactions in which attainable conversion levels are limited by equilibrium,

such as dehydrogenation, steam reforming, and esterification. In this type of reactor, reaction and separation occur simultaneously. In accordance with Le Chatelier's principle, equilibrium values shift by removing products from a reaction system, allowing conversion levels and product yields in the membrane reactor to exceed those in conventional reactors.

Both organopolymeric and inorganic membranes can be applied to membrane reactors. Inorganic membranes are advantageous compared with organopolymeric membranes for high temperature and/or high pressure applications. Among inorganic membranes, palladium alloy, amorphous silica and zeolite have so far been used for membrane reactors. Whereas, in particular, palladium and palladium alloy membranes were developed for the membrane reactor with hydrogen extraction, there were problems such as hydrogen embrittlement and high cost. Thus, development of amorphous silica and zeolite membrane for membrane reactor for dehydrogenation with hydrogen extraction has progressed in recent years. In this case of hydrogen production, lower reaction temperature is desirable from the view point of equipment deterioration and energy cost, because conventional hydrogen production reactions such as steam reforming of naphtha and methane need high reaction temperature above 1100 K. Compared to the conventional packed bed reactor, the membrane reactor can be operated at lower reaction temperature due to removal of hydrogen from the reaction system, inhibiting the formation of methane below 1100 K.

Zeolite membrane showed relatively high hydrogen permeance and selectivity [189-192]. Membrane reactors for WGSR using a H_2 selective MFI membrane modified with deposited silica were reported [193,194]. At 823 K, the packed bed membrane reactor achieved 81.7% of the level of CO conversion, which was higher than the equilibrium conversion, 65%. Xu and co-workers studied a H_2-selective zeolite membrane reactor for WGSR as well [195]. They demonstrated that their membrane reactor exhibited a high CO conversion of 95.4% which was higher than the equilibrium conversion of 93% at 573 K.

The improvement of the stability and selectivity of zeolite membranes at higher temperature is still an open question. It is supposed that cations occluded in zeolite framework inhibited the permeation of hydrogen molecules. Membranes of aluminophosphate ($AlPO_4$-n) or silicoaluminophosphate (SAPO-n), which have less or no ion exchange sites possibly blocking permeation paths in the zeolitic micropores, could be applied in dehydrogenation membrane reactors in the future.

Dehydrogenation of paraffin for olefin production is also strongly limited by thermodynamic equilibrium. Membrane reactor for olefin production has been studied in recent years. In particular, propane dehydrogenation with membrane separation is currently focused on, and then one can expect expansion of use for various reactants in the future, such as ethane,

butane, cyclohexane, and ethylbenzene. In either reaction, superior thermal and mechanical stability is required for H_2 selective membrane under severe conditions for dehydrogenation (> 773 K, < 2 MPa).

Nair and co-workers demonstrated an availability of propane dehydrogenation membrane reactor by using H_2 selective SAPO-34 membrane [189]. Propane conversion reached 70% exceeding equilibrium conversion with a high propylene selectivity of 85% by their membrane reactor operated at 873 K. In addition, they also studied the membrane reactor system for the propylene dehydrogenation by simulation [196]. They reported that the replacement of a conventional packed bed reactor with a packed bed membrane reactor increases the space-time yield of propylene production up to 45%. Kapteijn and co-workers studied *i*-butane dehydrogenation by using a H_2 permselective DD3R zeolite membrane reactor [190], and reported that *i*-butene yield reached 41%, where the equilibrium yield was 28%.

Many researchers have developed membrane reactors for the esterification using zeolite membranes. Compared with conventional reactors, these membrane reactors also lead to a higher conversion and a higher yield owing to the removal of water as a product of the esterification from the reaction system. Zeolite membranes having hydrophilic nature are expected to show a high water flux and permselectivity in the esterification reaction system.

Zeolite A (LTA) has Si/Al ratio =1 in its framework and thus develops strong hydrophilicity, resulting in that LTA membrane shows a high water flux [197-200]. Since the esterification reaction is generally operated under acidic atmosphere, the membrane is required to have acid resistance. Comparing the acid resistance of zeolite A with that of MOR membrane, MOR membrane showed better acid resistance in the membrane reactor tests [201,202]. Zeolite A is much more hydrophilic owing to its lowest Si/Al ratio (=1) among zeolites and, thus, the water flux through MOR membrane is smaller than that through zeolite A membrane.

Zeolite T membrane was also developed for the membrane esterification reactor with experimental and simulation approaches. Simulation results of vapour permeation-aided esterification of lactic acid with ethanol, using a simple model incorporated second-order reversible reaction with separation, showed good agreement with experimental results [203]. In addition, CHA zeolite membranes were successfully applied to the membrane reactor for the esterification of adipic acid with isopropyl alcohol and the yield of diisopropyl adipate was increased compared with the esterification without CHA-type zeolite membrane [204]. The water flux through CHA zeolite membrane was decreased after 10 times use in the esterification. In this paper, the authors claimed that such a decrease of water flux took place by the adhesion of sublimed adipic acid rather than by problem of acid resistance.

Xylene isomerisation is also limited by thermodynamic equilibrium. When an extractor-type

membrane reactor using MFI-type zeolite membrane that shows *p*-xylene permselective performance is applied for this reaction, *p*-xylene selectivity can be enhanced by the removal of *p*-xylene from the product. This type of membrane reactor is considered to show full use of the unique characteristics of zeolite membranes having uniform pore size derived from their crystal structures. Compared with the conventional packed bed reactor, membrane reactor using MFI membrane showed the enhancement of *p*-xylene selectivity and yield [205-207]. However, the practical use of membrane reactor for the xylene isomerisation still suffers from the insufficient flux and selectivity through MFI membrane. Development of a membrane showing high permselective performance is the key issue for this type of membrane reactor. On the other hand, MOFs membranes have been rarely reported for membrane reactors, although these membranes can be expected in the future.

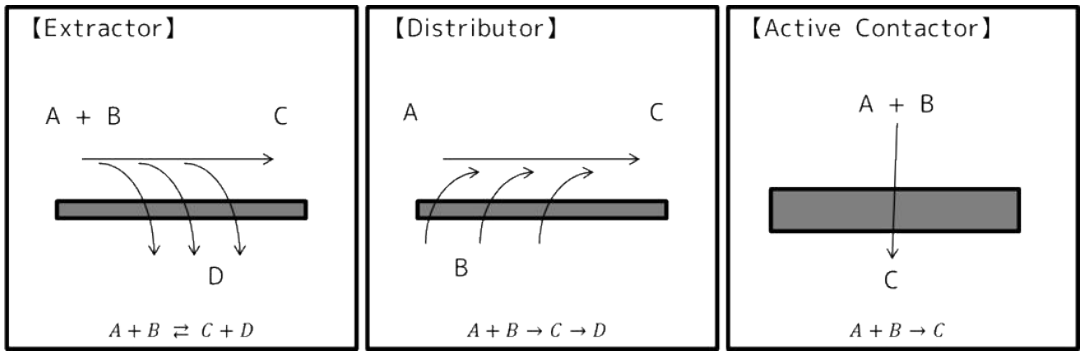

Figure 1.10. Schematic diagram of extractor, distributor and active contactor-type membrane reactors.

1.5. Olefin separation from gaseous mixture

Propylene and ethylene are very important raw feedstocks for the petrochemical industry. High purity is required for these olefins to use as feedstocks for polymer production. Separation processes of propylene/propane and ethylene/ethane mixtures by conventional cryogenic distillation are energetically intensive because the heat for liquefaction is hard to recover and the relative volatility of olefin and paraffin is close to unity. Membrane separation is expected to be a novel energy-saving process for gaseous mixture such as olefin purification [208,209].

Sholl and Lively pointed out that purification of propylene and ethylene requires as much as 0.3% of global energy use and suggested that membrane-based separation should be introduced for olefin purification [210]. Hence, many types of membranes, including polymeric [211], silica [212], metal-organic framework (MOF) [54,55,77,213-216], and carbon molecular sieving membranes [217], have been reported previously for propylene separation.

1.5.1. Olefin production and purification

Ethylene, propylene and butenes were purified from gaseous mixtures of C_1-C_4 hydrocarbons produced by various processes, such as naphtha cracking, fluid catalytic cracking. Currently, ethylene and propylene were purified from a mixture of C_1-C_4 hydrocarbons by a series of distillations [218], as shown in Figure 1.11. In this scheme, methane was removed by the first distillation tower, and then ethylene and ethane were separated from the remained C_2-C_4 mixture. C_4 hydrocarbons were, then, separated from C_3-C_4 mixture. The obtained mixture of ethylene/ethane and propylene/propane were fed to distillation towers for ethylene and propylene purifications, respectively. These distillation towers for ethylene and propylene purification consume most of the energy of the whole purification system mainly because of a small deference of boiling points at low temperature and a high reflux ratio (Δb.p. of ethylene and ethane, 15 K; Δb.p. of propylene and propane, 5.6 K).

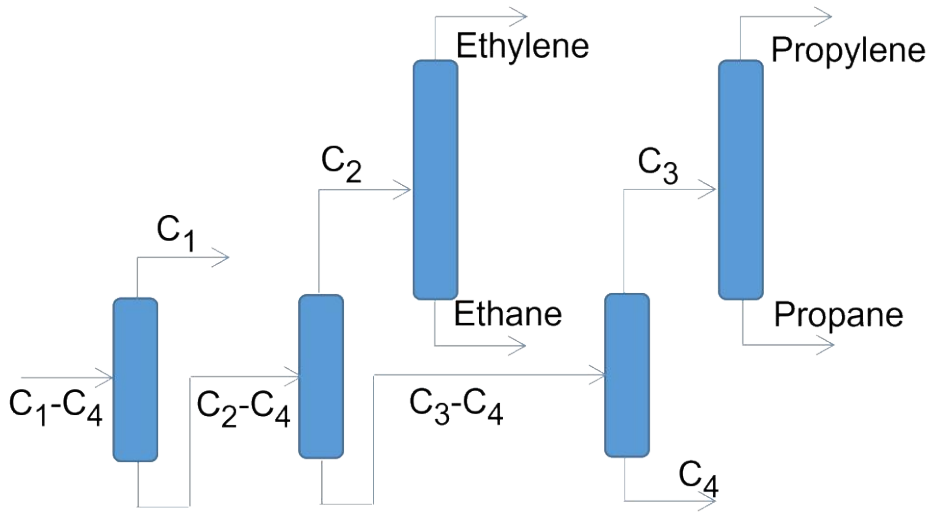

Figure 1.11. Typical cryogenic distillation for olefin purification from a mixture of C_1-C_4 hydrocarbons.

1.5.2. Membrane and membrane-distillation hybrid separation for olefin

Many membrane and membrane-distillation hybrid separation processes for olefin purification have been suggested for last decades [208,209,218-224]. Required membrane propery, separation factor and permeation performance, was investigated in these reports to apply olefin selectivfe membranes to olefin purification processes. In addition, the configulation of membrane modules and distilation towers were widely investigated. The energy and economic effects of membrane separation was also studied.

Configulation of membrane modules in membrane separation for olefin is suggested as

shown in Figure 1.12(a) [219-221]. Raw stream, a mixture of olefin and paraffin, is fed to the first membrane module including olefin-selective membrane. Olefin and paraffin enriched gases come out to permeate and retatntate sides, respectively. If the purity of olefin in permeate does not reached required standard because of unsatisfying separation performance, the permeate is send to the next membrane module. In addition, a part of retantate gas is recycled to improve olefin recovery ratio if the retantate includes much amount of olefin.

Configulation of membrane-distillation hybrid separation process is more complex. In this case, the location of membrane module is important parameter [208,209,219-224]. As shown in Figures 1.12(b), (c-1) and (c-2) membrane module is located before or after a ditillation tower. In the case of configulation(b), the permeate and retantate from a membrane module are sent to distillation tower. In the configulation(c-1), the top stream from a distillation tower are fed to a membrane module, and then permeate of membrane module will be product olefins. The side stream is bring into a membrane module in configulation(c-2) and the both permeate and retantate is returned to distillation tower. In addition, the combinations of configulations(b) and (c) are also suggested, as shown in Figures 1.12(d-1) and (d-2). A number of membrane modules in hybrid process is also parameter as in the case of membrane separation process.

In this decade, economic evaluation of the separation process for propylene/propane and ethylene/ethane by using membrane have been widely studied. In table 1.8, I summerized the results of economic estimations previously reported [209,218-224]. Although the economic efficiency of membrane-based separation process is strongly affected by some parameters such as feed purity, performance of membrane and membrane cost, the total annual cost in membrane-based separation shrinks compared with conventional cryogenic distillation. From these results, the membrane which satisfies the permeance of 3 x 10^{-8} mol m^{-2} s^{-1} Pa^{-1}, the separation factor of 30, and the life-time of 2 years at the same time must contribute to implementation of membrane-based separation process for the propylene/propane misture.

Although membrane separation is the best way for energy-saving in the course of olefin purification, required property for membrane is extremely high. The energy consumption in distillation tower is totally removed and the electlic energy for compresser is required instead. CAPEX is simply decided by the balance of the price of distillation tower and membrane.

Membrane-distillation hybrid processes has high pottential for energy-saving as well, and requied performance of membrane is feasible. The energy for condenser and reboiler in distillation is greatly reduced and the small amount of energy for compresser is additionally required. Membrane-distillation hybrid processes has potentials up to 60% of energy-consumption and operating cost reduction compared with conventional cryogenic distillation.

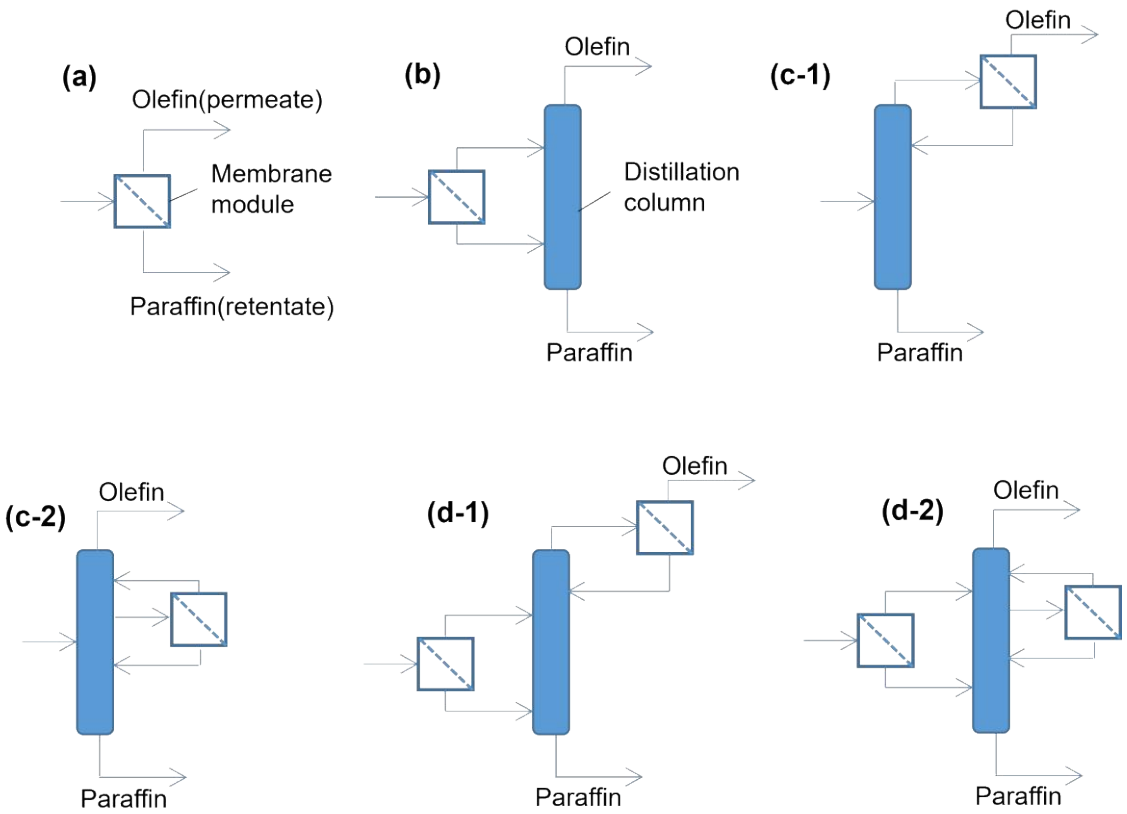

Figure 1.12. Configulations of membrane separation and membrane-distillation hybrid separation.processes.

Table 1.8 Economic evaluation of the separation process for propylene/propane and ethylene/ethane by using membrane

			Feed					Product specification			Assumed membrane performance					
No.	Components	Configulations*1	Flow rate / kmol h^{-1} Olefin	Flow rate / kmol h^{-1} paraffin	Propylene purity / -	Total pressure / MPa	Temperature / K	Propylene purity / -	Propylene recovery ratio / -	Pressure / MPa	Permeance / 10^{-9} mol m^{-2} s^{-1} Pa^{-1}	Permeance ratio ($C_3^=/C_3$) / -	Relative membrane Cost / \$ m^{-2}	Membrane area / m^2	Total membrane cost / MM\$	Membrane life / yr
1	$C_3^=/C_3$	(a)	180	180	0.50	1.80	323	0.9950	0.950	1.80	0.335		156	16163	2.52	15
2	$C_3^=/C_3$	(a)	1433	159	0.90	2.04	N.D.	0.9950	0.995	2.04	1000	100	18182	3247	59.04	5
3	$C_3^=/C_3$	(a)	1433	159	0.90	2.04	N.D.	0.9950	0.995	2.04	1000	100	4545	3247	14.76	5
4	$C_3^=/C_3$	(b)	1433	159	0.90	2.04	N.D.	0.9950	0.995	2.04	1000	100	18182	500	9.09	5
5	$C_3^=/C_3$	(b)	1433	159	0.90	2.04	N.D.	0.9950	0.995	2.04	1000	100	4545	500	2.27	5
6	$C_3^=/C_3$	(a)	1433	159	0.90	2.04	N.D.	0.9950	0.995	2.04	7	42	N.D.	104070	N.D.	N.D.
7	$C_3^=/C_3$	(b)	1433	955	0.60	2.04	N.D.	0.9950	0.995	2.04	7	42	N.D.	47217	N.D.	N.D.
8	$C_3^=/C_3$	(b)	1433	159	0.90	2.04	N.D.	0.9950	0.995	2.04	7	42	N.D.	32948	N.D.	N.D.
9	$C_3^=/C_3$	(c-1)	1433	955	0.60	2.04	N.D.	0.9950	0.995	2.04	7	42	N.D.	37956	N.D.	N.D.
10	$C_3^=/C_3$	(c-1)	1433	159	0.90	2.04	N.D.	0.9950	0.995	2.04	7	42	N.D.	37965	N.D.	N.D.
11	$C_3^=/C_3$	(b)	180	180	0.50	1.80	323	0.9950	0.950	1.80	37.2	209	20	2800	0.06	2
12	$C_3^=/C_3$	(b)	180	180	0.50	1.80	323	0.9950	0.950	1.80	37.2	209	200	2800	0.56	2
13	$C_3^=/C_3$	(b)	180	180	0.50	1.80	323	0.9950	0.950	1.80	30.5	50	20	2900	0.06	2
14	$C_3^=/C_3$	(b)	180	180	0.50	1.80	323	0.9950	0.950	1.80	30.5	50	200	2900	0.58	2
15	$C_3^=/C_3$	(b)	180	180	0.50	1.80	323	0.9950	0.950	1.80	12.4	8.9	20	5300	0.11	2
16	$C_3^=/C_3$	(b)	180	180	0.50	1.80	323	0.9950	0.950	1.80	12.4	8.9	200	5300	1.06	2
17	$C_3^=/C_3$	(b)	180	180	0.50	1.80	323	0.9950	0.950	1.80	44.9	17	200	1600	0.32	2
18	$C_3^=/C_3$	(b)	531	22	0.91	1.97	308	0.9980	0.868	1.90	7.04	42	107.6	8350	0.90	N.D.
19	$C_2^=/C_2$	(b)	2050	362	0.85	2.00	255	0.9995	0.999	2.00	150	94	1920	N.D.	N.D.	2
20	$C_2^=/C_2$	(c-1)	60	40	0.60	2.00	253	0.9950	0.995	2.00	13.9	4.72	200	121.9	0.02	2
21	$C_2^=/C_2$	(b)	2000	500	0.80	2.00	255	0.9995	0.995	1.90	28	30	100	15000	1.50	5
22	$C_2^=/C_2$	(b)	2000	500	0.80	2.00	255	0.9995	0.995	1.90	28	100	100	15000	1.50	5

*1 Details of configulation is shown in figure 1.12

*2 1.00 USD = 0.833 EURO = 110 JPY

*3 N.D. means No Data

Table 1.8 Continued

No.	Calculated results										Ref.
	Energy consumption in conventional distillation / MW	Energy consumption in membrane-based separation / MW	Reduction of energy consumption / -	CAPEX of conventional distillation /MM$	CAPEX of membrane-based separation /MM$	OPEX of conventional distillation /MM$ yr^{-1}	OPEX of membrane-based separation /MM$ yr^{-1}	Total annual cost of conventional distillation /MM$ yr^{-1}	Total annual cost of membrane-based separation /MM$ yr^{-1}	Reduction of total annual cost / -	
1	N.D.	N.D.	N.D.	8.9	7.02	4.1	1.77	4.69	2.24	0.52	219
2	74.5	24	0.68	33.3	62.7	19.6	4.6	26.2	17.1	0.35	220
3	74.5	24	0.68	33.3	18.4	19.6	4.6	26.2	8.28	0.68	220
4	74.5	29	0.61	33.3	24.9	19.6	7.38	26.2	12.3	0.53	220
5	74.5	29	0.61	33.3	17.9	19.6	7.38	26.2	11	0.58	220
6	73	22	0.70	N.D.	N.D.	N.D.	N.D.	N.D.	N.D.	N.D.	221
7	93	64	0.31	N.D.	N.D.	N.D.	N.D.	N.D.	N.D.	N.D.	221
8	73	25	0.66	N.D.	N.D.	N.D.	N.D.	N.D.	N.D.	N.D.	221
9	93	82	0.12	N.D.	N.D.	N.D.	N.D.	N.D.	N.D.	N.D.	221
10	73	27	0.63	N.D.	N.D.	N.D.	N.D.	N.D.	N.D.	N.D.	221
11	N.D.	N.D.	N.D.	N.D.	N.D.	N.D.	N.D.	4.05	1.78	0.56	222
12	N.D.	N.D.	N.D.	N.D.	N.D.	N.D.	N.D.	4.05	2.04	0.50	222
13	N.D.	N.D.	N.D.	N.D.	N.D.	N.D.	N.D.	4.05	2.5	0.38	222
14	N.D.	N.D.	N.D.	N.D.	N.D.	N.D.	N.D.	4.05	2.6	0.36	222
15	N.D.	N.D.	N.D.	N.D.	N.D.	N.D.	N.D.	4.05	3.34	0.18	222
16	N.D.	N.D.	N.D.	N.D.	N.D.	N.D.	N.D.	4.05	3.73	0.08	222
17	N.D.	N.D.	N.D.	N.D.	N.D.	N.D.	N.D.	4.05	3.13	0.23	222
18	N.D.	N.D.	N.D.	9.6	14.9	7.8	4.1	9.7	6.2	0.36	223
19	60.2	N.D.	N.D.	26.5	20.7	8.83	6.63	N.D.	N.D.	N.D.	218
20	N.D.	N.D.	N.D.	N.D.	N.D.	N.D.	N.D.	0.581	0.467	0.20	209
21	41.9	N.D.	N.D.	N.D.	N.D.	N.D.	N.D.	9.4	9.4	0.00	224
22	41.9	N.D.	N.D.	N.D.	N.D.	N.D.	N.D.	9.4	8.8	0.06	224

*1 Details of configulation is shown in figure 1.12

*2 1.00 USD = 0.833 EURO = 110 JPY

*3 N.D. means No Data

1.5.3. Membrane materials for olefin separation; Molecular sieving or affinity-based separation

During the last decades, propylene/propane and ethylene/ethane separation have been tried with various types of membranes on the basis of molecular sieving effect or interaction between membrane and olefin.

Understanding adsorption and diffusion phenomena in micropores is essential for an understanding of the separation mechanism using membranes made of microporous materials such as zeolites and MOFs. Permeation phenomena were explained generally by an adsorption-diffusion model in which the permeation selectivity can be expressed as the product of adsorption and diffusion selectivities [53,225,226]. In other words, permeation selectivity is mainly governed by adsorption selectivity when diffusion selectivity is low, and vice versa.

Following studies of the ZIF-8 membrane for propylene/propane separation by Lai *et al.* [54,213], ZIF-8 membranes have been researched extensively [55,77,214-216]. ZIF-8 membranes have great potential for propylene/propane separation on the basis of diffusion selectivity [55,216]. Li *et al.* studied the adsorption and diffusion properties of propylene and propane in the micropores of ZIF-8 [55]. It was pointed out that although the heats of adsorption and adsorption capacities for propylene and propane are similar, the diffusion coefficient of propylene is 125 times greater than that of propane. The slightly smaller size of propylene contributes to a larger diffusion rate in the micropores of ZIF-8 compared with propane. Hara *et al.* have discussed the contribution of adsorption and diffusion for propylene/propane separation through ZIF-8 membranes, and they concluded that the separation is governed mostly by diffusive separation [216].

Caro *et al.* investigated the contribution of adsorption and diffusion processes to ethylene/ethane separation with ZIF-8 membrane [53]. They reported that the estimated ethylene/ethane permeation selectivity of 1.4, as the product of adsorption selectivity of 0.5 and diffusion selectivity of 2.7, was close to the measured permeation selectivity of 2.4. In this case, both adsorption and diffusion selectivity probably contributed to permeation selectivity.

Olefin/paraffin separation based on molecular sieving effect by silica, CMS, and MOF have previously been reported [54,212,217,227,228]. Koros *et al.* reported ethylene/ethane separation with Matrimid® derived CMS hollow fiber membrane [227]. Their membrane showed the ethylene selectivity of 12 with the ethylene permeance of 8.3×10^{-11} mol m^{-2} s^{-1} Pa^{-1}. Morooka *et al*. performed propylene/propane separation with a carbonized BPDA-pp'ODA polyimide membrane [217]. They reported the propylene selectivity of 33 with its permeance of 2.9×10^{-9} mol m^{-2} s^{-1} Pa^{-1}. Kanezashi *et al*. prepared a BTESM-derived silica membrane and applied it to propylene/propane separation [212]. The membrane showed the propylene selectivity of 33 with

the permeance of 2.8×10^{-8} mol m^{-2} s^{-1} Pa^{-1}. These inorganic membranes separate the olefin/paraffin mixtures by a molecular sieving effect. Altogether, olefins preferentially penetrate through the membranes because of their slightly small sizes.

These inorganic membranes, silica, carbon molecular sieving (CMS), metal-organic framework (MOF) and zeolite membranes are expected to have high chemical and pressure resistance, and thus have become recognized as candidates for olefin separation.

Polymeric membranes for olefin separation has often been reported. In particular, Ag-containing polymeric membranes were extensively studied and showed superior separation performance by strong interaction between membrane and olefin [211,229,230]. Ag cations in facilitated transport membranes play as carrier for the transport of olefins. Kim *et al*. prepared an $AgBF_4$-cellulose acetate membrane having the ethylene selectivity of 280 in ethylene/ethane separation [229]. Ren *et al*. reported the PEI/Pebax2533/$AgBF_4$ composite membrane showing an excellent selectivity as high as 4400 with propylene permeance of 1.2×10^{-8} mol m^{-2} s^{-1} Pa^{-1} for propylene/propane mixture [211]. Fallanza *et al.* adapted a supported ionic liquid membranes containing Ag for propylene/propane separation [230]. The membrane showed the propylene selectivity of 19.5 with its permeance of 1.5×10^{-8} mol m^{-2} s^{-1} Pa^{-1}.

Whereas these Ag containing polymeric membranes such as liquid phase or solid phase facilitated transport membranes possess great advantage in olefin selectivity, these membranes have difficulty in stability owing to their poor chemical and mechanical strength. In particular, liquid phase-facilitated transport membranes showed high olefin selectivities only in the presence of water and readily lose their olefin selectivity by leakage of carrier.

1.5.4. Affinity-based separation by using zeolite membrane for olefin recovery

Zeolites have been attracted attention as membrane material because of their unique molecular sieving and adsorption properties based on their wide variety of crystalline microporous structures. Matsukata *et al.* previously reported preparation of FAU-type zeolite membrane and examination of its separation property for the water/2-propanol binary system [231].

It is also known that separation performance appears due to adsorption selectivity other than the molecular sieving effect described above. A membrane made of silicalite-1, all-silica zeolite with the MFI topology, showed ethanol-selective permeation from an ethanol/water mixture due to its strong hydrophobicity [225,232,233]. Sano *et al.* were the first to report that silicalite-1 membrane exhibited a high ethanol permselectivity [232,233]. Nomura *et al.* investigated the transport mechanism of ethanol and water through silicalite-1 membrane [225]. They reported that the water permeance decreased in the presence of ethanol. While the diffusion coefficients

of ethanol and water in silicalite-1 membrane are almost the same, the amount of ethanol adsorbed was approximately 10 times larger than that of water, resulting in a membrane with high ethanol selectivity. This selective permeation of ethanol from an aqueous solution by hydrophobic zeolite membrane was the study that triggered research on zeolite membranes utilizing adsorption selectivity.

Sawamura *et al.* [234,235] have reported that selective permeation for water vapor of MOR-type zeolite membrane from hydrogen and methanol. Although the molecular size of hydrogen and water is almost the same, this hydrophilic membrane exhibited high water selectivity by affinity-based separation at high temperatures as high as 523 K. Sawamura *et al.* have also reported a reverse-selective Na-ZSM-5 membrane which showed high methanol selectivity against hydrogen despite the bigger molecular size of methanol [136]. These studies are good examples of affinity-based separation using unique adsorption properties of zeolites.

Here I pay attention to Ag-exchanged zeolite as membrane material for olefin recovery. Since zeolite can capture and hold cation as exchanged ion in their microchannels, I aimed at preparing Figure 1.13 shows the conceptual diagram of Ag-exchanged zeolite membrane for olefin purification by using affinity-based separation. Ag-exchanged membranes and investigating their olefin/paraffin separation properties in this thesis. Both characters of high stability in inorganic membrane and high selectivity in Ag containing polymeric membrane are expected for Ag-exchanged zeolite membrane. This is the first report about Ag-exchanged zeolite membrane for olefin/paraffin separation in our best knowledge.

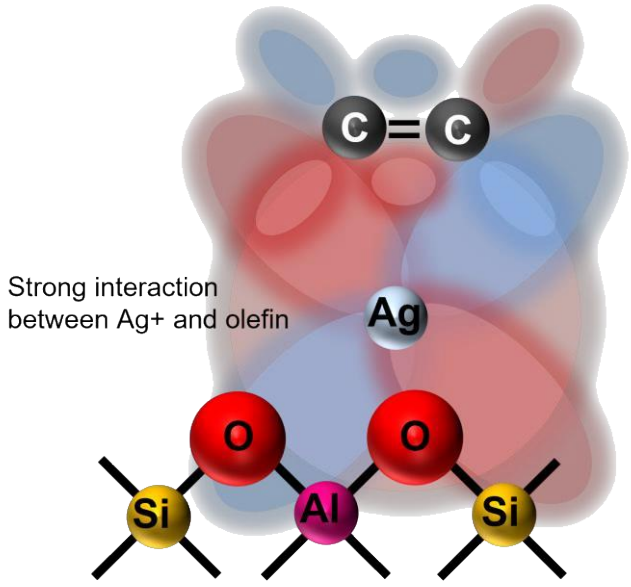

Figure 1.13. conceptual diagram of Ag-exchanged zeolite membrane for olefin purification by using affinity-based separation.

1.6. Summary

Separation by zeolite membrane has started to be used in relatively small-scale processes such as the recycle of organic solvents and food manufacturing since the late 1990s. However, there are issues that need to be solved to apply zeolite membranes to large-scale processes like gas separation or hydrocarbon separation.

Zeolite membranes including SAPO-34, SSZ-13, and MFI exhibit nearly sufficient permselectivity for CO_2 separation in laboratory scale especially for natural gas upgrading. Scale up and durability test is next important issues for practical applications. For hydrogen separation, membrane development will continue for a while in lab scale. In addition, study on membrane reactor systems will continue as well. The selectivity of zeolite membranes to hydrogen would be difficult to overwhelm those of carbon and Pd membranes for the future, so that zeolite membranes will be applied to relatively severe uses such as membrane reactors for WGSR and dehydrogenation reactions.

Additionally, some novel applications such as noble gas separation and olefin separations are also expected. Huge amount of energy is consumed in olefin purification processes as high as 0.3% of global energy use. Drastic reduction of such energy consumption is expected by introduction of membrane and membrane-based separation process. Therefore, many kinds of membranes for olefin purification have been developed in the last decade.

In propylene/propane separation, silica and ZIF-8 membrane exhibited good permeation and separation performance for propylene by a molecular sieving effect. In addition, Ag+-containing polymeric membranes showed excellent separation performance. However, these polymeric membranes have poor durability because of low thermal and mechanical strength.

Since zeolite can occlude cation in its micropore as exchanged ion, I have studied Ag-exchanged zeolite as membrane material. Ag-exchanged zeolite is expected as both specialties of inorganic membrane, high permeability and durability, and Ag-containing organic membrane, high selectivity.

References

[1] Bein, T.; Brown, K.; Frye, G.C.; Brinker, C.J. Molecular Sieve Sensors for Selective Detection at the Nanogram Level. *J. Am. Chem. Soc*. **1989**, 111, 7640.

[2] Meier, B.; Werner, T.; Klimant, I.; Wolfbeis, O.S. Novel oxygen sensor material based on a ruthenium bipyridyl complex encapsulated in zeolite Y: dramatic differences in the efficiency of luminescence quenching by oxygen on going from surface-adsorbed to zeolite-encapsulated

fluorophores. *Sens. Actuators, B* **1995**, 29, 240.

[3] Urbiztondo, M.A.; Pellejero, I.; Villarroya, M.; Sese, J.; Pina, M.P.; Dufour, I.; Santamaria, J. Zeolite-modified cantilevers for the sensing of nitrotoluene vapors. *Sens. Actuators, B* **2009**, 137, 608.

[4] Liu, J.; Sun, F.; Zhang, F.; Wang, Z.; Zhang, R.; Wang, C.; Qui, S. In situ growth of continuous thin metal–organic framework film for capacitive humidity sensing. *J. Mater. Chem*. **2011**, 21, 3775.

[5] Kung, C.W.; Chang, T.H.; Chou, L.Y.; Hupp, J.T.; Farha, O.K.; Ho, K.C. Porphyrin-based metal–organic framework thin films for electrochemical nitrite detection. *Electrochem. Commun.* **2015**, 58, 51.

[6] Wang, Z.; Wang, H.; Mitra, A.; Huang, L.; Yan, Y. Pure-Silica Zeolite Low-k Dielectric Thin Films. *Adv. Mater.* **2001**, 13, 746.

[7] Eslava, S.; Baklanov, M.R.; Neimark, A.V.; Iacopi, F.; Kirschhock, C.E.A.; Maex, K.; Martens, J.A. Evidence of Large Voids in Pure-Silica-Zeolite Low-k Dielectrics Synthesized by Spin-on of Nanoparticle Suspensions. *Adv. Mater.* **2008**, 20, 3110.

[8] Jahan, M.; Bao, Q.; Loh, K.P. Electrocatalytically Active Graphene−Porphyrin MOF Composite for Oxygen Reduction Reaction. *J. Am. Chem. Soc.* **2012**, 134, 6707.

[9] Alvaro, M.; Carbonell, E.; Ferrer, B.; Llabrés I Xamena, F. X.; Garcia, H. Semiconductor Behavior of a Metal-Organic Framework (MOF). *Chem. Eur. J.* **2007**, 13, 5106.

[10] Zhang, X.; Lai, E.S.M.; Martin-Aranda, R.; Yeung, K.L. An investigation of Knoevenagel condensation reaction in microreactors using a new zeolite catalyst. *Appl. Catal. A* **2004**, 261, 109.

[11] Rebrov, E.V.; Seijger, G.B.F.; Calis, H.P.A.; de Croon, M.H.J.M.; van den Bleek, C.M.; Schouten, J.C. The preparation of highly ordered single layer ZSM-5 coating on prefabricated stainless steel microchannels. *Appl. Catal. A* **2001**, 206, 125.

[12] Wan, Y.S.S.; Chau, J.L.H.; Gavriilidis, A.; Yeung, K.L. Design and fabrication of zeolite-based microreactors and membrane microseparators. *Micropor. Mesopor. Mater.* **2001**, 42, 157.

[13] Huo, J.; Aguilera-Sigalat, J.; El-Hankari, S.; Bradshaw, D. Magnetic MOF microreactors for recyclable sizeselective biocatalysis. *Chem. Sci.* **2015**, 6, 1938.

[14] Elimelech, M.; Phillip, W.A. The Future of Seawater Desalination: Energy, Technology, and the Environment. *Science* **2011**, 333, 712.

[15] Avlonitis, S.A.; Kouroumbas, K.; Vlachakis, N. Energy consumption and membrane replacement cost for seawater RO desalination plants. *Desalination* **2003**, 157, 151.

[16] Schiermeier, Q. Purification with a pinch of salt. *Nature* **2008**, 452, 260.

[17] Le-Clech, P.; Chen, V.; Fane, T.A.G. Fouling in membrane bioreactors used in wastewater treatment. *J. Membr. Sci.* **2006**, 284, 17.

[18] Meng, F.; Chae, S.R.; Drews, A.; Kraume, M.; Shin, H.S.; Yang, F. Recent advances in membrane bioreactors (MBRs): Membrane fouling and membrane material. *Water Res.* **2009**, 43, 1489.

[19] Riedl, K.; Girard, B.; Lencki, R.W. Influence of membrane structure on fouling layer morphology during apple juice clarification. *J. Membr. Sci.* **1998**, 139, 155.

[20] Rektor, A.; Pap, N.; Kokai, Z.; Szabo, R.; Vatai, G.; Bekassy-Molnar, E. Application of membrane filtration methods for must processing and preservation. *Desalination* **2004**, 162, 271.

[21] Itoh, N.; Akiha, T.; Sato, T. Preparation of thin palladium composite membrane tube by a CVD technique and its hydrogen permselectivity. *Catal. Today* **2005**, 104, 231.

[22] Uemiya, S.; Sato, N.; Ando, H.; Kude, Y.; Matsuda, T.; Kikuchi, E. Separation of hydrogen through palladium thin film supported on a porous glass tube. *J. Membr. Sci.* **1991**, 56, 303.

[23] Barbieri, G.; Violante, V.; Maio, F.P.D.; Criscuoli, A.; Drioli, E. Methane Steam Reforming Analysis in a Palladium-Based Catalytic Membrane Reactor. *Ind. Eng. Chem. Res.* **1997**, 36, 3369.

[24] Kiyono, M.; Williams, P.J.; Koros, W.J. Effect of pyrolysis atmosphere on separation performance of carbon molecular sieve membranes. *J. Membr. Sci.* **2010**, 359, 2.

[25] Yoshimune, M.; Fujikawa, I.; Haraya, K. Carbon molecular sieve membranes derived from trimethylsilyl substituted poly(phenylene oxide) for gas separation. *Carbon* **2007**, 45, 553.

[26] Gopalakrishnan, S.; da Costa, J.C.D. Hydrogen gas mixture separation by CVD silica membrane. *J. Membr. Sci.* **2008**, 323, 144.

[27] Nomura, M.; Ono, K.; Gopalakrishnan, S.; Sugawara, T.; Nakao, S. Preparation of a stable silica membrane by a counter diffusion chemical vapor deposition method. *J. Membr. Sci.* **2005**, 251, 151.

[28] Kanezashi, M.; Yada, K.; Yoshioka, T.; Tsuru, T. Organic–inorganic hybrid silica membranes with controlled silica network size: Preparation and gas permeation characteristics. *J. Membr. Sci.* **2010**, 348, 310.

[29] Carreon, M.L.; Li, S.; Carreon, M.A. AlPO-18 membranes for CO_2/CH_4 separation. *Chem. Commun.* **2012**, 48, 2310.

[30] Wu, T.; Wang, B.; Lu, Z.; Zhou, R.; Chen X. Alumina-supported AlPO-18 membranes for CO_2/CH_4 separation. *J. Membr. Sci.* **2014**, 471, 338.

[31] Hasegawa, Y.; Hotta, H.; Sato, K.; Nagase, T.; Mizukami, F. Preparation of novel chabazite (CHA)-type zeolite layer on porous α-Al_2O_3 tube using template-free solution. *J. Membr. Sci.*

2010, 347, 193.

[32] Li, S.; Falconer, J.L.; Noble, R.D. SAPO-34 membranes for CO_2/CH_4 separation. *J. Membr. Sci.* **2004**, 241, 121.

[33] Tian, Y.; Fan, L.; Wang, Z.; Qiu, S.; Zhu, G. Synthesis of a SAPO-34 membrane on macroporous supports for high permeance separation of a CO_2/CH_4 mixture. *J. Mater. Chem.* **2009**, 19, 7698.

[34] Hirota, Y.; Watanabe, K.; Uchida, Y.; Egashira, Y.; Yoshida, K.; Sasaki, Y.; Nishiyama, N. Coke deposition in the SAPO-34 membranes for examining the effects of zeolitic and non-zeolitic pathways on the permeation and separation properties in gas and vapor permeations. *J. Membr. Sci.* **2014**, 415, 176.

[35] Aoki, K.; Kusakabe, K.; Morooka, S. Gas permeation properties of A-type zeolite membrane formed on porous substrate by hydrothermal synthesis. *J. Membr. Sci.* **1998**, 141, 197.

[36] Okamoto, K.; Kita, H.; Horii, K.; Tanaka, K. Zeolite NaA Membrane: Preparation, Single-Gas Permeation, and Pervaporation and Vapor Permeation of Water/Organic Liquid Mixtures. *Ind. Eng. Chem. Res.* **2001**, 40, 163.

[37] Tomita, T.; Nakayama, K.; Sakai, H. Gas separation characteristics of DDR type zeolite membrane. *Micropor. Mesopor. Mater.* **2004**, 68, 71.

[38] van den Bergh, J.; Tihaya, A.; Kapteijn, F. High temperature permeation and separation characteristics of an all-silica DDR zeolite membrane. *Micropor. Mesopor. Mater.* **2010**, 132, 137.

[39] Lai, Z.; Tsapatsis, M.; Nicolich, J.P. Siliceous ZSM-5 membranes by secondary growth of *b*-oriented seed layers. *Adv. Funct. Mater.* **2004**, 14, 716.

[40] Hedlund, J.; Sterte, J.; Anthonis, M.; Bons, A.J.; Carstensen, B.; Corcoran, N.; Cox, D.; Deckman, H.; Gijnst, W.D.; de Moor, P.P.; Lai, F.; McHenry, J.; Mortier, W.; Reinoso, J.; Peters, J. High-flux MFI membranes. *Micropor. Mesopor. Mater.* **2002**, 52, 179.

[41] Li, G.; Kikuchi, E.; Matsukata, M. ZSM-5 zeolite membranes prepared from a clear template-free solution. *Micropor. Mesopor. Mater.* **2003**, 60, 225.

[42] Coronas, J.; Falconer, J. L.; Noble, R.D. Characterization and Permeation Properties of ZSM-5 Tubular Membranes. *AIChE J.* **1997**, 43, 1797.

[43] Kumakiri, I.; Yamaguchi, T.; Nakao, S. Preparation of Zeolite A and Faujasite Membranes from a Clear Solution. *Ind. Eng. Chem. Res.* **1999**, 38, 4682.

[44] Zhu, G.; Li, Y.; Zhou, H.; Liu, J.; Yang, W. Microwave synthesis of high performance FAU-type zeolite membranes: Optimization, characterization and pervaporation dehydration of alcohols. *J. Membr. Sci.* **2009**, 337, 47.

[45] Sato, K.; Sugimoto, K.; Sekine, Y.; Takada, M.; Matsukata, M.; Nakane, T. Application of FAU-type zeolite membranes to vapor/gas separation under high pressure and high temperature up to 5 MPa and 180 °C. *Micropor. Mesopor. Mater.* **2007**, 101, 312.

[46] Li, G.; Kikuchi, E.; Matsukata, M. Separation of water-acetic acid mixtures by pervaporation using a thin mordenite membrane. *Sep. Purif. Technol.* **2003**, 32, 199.

[47] Zhang, Y.; Xu, Z.; Chen, Q. Synthesis of small crystal polycrystalline mordenite membrane. *J. Membr. Sci.* **2002**, 210, 361.

[48] Furukawa, H.; Cordova, K. E.; O'Keeffe, M.; Yaghi, O.M. The Chemistry and Applications of Metal-Organic Frameworks. *Science* **2013**, 341, 1230444.

[49] Gul-E-Noor, F.; Jee, B.; Poppl, A.; Hartmann, M.; Himsl, D.; Bertmer, M. Effects of varying water adsorption on a $Cu_3(BTC)_2$ metal–organic framework (MOF) as studied by 1H and ^{13}C solid-state NMR spectroscopy. *Phys. Chem. Chem. Phys.* **2011**, 13, 7783.

[50] Cychosz, K.A.; Matzger, A.J. Water Stability of Microporous Coordination Polymers and the Adsorption of Pharmaceuticals from Water. *Langmuir* **2010**, 26, 17198.

[51] Li, Y.S.; Bux, H.; Feldhoff, A.; Li, G.L.; Yang, W.S.; Caro, J. Controllable Synthesis of Metal–Organic Frameworks: From MOF Nanorods to Oriented MOF Membranes. *Adv. Mater.* **2010**, 22, 3322.

[52] Kang, C.H.; Lin, Y.F.; Huang, Y.S.; Tung, K.L.; Chang, K.S.; Chen, J.T.; Hung, W.S.; Lee, K.R.; Lai, J.Y. Synthesis of ZIF-7/chitosan mixed-matrix membranes with improved separation performance of water/ethanol mixtures. *J. Membr. Sci.* **2013**, 438, 105.

[53] Bux, H.; Chmelik, C.; Krishna, R.; Caro, J. Ethene/ethane separation by the MOF membrane ZIF-8: Molecular correlation of permeation, adsorption, diffusion. *J. Membr. Sci.* **2011**, 369, 284.

[54] Pan, Y.; Li, T.; Lestari, G.; Lai, Z. Effective separation of propylene/propane binary mixtures by ZIF-8 membranes. *J. Membr. Sci.* **2012**, 390-391, 93-98.

[55] Hara, N.; Yoshimune, M.; Negishi, H.; Haraya, K.; Hara, S.; Yamaguchi, T. Diffusive separation of propylene/propane with ZIF-8 membranes. *J. Membr. Sci.* **2014**, 450, 215.

[56] Yang, T.; Chung, T.S. Room-temperature synthesis of ZIF-90 nanocrystals and the derived nano-composite membranes for hydrogen separation. *J. Mater. Chem. A* **2013**, 1, 6081.

[57] Huang, A.; Dou, W.; Caro, J. Steam-Stable Zeolitic Imidazolate Framework ZIF-90 Membrane with Hydrogen Selectivity through Covalent Functionalization. *J. Am. Chem. Soc.* **2010**, 132, 15562.

[58] Hu, Y.; Dong, X.; Nan, J.; Jin, W.; Ren, X.; Xu, N.; Lee, Y.M. Metal–organic framework membranes fabricated via reactive seeding. *Chem. Commun.* **2011**, 47, 737.

[59] Basu, S.; Cano-Odena, A.; Vankelecom, I.F.J. MOF-containing mixed-matrix membranes

for CO_2/CH_4 and CO_2/N_2 binary gas mixture separations. *Sep. Purif. Technol.* **2011**, 81, 31.

[60] Guerrero, V.V.; Yoo, Y.; McCarthy, M.C.; Jeong, H.K. HKUST-1 membranes on porous supports using secondary growth. *J. Mater. Chem.* **2010**, 20, 3938.

[61] Nan, J.; Dong, X.; Wang, W.; Jin, W.; Xu, N. Step-by-Step Seeding Procedure for Preparing HKUST-1 Membrane on Porous α-Alumina Support. *Langmuir* **2011**, 27, 4309.

[62] Zornoza, B.; Martinez-Joaristi, A.; Serra-Crespo, P.; Tellez, C.; Coronas, J.; Gascon, J.; Kapteijn, F. Functionalized flexible MOFs as fillers in mixed matrix membranes for highly selective separation of CO_2 from CH_4 at elevated pressures. *Chem. Commun.* **2011**, 47, 9522.

[63] Lin. R.; Ge, L.; Hou, L.; Strounina, E.; Rudolph, V.; Zhu, Z. Mixed Matrix Membranes with Strengthened MOFs/Polymer Interfacial Interaction and Improved Membrane Performance. *ACS Appl. Mater. Interfaces* **2014**, 6, 5609.

[64] Sato, K.; Sugimoto, K.; Nakane, T. Preparation of higher flux NaA zeolite membrane on asymmetric porous support and permeation behavior at higher temperatures up to 145 ◦C in vapor permeation. *J. Membr. Sci.* **2008**, 307, 181.

[65] Wang, Z.; Shao, Q.G.J.; Yan, Y. High Performance Zeolite LTA Pervaporation Membranes on Ceramic Hollow Fibers by Dipcoating-Wiping Seed Deposition. *J. Am. Chem. Soc.* **2009**, 131, 6910.

[66] Brown, A.J.; Brunelli, N.A.; Eum, K.; Rashidi, F.; Johnson, J.R.; Koros, W.J.; Jones, C.W.; Nair, S. Interfacial microfluidic processing of metal-organic framework hollow fiber membranes. *Science* **2014**, 345, 72.

[67] Liu, X.; Demir, N.K.; Wu, Z.; Li, K. Highly Water-Stable Zirconium Metal−Organic Framework UiO-66 Membranes Supported on Alumina Hollow Fibers for Desalination. *J. Am. Chem. Soc.* **2015**, 137, 6999.

[68] Ping, E.W.; Zhou, R.; Funke, H.H.; Falconer, J.L.; Nobel, R.D. Seeded-gel synthesis of SAPO-34 single channel and monolith membranes, for CO_2/CH_4 separations. *J. Membr. Sci.* **2012**, 415, 7705.

[69] Kalipcilar, H.; Gade, S.K.; Nobel, R.D.; Falconer, J.L. Synthesis and separation properties of B-ZSM-5 zeolite membranes on monolith supports. *J. Membr. Sci.* **2002**, 210, 113.

[70] Morigami, Y.; Kondo, M.; Abe, J.; Kita, H.; Okamoto, K. The first large-scale pervaporation plant using tubular-type module with zeolite NaA membrane. *Sep. Purif. Technol.* **2001**, 25, 251.

[71] Kondo, M.; Komori, M.; Kita, H.; Okamoto, K. Tubular-type pervaporation module with zeolite NaA membrane. *J. Membr. Sci.* **1997**, 133, 133.

[72] Nishiyama, N.; Ueyama, K.; Matsukata, M. Synthesis of defect-free zeolite-alumina composite membranes by a vapor-phase transport method. *Micropor. Mater.* **1996**, 7, 299.

[73] Matsufuji, T.; Nakagawa, S.; Nishiyama, N.; Matsukata, M.; Ueyama, K. Synthesis and permeation studies of ferrierite/alumina composite membranes. *Micropor. Mesopor. Mater.* **2000**, 38, 43.

[74] Kikuchi, E.; Yamashita, K.; Hiromoto, S.; Ueyama, K.; Matsukata, M. Synthesis of a zeolitic thin layer by a vapor-phase transport method: appearance of a preferential orientation of MFI zeolite. *Micropor. Mater.* **1997**, 11, 107.

[75] Matsufuji, T.; Nishiyama, N.; Matsukata, M.; Ueyama, K. Separation of butane and xylene isomers with MFI-type zeolitic membrane synthesized by a vapor-phase transport method. *J. Membr. Sci.* **2000**, 178, 25.

[76] Hara, N.; Yoshimune, M.; Negishi, H.; Haraya, K.; Hara, S.; Yamaguchi, T. Thickness Reduction of the Zeolitic Imidazolate Framework-8 Membrane by Controlling the Reaction Rate during the Membrane Preparation. *J. Chem. Eng. Jpn.* **2014**, 47, 770.

[77] Kwon, H.T.; Jeong, H.K. In Situ Synthesis of Thin Zeolitic−Imidazolate Framework ZIF-8 Membranes Exhibiting Exceptionally High Propylene/Propane Separation. *J. Am. Chem. Soc.* **2013**, 135, 10763.

[78] Li, Y.; Wee, L.H.; Volodin, A.; Martiens, J.A.; Vankelecom, I.F.J. Polymer supported ZIF-8 membranes prepared via an interfacial synthesis method. *Chem. Commun.* **2015**, 51, 918.

[79] Kusakabe, K.; Kuroda, T.; Murata, A.; Morooka, S. Formation of a Y-Type Zeolite Membrane on a Porous α-Alumina Tube for Gas Separation. *Ind. Eng. Chem. Res.* **1997**, 36, 649.

[80] Tao, K.; Cao, L.; Lin, Y.; Kong, C.; Chen, L. A hollow ceramic fiber supported ZIF-8 membrane with enhanced gas separation performance prepared by hot dip-coating seeding. *J. Mater. Chem. A* **2013**, 1, 13046.

[81] Xiao, W.; Chen, Z.; Zhou, L.; Yang, J.; Lu, J.; Wang, J. A simple seeding method for MFI zeolite membrane synthesis on microporous support by microwave heating. *Micropor. Mesopor. Mater.* **2011**, 142, 154.

[82] Yang, J.; Li, H.; Xu, J.; Wang, J.; Meng, X.; Bai, K.; Lu, J.; Zhang, Y.; Yin, D. Influences of inorganic salts on the pervaporation properties of zeolite NaA membranes on macroporous supports. *Micropor. Mesopor. Mater.* **2014**, 192, 60.

[83] Chen, X.; Wang, J.; Yin, D.; Yang, J.; Lu, J.; Zhang, Yan.; Chen, Z. High-Performance Zeolite T Membrane for Dehydration of Organics by a New Varying Temperature Hot-Dip Coating Method. *AIChE J.* **2013**, 59, 936.

[84] Mintova, S.; Bein, T. Microporous Films Prepared by Spin-Coating Stable Colloidal Suspensions of Zeolites. *Adv. Mater.* **2001**, 13, 1880.

[85] Tosheva, L.; Mihailova, B.; Wee, L.K.; Gasharova, B.; Garbev, K.; Doyle, A.M. Indirect

Observation of Structured Incipient Zeolite Nanoparticles in Clear Precursor Solutions. *Angew. Chem. Int. Ed.* **2008**, 47, 8650.

[86] Algieri, C.; Bernardo, P.; Barbieri, G.; Drioli, E. A novel seeding procedure for preparing tubular NaY zeolite membranes. *Micropor. Mesopor. Mater.* **2009**, 119, 129.

[87] Huang, A.; Lin, Y.S.; Yang, W. Synthesis and properties of A-type zeolite membranes by secondary growth method with vacuum seeding. *J. Membr. Sci.* **2004**, 245, 41.

[88] Ji, C.; Tian, Y.; Li, Y.; Lin, Y.S. Thin oriented AFI zeolite membranes for molecular sieving separation. *Micropor. Mesopor. Mater.* **2014**, 186, 80.

[89] Melgar, V.M.A.; Kwon, H.T.; Kim, J. Direct spraying approach for synthesis of ZIF-7 membranes by electrospray deposition. *J. Membr. Sci.* **2014**, 459, 190.

[90] Seike, T.; Matsuda, M.; Miyake, M. Preparation of FAU type zeolite membranes by electrophoretic deposition and their separation properties. *J. Mater. Chem.* **2002**, 12, 366.

[91] Liu, Y.; Yang, Z.; Yu, C.; Gu, X.; Xu, N. Effect of seeding methods on growth of NaA zeolite membranes. *Micropor. Mesopor. Mater.* **2011**, 143, 348.

[92] Hedlund, J.; Jareman, F.; Bons, A.J.; Anthonis, M. A masking technique for high quality MFI membranes. *J. Membr. Sci.* **2003**, 222, 163.

[93] Pan, M.; Lin, Y.S. Template-free secondary growth synthesis of MFI type zeolite membranes. *Micropor. Mesopor. Mater.* **2001**, 43, 319.

[94] Zhou, L.; Yang, J.; Li, G.; Wang, J.; Zhang, Y.; Lu, J.; Yin, D. Highly H_2 permeable SAPO-34 membranes by steam-assisted conversion seeding. *Int. J. Hydrog. Energy* **2014**, 39, 14949.

[95] Bradshaw, D.; Garai, A.; Huo, Metal–organic framework growth at functional interfaces: thin films and composites for diverse applications. *J. Chem. Soc. Rev.* **2012**, 41, 2344.

[96] Lai, Z.; Bonilla, G.; Diaz, I.; Nery, J.G.; Sujaoti, K.; Amat, M. A.; Kokkoli, E.; Terasaki, O.; Thompson, R.W.; Tsapatsis, M.; Vlachos, D.G. Microstructural Optimization of a Zeolite Membrane for Organic Vapor Separation. *Science* **2003**, 300, 456.

[97] Boudreau, L.C.; Kuck, J.A.; Tsapatsis, M. Deposition of oriented zeolite A films: in situ and secondary growth. *J. Membr. Sci.* **1999**, 152, 41.

[98] Lai, R.; Gavalas, G. R. Surface Seeding in ZSM-5 Membrane Preparation. *Ind. Eng. Chem. Res.* **1998**, 37, 4275.

[99] Li, G.; Kikuchi, E.; Matsukata, M. The control of phase and orientation in zeolite membranes by the secondary growth method. *Micropor. Mesopor. Mater.* **2003**, 62, 211.

[100] Jeong, H.K.; Krohn, J.; Sujaoti, K.; Tsapatsis, M. Oriented Molecular Sieve Membranes by Heteroepitaxial Growth. *J. Am. Chem. Soc.* **2002**, 124, 12966.

[101] Sakai, M.; Fujimaki, N.; Kobayashi, G.; Yasuda, N.; Oshima, Y.; Seshimo, M.; Matsukata,

M. Formation process of *BEA-type zeolite membrane under OSDA-free conditions and its separation property. *Micorpor. Mesopor. Mater.* **2019**, 284, 360-365.

[102] Membrane Technology, "Japanese firms work together to produce and sell zeolite membranes." **2016**, 10, 3.

[103] Membrane Technology, "Zeolite-based membrane element developed." **2011**, 7, 3.

[104] Urtiaga, A.; Gorri, E.D.; Casado, C.; Ortiz, I. Pervaporative dehydration of industrial solvents using a zeolite NaA commercial membrane. *Sep. Purif. Technol.* **2003**, 32, 207.

[105] Hoof. V.V.; Dotremont, C.; Buekenhoudt, A. Performance of Mitsui NaA type zeolite membranes for the dehydration of organic solvents in comparison with commercial polymeric pervaporation membranes. *Sep. Purif. Technol.* **2006**, 48, 304.

[106] Nomura, M.; Yamaguchi, T.; Nakao, S. Transport phenomena through intercrystalline and intracrystalline pathways of silicalite zeolite membranes. *J. Membr. Sci.* **2001**, 187, 203.

[107] Mirth, G.; Cejka, J.; Lercher, J.A. Transport and Isomerization of Xylenes over HZSM-5 Zeolites. *J. Catal.* **1993**, 139, 24.

[108] Hong, M.; Li, S.; Funke, H.H.; Falconer, J.L.; Noble, R.D. Ion-exchanged SAPO-34 membranes for light gas separations. *Micropor. Mesopor. Mater.* **2007**, 106, 140.

[109] Sakai, M.; Tomaki, K.; Matsukata, M. Control of pore size of silicalite-1 membrane with pyrolytic carbon. Proceeding of 14th International Conference on Inorganic Membranes 2016, P1.

[110] Sandstorm, L.; Lindmark, J.; Hedlund, J. Separation of methanol and ethanol from synthesis gas using MFI membranes. *J. Membr. Sci.* **2010**, 360, 265.

[111] Karimi, S.; Korelskiy, D.; Yu, L.; Mouzon, J.; Khodadadi, A.A.; Mortazavi, Y.; Esmaeili, M.; Hedlund, J. A simple method for blocking defects in zeolite membranes. *J. Membr. Sci.* **2015**, 489, 270.

[112] Caro, J.; Noack, M.; Kolsch, P. Zeolite Membranes: From the Laboratory Scale to Technical Applications. *Adsorption* **2005**, 11, 215.

[113] Hedlund, J.; Korelskiy, D.; Sandstorm, L.; Lindmark, J. Permporometry analysis of zeolite membranes. *J. Membr. Sci.* **2009**, 345, 276.

[114] Tsuru, T.; Hino, T.; Yoshioka, T.; Asaeda, M. Permporometry characterization of microporous ceramic membranes. *J. Membr. Sci.* **2001**, 186, 257.

[115] Kumakiri, I.; Stange, M.; Peters, T.A.; Klette, H.; Kita, H.; Bredesen, R. Membrane characterisation by a novel defect detection technique. *Micropor. Mesopor. Mater.* **2008**, 115, 33.

[116] Funke, H.H.; Tokay, B.; Zhou, R.; Ping, E.W.; Zhang, Y.; Falconer, J.L.; Noble, R.D. Spatially resolved gas permeation through SAPO-34 membranes. *J. Membr. Sci.* **2012**, 409, 212.

[117] Bonilla, G.; Tsapatsis, M.; Vlachos, D. G.; Xomeritakis, G. Fluorescence confocal optical microscopy imaging of the grain boundary structure of zeolite MFI membranes made by secondary (seeded) growth. *J. Membr. Sci.* **2001**, 182, 103-109.

[118] Snyder, M.A.; Lai, Z.; Tsapatsis, M.; Vlachos, D.G. Combining simultaneous reflectance and fluorescence imaging with SEM for conclusive identification of polycrystalline features of MFI membranes. *Micropor. Mesopor. Mater.* **2004**, 76, 29.

[119] Kosinov, N.; Sripathi V.G.P.; Hensen, E.J.M. Improving separation performance of high-silica zeolite membranes by surface modification with triethoxyfluorosilane. *Micropor. Mesopor. Mater.* **2014**, 194, 24.

[120] Nomura, M.; Yamaguchi T.; Nakao, S. Silicalite Membranes Modified by Counterdiffusion CVD Technique. *Ind. Eng. Chem. Res.* **1997**, 36, 4217.

[121] Yan, Y.; Davis M.E.; Gavalas, G.R. Preparation of highly selective zeolite ZSM-5 membranes by a post-synthetic coking treatment. *J. Membr. Sci.* **1997**, 123, 95.

[122] Hong, S.; Kim, D.; Jeong, Y.; Kim, E.; Jung, J.C.; Choi, N.; Nam, J.; Yip, A.C.K.; Choi, J. Healing of Microdefects in SSZ-13 Membranes via Filling with Dye Molecules and Its Effect on Dry and Wet CO_2 Separations. *Chem. Mater.* **2018**, 30, 3346.

[123] Sakai, M.; Hori, H.; Matsukata, M. Self-defect-healing of silicalite-1 membrane in alkaline aqueous solution with surfactant. *Mater. Adv.* **2021**, 2, 3892-3897.

[124] Xomeritakis, G.; Lai, Z.; Tsapatsis, M. Separation of xylene isomer vapors with oriented MFI membranes made by seeded growth. *Ind. Eng. Chem. Res.* **2001**, 40, 544–552.

[125] Korelskiy, D.; Leppajarvi, T.; Zhou, H.; Grahn, M.; Tanskanen, J.; Hedlund, J. High flux MFI membranes for pervaporation. *J. Membr. Sci.* **2013**, 427, 381–389.

[126] Kim, D.; Jeon, M.Y.; Stottrup, B.L.; Tsapatsis, M. para-Xylene Ultra-selective Zeolite MFI Membranes Fabricated from Nanosheet Monolayers at the Air–Water Interface. *Angew. Chem. Int. Ed.* **2018**, 57, 480–485.

[127] Ueno, K.; Negishi, H.; Okuno, T.; Tawarayama, H.; Ishikawa, S.; Miyamoto, M.; Uemiya, S.; Oumi, Y. Effects of seed crystal type on the growth and microstructures of silicalite-1 membranes on tubular silica supports via gel-free steam-assisted conversion. *Micropor. Mesopor. Mater.* **2019**, 289, 109645.

[128] Heink, W.; Kärger, J.; Naylor, T.; Winkler, U. PFG NMR study of the transport properties of A-type zeolite membranes. *Chem. Commun.* **1999**, 57–58.

[129] Hirosawa, F.; Miyagawa, M.; Takaba, H. Selectivity enhancement by the presence of grain boundary in chabazite zeolite membranes investigated by non-equilibrium molecular dynamics. *J. Membr. Sci.* **2021**, 632, 119348.

[130] Yu, M.; Falconer, J.L.; Amundsen, T.J.; Hong, M.; Noble, R.D. A Controllable

Nanometer-Sized Valve. *Adv. Mater.* **2007**, 19, 3032–3036.

[131] Sakai, M.; Sasaki, Y.; Kaneko, T.; Matsukata, M. Contribution of Pore-Connectivity to Permeation Performance of Silicalite-1 Membrane; Part I, Pore Volume and Effective Pore Size. *Membranes* **2021**, 11, 382.

[132] Kondo, M.; Yamamura, T.; Yukitake, T.; Matsuo, Y.; Kita, H.; Okamoto, K. IPA purification for lens cleaning by vapor permeation using zeolite membrane. *Sep. Purif. Technol.* **2003**, 32, 191.

[133] Nomura, M.; Uchida, M. JP 2017018848.

[134] Sakai, M.; Kaneko, T.; Sasaki, Y.; Sekigawa, M.; Matsukata, M. Formation Process of Columnar Grown (101)-Oriented Silicalite-1 Membrane and Its Separation Property for Xylene Isomer. *Crystals* **2020**, 10, 949.

[135] Schmitt, M.; Christmann, M.; Ueno, N.; Kyotani, T.; Kakiuchi, H. Must concentration by new zeolite membrane (KonKer^{TM}) technology. BIO web Conferences 39th World Congress of Vine and Wine, **2016**, 7.

[136] Sawamura, K.; Izumi, T.; Kawasaki, K.; Daikohara, S.; Ohsuna, T.; Takada, M.; Sekine, Y.; Kikuchi, E.; Matsukata, M. Reverse-selective microporous membrane for gas separation. *Chem. Asian J.* **2009**, 4, 1070-1077.

[137] NIKKEI ASIA, "Mitsubishi Chemical strains out profit with zeolites." http://asia.nikkei.com/magazine/20160512-WEALTHIER-UNHEALTHIER/Tech-Science/Mitsubishi-Chemical-strains-out-profit-with-zeolites

[138] Lixiong, Z.; Mengdong, J.; Enze, M. Synthesis of SAPO-34/ceramic composite membranes. *Stud. Surface Sci.Catal.* **1997**, 105, 2211-2216.

[139] Carreon, M.A.; Li, S.; Falconer, J.L.; Noble, R.D. SAPO-34 seeds and membranes prepared using multiple structure directing agents. *Adv. Mater.* **2007**, 20, 729-732.

[140] Carreon, M.A.; Li, S.; Falconer, J.L.; Noble, R.D. Alumina-supported SAPO-34 membranes for CO_2/CH_4. *J. Am. Chem. Soc.* **2008**, 130, 5412-5413.

[141] Poshusta, J.C.; Tuan, V.A.; Pape, A.; Noble, R.D.; Falconer, J.L. Separation of light gas mixtures using SAPO-34 membranes. *AIChE J.* **2000**, 46, 779-789.

[142] Poshusta, J.C.; Tuan, V.A.; Falconer, J.L.; Noble, R.D. Synthesis and permeation properties of SAPO-34 tubular membranes. *Ind. Eng. Chem. Res.* **1998**, 37, 3924-3929.

[143] Li, S.; Martinek, J.G.; Falconer, J.L.; Noble, R.D.; Gardner, T.Q. High-pressure CO_2/CH_4 separation using SAPO-34 membranes. *Ind. Eng. Chem. Res.* **2005**, 44, 3220-3228.

[144] Kosinov, N.; Auffret, C.; Gucuyener, C.; Szyja, B.M.; Gascon, J.; Kapteijn, F.; Hensen, E.J.M. High flux high-silica SSZ-13 membrane for CO_2 separation. *J. Mater. Chem. A* **2014**, 2, 13083-13092.

[145] Zheng, Y.; Hu, N.; Wang, H.; Bu, N.; Zhang, F.; Zhou, R. Preparation of steam-stable high-silica CHA (SSZ-13) membranes for CO_2/CH_4 and C_2H_4/C_2H_6 separation. *J. Membr. Sci.* **2015**, 475, 303-310.

[146] Kalipcilar, H.; Bowen, T.C.; Noble, R.D.; Falconer, J.L. Synthesis and separation performance of SSZ-13 zeolite membranes on tubular supports. *Chem. Mater.* **2002**, 14, 3458-3464.

[147] Kosinov, N.; Auffret, C.; Sripathi, V.G.P.; Gucuyener, C.; Gascon, J.; Kapteijn, F.; Hensen, E.J.M. Influence of support morphology on the detemplation and permeation of ZSM-5 and SSZ-13 zeolite membranes. *Micropor. Mesopor. Mater.* **2014**, 197, 268-277.

[148] Yoshihara, K., Sakai, M., Matsukata, M., 2017, Unpublished results.

[149] Lindmark, J.; Hedlund, J. Modification of MFI membranes with amine groups for enhanced CO_2 selectivity. *J. Mater. Chem.* **2010**, 20, 2219-2225.

[150] Lindmark, J.; Hedlund, J. Carbon dioxide removal from synthesis gas using MFI membranes. *J. Membr. Sci.* **2010**, 360, 284-291.

[151] Sandstrom, J.; Sjoberg, E.; Hedlund, J. Very high flux MFI membrane for CO_2 separation. *J. Membr. Sci.* **2011**, 380, 232-240.

[152] Sjoberg, E.; Barnes, S.; Korelskiy, D.; Hedlund, J. MFI membranes for separation of carbondioxide from synthesis gas at high pressures. *J. Membr. Sci.* **2015**, 486, 132-137.

[153] Zhou, M.; Korelskiy, D.; Ye, P.; Grahn, M.; Hedlund, J. A uniformly oriented MFI membrane for improved CO_2 separation. *Ange. Chem. Int. Ed.* **2014**, 53, 3492-3495.

[154] Venna, S.R.; Carreon, M.A. Amino-functionalized SAPO-34 membranes for CO_2/CH_4 and CO_2/N_2 separation. *Langmuir* **2011**, 27, 2888-2894.

[155] Bo, L.; Rongfei, Z.; Na, B.; Qing, W.; Shenglai, Z.; Bin, W.; Kita, H. Room-temperature ionic liquids modified zeolite SSZ-13 membranes for CO_2/CH_4 separation. *J. Membr. Sci.* **2017**, 524, 12-19.

[156] Li, S.; Alvarado, G.; Falconer, J.L.; Noble, R.D. Effects of impurities on CO_2/CH_4 separations through SAPO-34 membranes. *J. Membr. Sci.* **2005**, 251, 59-66.

[157] Li, S.; Carreon, M.A.; Zhang, Y.; Funke, H.H.; Noble, R.D.; Falcone, J.L. Scale-up of SAPO-34 membranes for CO_2/CH_4 separation. J. Membr. Sci. **2010**, 352, 7-13.

[158] Chen, Y.; Zhang, Y.; Zhang, C.; Jiang, J.; Gu, X. Fabrication of high-flux SAPO-34 membrane on α-Al_2O_3 four-channel hollow fibers for CO_2 capture from CH_4. *J. CO_2 Util.* **2017**, 18, 30-40.

[159] Chew, T.L.; Ahmad, A.L.; Bhatia, S. Ba-SAPO-34 membrane synthesized from microwave heating and its performance for CO_2/CH_4 gas separation. *Chem. Eng. J.* **2011**, 171, 1053-1059.

[160] Bing, L.; Liu, X.; Zhang, B. Synthesis of thin CrAPSO-34 membranes by microwave-assisted secondary growth. *J. Mater. Sci.* **2016**, 51, 1476-1483.

[161] Wang, B.; Hu, N.; Wang, H.; Zheng, Y.; Zhou, R. Improved AlPO-18 membranes for light gas separation. *J. Mater. Chem. A* **2015**, 3, 12205-12212.

[162] Wang, L.; Zhang, C.; Gao, X.; Peng, L.; Jiang, J.; Gu, X. Preparation of defect-free DDR zeolite membranes by eliminating template with ozone at low temperature. *J. Membr. Sci.* **2017**, 539, 152-160.

[163] Cui, Y.; Kita, H.; Okamoto, K. Preparation and gas separation properties of zeolite T membrane. *Chem. Commun.* **2003**, 0, 2154-2155.

[164] van der Broeke, L.J.P.; Bakker, W.J.W.; Kapteijn, F.; Moulijn, J.A. Binary permeation through a silicalite-1 membrane. *AIChE J.* **1999,** 45, 976-985.

[165] Huang, A.; Wang, N.; Caro, J. Synthesis of multi-layer zeolite LTA membranes with enhanced gas separation performance by using 3-aminopropyltriethoxysilane as interlayer. *Micropor. Mesopor. Mater.* **2012**, 164, 294-301.

[166] Hong, M.; Li, S.; Falconer, J.L.; Noble, R.D. Hydrogen purification using a SAPO-34 membrane. *J. Membr. Sci.* **2008**, 307, 277-283.

[167] Guan, G.; Tanaka, T.; Kusakabe, K.; Sotowa, K.; Morooka, S. Characterization of $AlPO_4$-type molecular sieving membranes formed on a porous α-alumina tube. *J. Membr. Sci.* **2003**, 214, 191-198.

[168] Korelskiy, D.; Ye, P.; Fouladvand, S.; Karimi, S.; Sjoberg, E.; Hedlund, J. Efficient ceramic zeolite membranes for CO_2/H_2 separation. *J. Mater. Chem. A* **2015**, 3, 12500-12506.

[169] Hong, M.; Falconer, J.L.; Noble, R.D. Modification of zeolite membranes for H_2 separation by catalytic cracking of methyldiethoxysilane. *Ind. Eng. Chem. Res.* **2005**, 44, 4035-4041.

[170] Li. S.; Fan, C.Q. High-flux SAPO-34 membrane for CO_2/N_2 separation. *Ind. Eng. Chem. Res.* **2010**, 49, 4399-4404.

[171] Guo, H.; Zhu, G.; Li, H.; Zou, X.; Yin, X.; Yang, W.; Qiu, S.; Xu, R. Hierarchical growth of large-scale ordered zeolite silicalite-1 membranes with high permeability and selectivity for recycling CO_2. *Ange. Chem. Int. Ed.* **2006**, 45, 7053-7056.

[172] Shin, D.W.; Hyun, S.H.; Cho, C.H.; Han, M.H. Synthesis and CO_2/N_2 gas permeation characteristics of ZSM-5 zeolite membranes. *Micropor. Mesopor. Mater.* **2005**, 85, 313-323.

[173] Tiscornia, I.; Kumakiri, I.; Bredesen, R.; Tellez, C.; Coronas, J. Microporous titanosilicate ETS-10 membrane for high pressure CO_2 separation. *Sep. Purif. Technol.* **2010**, 73, 8-12.

[174] Kusakabe, K.; Kuroda, T.; Uchino, K.; Hasegawa, Y.; Morooka, S. Gas permeation properties of ion-exchanged faujasite-type zeolite membranes. *AIChE J.* **1999**, 45, 1220-1226.

[175] Weh, K.; Noack, M.; Sieber, I.; Caro, J. Permeation of single gases and gas mixtures through faujasite-type molecular sieve membranes. *Micropor. Mesopor. Mater.* **2002**. 54, 27-36.

[176] Wu, T.; Diaz, M.C.; Zheng, Y.; Zhou, R.; Funke, H.H.; Falconer, J.L.; Noble, R.D. Influence of propane on CO_2/CH_4 and N_2/CH_4 separations in CHA zeolite membranes. *J. Membr. Sci.* **2015**, 473, 201-209.

[177] Zong, Z.; Carreon, M.A. Thin SAPO-34 membranes synthesized in stainless steel autoclaves for N_2/CH_4 separation. *J. Membr. Sci.* **2017**, 524, 117-123.

[178] Zong, Z.; Elsaidi, S.K.; Thallapally, P.K.; Carreon, M.A. Highly permeable AlPO-18 membranes for N_2/CH_4 separation. *Ind. Eng. Chem. Res.* **2017**, 56, 4113-4118.

[179] Guan, G.; Kusakabe, K.; Morooka, S. Synthesis and permeation properties of ion-exchanged ETS-4 tubular membranes. *Micropor. Mesopor. Mater.* **2001**, 50, 109-120.

[180] Hong, Z.; Sun, F.; Chen, D.; Zhang, C.; Gu, X.; Xu, N. Improvement of hydrogen-separating performance by on-stream catalytic cracking of silane over hollow fiber MFI zeolite membrane. *Int. J. Hydrog. Energy* **2013**, 38, 8409-8414.

[181] Huang, A.; Caro, J. Highly oriented, neutral and cation-free $AlPO_4$ LTA: from a seed crystal monolayer to a molecular sieve membrane. *Chem. Commun.* **2011**, 47, 4201-4203.

[182] Kumakiri, I.; Qiu, L.; Tanaka, K.; Kita, H.; Saito, T.; Nishida, R. Application of MFI zeolite membrane prepared with fluoride ions to hydrogen/toluene separation. *J. Chem. Eng. J.* **2016**, 49, 753-755.

[183] Li, X.; Li, K.; Tao, S.; Ma, H.; Xu, R.; Wang, B.; Wang, P.; Tian, Z. Ionothermal synthesis of LTA-type aluminophosphate molecular sieve membranes with gas separation performance. *Micropor. Mesopor. Mater.* **2016**, 228, 45-53.

[184] Zhou, C.; Yuan, C.; Zhu, Y.; Caro, J.; Huang, A. Facile synthesis of zeolite FAU molecular sieve membranes on bio-adhesive polydopamine modified Al_2O_3 tubes. *J. Membr. Sci.* **2015**, 494, 174-181.

[185] Funke, H.H.; Chen, M.Z.; Prakash, A.N.; Falconer, J.L.; Noble, R.D. Separating molecules by size in SAPO-34 membranes. *J. Membr. Sci.* **2014**, 456, 185-191.

[186] Ye, P.; Grahn, M.; Korelskiy, D.; Hedlund J. Efficient separation of N_2 and He at low temperature using MFI membranes. *AIChE J.* **2016**, 62, 2833-2842.

[187] Feng, X.; Zong, Z.; Elsaidi, S.K.; Jasinski, J.B.; Krishna, R.; Thallapally, P.K.; Carreon, M.A. Kr/Xe Separation over a Chabazite Zeolite Membrane. *J. Am. Chem. Soc.* **2016**, 138, 9791-9794.

[188] Kwon, Y.H.; Kiang, C.; Benjamin, E.; Crawford, P.; Nair, S.; Bhave, R. Krypton-Xenon separation properties of SAPO-34 zeolite materials and membranes. *AIChE J.* **2017**, 63, 762-769.

[189] Kim, S.J.; Liu, Y.; Moore, J.S.; Dixit, R.S.; Pendergast Jr., J.G.; Sholl, D.; Jones, C.W.; Nair, S. Thin Hydrogen-Selective SAPO-34 Zeolite Membranes for Enhanced Conversion and Selectivity in Propane Dehydrogenation Membrane Reactors. *Chem. Mater.* **2016**, 28, 4397.

[190] van den Bergh, J.; Gucuyener, C.; Gascon, J.; Kapteijn, F. Isobutane dehydrogenation in a DD3R zeolite membrane reactor. *Chem. Eng. J.* **2011**, 166, 368.

[191] Illgen, D.; Schafer, R.; Noack M.; Kolsch, P.; Kuhnle, A.; Caro, Membrane supported catalytic dehydrogenation of iso-butane using an MFI zeolite membrane reactor. *J. Catal. Commun.* **2001**, 2, 11.

[192] Ciavarella, P.; Casanave, D.; Moueddeb, H.; Miachon, S.; Fiaty, K.; Dalmon, J.A. Isobutane dehydrogenation in a membrane reactor Influence of the operating conditions on the performance. *Catal. Today* **2001**, 67, 177.

[193] Tang, Z.; Kim, S.J.; Reddy, G.K.; Dong, J.; Smirniotis, P. Modified zeolite membrane reactor for high temperature water gas shift reaction. *J. Membr. Sci.* **2010**, 354, 114-122.

[194] Kim, S.J.; Xu, Z.; Reddy, G.K.; Smirniotis, P.; Dong, J. Effect of pressure on high-temperature water gas shift reaction in microporous zeolite membrane reactor. *Ind. Eng. Chem. Res.* **2012**, 51, 1364-1375.

[195] Zhang, Y.; Wu, Z.; Hong, Z.; Gu, X.; Xu, N. Hydrogen-selective zeolite membrane reactor for low temperature water gas shift reaction. *Chem. Eng. J.* **2012**, 197, 314-321.

[196] Choi, S.W.; Sholl, D.S.; Nair, S. Modeling and process simulation of hollow fiber membrane reactor systems for propane dehydrogenation. *AIChE J.* **2017**, 63, 4519-4531.

[197] Jafar, J.J.; Budd, P. M.; Hughes, R. Enhancement of esterification reaction yield using zeolite A vapour permeation membrane. *J. Membr. Sci.* **2002**, 199, 117.

[198] Peng, X.; Lei, Q.; Lv, G.; Zhang, X. Zeolite membrane-assisted preparation of high fatty esters. *Sep. Purif. Technol.* **2012**, 89, 84.

[199] Li, W.; Liu, W.; Xing, W.; Xu, N. Esterification of Acetic Acid and *n*-Propanol with Vapor Permeation Using NaA Zeolite Membrane. *Ind. Eng. Chem. Res.* **2013**, 52, 6336.

[200] Han, Y.; Lv. E.; Ma, L.; Lu, J.; Chen, K.; Ding, J. Coupling membrane pervaporation with a fixed-bed reactor for enhanced esterification of oleic acid with ethanol. *Energy Convers. Manage.* **2015**, 106, 1379.

[201] de la Iglesia, O.; Mallada, R.; Menendez, M.; Coronas, J. Continuous zeolite membrane reactor for esterification of ethanol and acetic acid. *Chem. Eng. J.* **2007**, 131, 35.

[202] Tanaka, K.; Yoshikawa, R.; Ying, C.; Kita, H.; Okamoto, K. Application of zeolite T membrane to vapor-permeation-aided esterification of lactic acid with ethanol. *Chem. Eng. Sci.* **2002**, 57, 1577.

[203] Zhang, W.; Na, S.; Li, W.; Xing, W. Kinetic Modeling of Pervaporation Aided

Esterification of Propionic Acid and Ethanol Using T-Type Zeolite Membrane. *Ind. Eng. Chem. Res.* **2015**, 54, 4940.

[204] Hasegawa, Y.; Abe, C.; Mizukami, F.; Kowata, Y.; Hanaoka, T. Application of a CHA-type zeolite membrane to the esterification of adipic acid with isopropyl alcohol using sulfuric acid catalyst. *J. Membr. Sci.* **2012**, 415, 368.

[205] van Dyk, L.; Lorenzen, L.; Miachon, S.; Dalmon, J.A. Xylene isomerization in an extractor type catalytic membrane reactor. *Catal. Today* **2005**, 104, 274.

[206] Zhang, C.; Hong, Z.; Gu, X.; Zhong, Z.; Jin, W.; Xu, N. Silicalite-1 Zeolite Membrane Reactor Packed with HZSM-5 Catalyst for meta-Xylene Isomerization. *Ind. Eng. Chem. Res.* **2009**, 48, 4293.

[207] Daramola, M.O.; Burger, A.J.; Giroir-Fendler, A.; Miachon, S.; Lorenzen, L. Extractor-type catalytic membrane reactor with nanocomposite MFI-alumina membrane tube as separation unit: Prospect for ultra-pure para-Xylene production from m-Xylene isomerization over Pt-HZSM-5 catalyst. *Appl. Catal. A* **2010**, 386, 109.

[208] Benali, M.; Aydin, B. Ethane/Ethylene and Propane/Propylene Separation in Hybrid Membrane Distillation Systems: Optimization and Economic Analysis. *Sep. Purif. Technol.* **2010**, 73, 377-390.

[209] Caballero, J.A.; Grossmann, I.E.; Keyvani, M.; Lenz, E.S. Design of Hybrid Distillation – Vapor Membrane Separation System. *Ind. Eng. Chem. Res.* **2009**, 48, 9151-9162.

[210] Sholl, D.S.; Lively, R.P. Seven Chemical Separations to Change the World. *Nature* **2016**, 532, 435-437.

[211] Wang, Y.; Ren, J.; Deng, M. Ultrathin Solid Polymer Electrolyte PEI/Pebax2533/$AgBF_4$ Composite Membrane for Propylene/Propane Separation. *Sep. Purif. Technol.* **2011**, 77, 46-52.

[212] Kanezashi, M.; Shazwani, W.N.; Yoshioka, T.; Tsuru, T. Separation of Propylene/Propane Mixtures by Bis(triethoxysilyl) methane (BTESM)-Derived Silica Membranes Fabricated at Different Calcination Temperatures. *J. Membr. Sci.* **2012**, 415-416, 478-485.

[213] Pan, Y.; Lai, Z. Sharp Separation of C2/C3 Hydrocarbon Mixtures by Zeolitic Imidazolate Framework-8 (ZIF-8) Membranes Synthesized in Aqueous Solutions, *Chem. Commun.* **2011**, 47, 10275-10277.

[214] Ma, X.; Kumar, P.; Mittal, N.; Khlyustova, A.; Daoutidis, P.; Mkhoyan, K.A.; Tsapatsis, M. Zeolitic Imidazolate Framework Membranes Made by Ligand-Induced Permsectivation. *Science* **2018**, 361, 1008-1011.

[215] Rashidi, F.; Leisen, J.; Kim, S.J.; Rownaghi, A.A.; Jones, C.W.; Nair, S. All-Nanoporous Hybrid Membranes: Redefining Upper Limits on Molecular Separation Properties. *Angew. Chem. Int. Ed.* **2019**, 58, 236-239.

[216] Li, K.; Olson, D.H.; Seidel, J.; Emge, T.J.; Gong, H.; Zeng, H.; Li, J. Zeolitic Imidazolate Frameworks for Kinetic Separation of Propane and Propene. *J. Am. Chem. Soc.* **2009**, 131, 10368-10369.

[217] Hayashi, J.; Mizuta, H.; Yamamoto, M.; Kusakabe, K.; Morooka, S.; Suh, S.-H. Separation of Ethane/Ethylene and Propane/Propylene Systems with a Carbonized BPDA-pp'ODA Polyimide Membrane. *Ind. Eng. Chem. Res.* **1996**, 35, 4176-4181.

[218] Motelica, A.; Bruinsma, O.S.L.; Kreiter, R.; Exter, M.; Vente, J.F. Membrane Retrofit Option for Paraffin/Olefin Separation – A Technoeconomic Evaluation. *Ind. Eng. Chem. Res.* **2012**, 51, 6977-6986.

[219] Zarca, R.; Ortiz, A.; Gorri, D.; Biegler, L.T.; Ortiz, I. Optimization of multistage olefin/paraffin membrane separation processes through rigorous modeling. *AIChE J.* **2019**, 65, e16588.

[220] Takane, K.; Suzuki, K.; Matsuda, K.; Yamaki, T.; Endo, A. Design and Economic Evaluation of the Separation Processes using Inorganic Membrane Technology. *MEMBRANE* **2019**, 44, 163-168.

[221] Yamaki, T.; Yoshimune, M.; Hara, N.; Negishi, H. Design and Economic Evaluation of the Separation Processes using Inorganic Membrane Technology. *J. Jpn. Petrol. Inst.* **2019**, 62, 80-86.

[222] Zarca, R.; Ortiz, A.; Gorri, D.; Biegler, L.T.; Ortiz, L. Optimized distillation coupled with state-of-the-art membranes for propylene purification. *J. Membr. Sci.* **2018**, *556*, 321-328.

[223] Amedi, H.R.; Aghajani, M. Economic Estimation of Various Membranes and Distillation for Propylene and Propane Separation. *Ind. Eng. Chem. Res.* **2018**, *57*, 4366-4376.

[224] Ploegmakers, J.; Jelsma, A.R.T.; van der Ham, A.G.J.; Nijmeijer, K. Economic Evaluation of Membrane Potential for Ethylene/Ethane Separation in a Retrofitted Hybrid Membrane-Distillation Plant Using Unisim Design. *Ind. Eng. Chem. Res.* **2013**, 52, 6524-6539.

[225] Nomura, M.; Yamaguchi, T.; Nakao, S. Ethanol/Water Transport through Silicalite Membranes. *J. Membr. Sci.* **1998**, 144, 161-171.

[226] Krishna, R. Describing the Diffusion of Guest Molecules inside Porous Structures. *J. Phys. Chem. C* **2009**, 113, 19756-19781.

[227] Xu, L.; Rungta, M.; Koros, W.J. Matrimid® Derived Carbon Molecular Sieve Hollow Fiber Membranes for Ethylene/Ethane Separation. *J. Membr. Sci.* **2011**, 380, 138-147.

[228] Liu, D.; Ma, X.; Xi, H.; Lin, Y.S. Gas Transport Properties and Propylene/Propane Separation Characteristics of ZIF-8 membranes. *J. Membr. Sci.* **2014**, 451, 85-93.

[229] Ryu, J.H.; Lee, H.; Kim, Y.J.; Kang, Y.S.; Kim, H.S. Facilitated Olefin Transport by Reversible Olefin Coordination to Silver Ions in a Dry Cellulose Acetate Membrane. *Chem. Eur.*

J. **2001**, 7, 1525-1529.

[230] Fallanza, M.; Ortiz, A.; Gorri, D.; Ortiz, I. Experimental Study of Separation of Propane/Propylene Mixtures by Supported Ionic Liquid Membranes Containing Ag^{+}-RTILs as Carrier. *Sep. Purif. Technol.* **2012**, 97, 83-89.

[231] Sawamura, K.; Furuhata, T.; Sekine, Y.; Kikuchi, E.; Subramanian, B.; Matsukata, M. Zeolite Membrane for Dehydration of Isopropylalcohol-Water Mixture by Vapor Permeation. *ACS Appl. Mater. Interfaces* **2015**, 7, 13728-13730.

[232] Sano, T.; Yanagishita, H.; Kiyozumi, Y; Kitamoto, D.; Mizukami, F. Separation of Ethanol/Water Mixture by Silicalite Membrane. *Chem. Lett.* **1992**, 21, 2413-2414.

[233] Sano, T.; Yanagishita, H.; Kiyozumi, Y; Mizukami, F.; Haraya, K. Separation of Ethanol/Water Mixture by Silicalite Membrane on Pervaporation. *J. Membr. Sci.* **1944**, 95, 221-228.

[234] Sawamura, K.; Shirai, T.; Ohsuna, T.; Hagino, T.; Takada, M.; Sekine, Y.; Kikuchi, E.; Matsukata, M. Separation Behavior of Steam from Hydrogen and Methanol through Mordenite Membrane. *J. Chem. Eng. J.* **2008**, 41, 870-877.

[235] Sawamura, K.; Shirai, T.; Takada, M.; Sekine, Y.; Kikuchi, E.; Matsukata, M. Selective permeation and separation of steam from water–methanol–hydrogen gas mixtures through mordenite membrane. *Catal. Today* **2008**, 132, 182-187.

Chapter 2 Preparation of Ag-exchanged X-type zeolite membrane and its olefin separation performance

2.1. Introduction

Propylene and ethylene are very important raw feedstocks for the petrochemical industry. Separation processes of propylene/propane and ethylene/ethane mixtures by conventional cryogenic distillation are energetically intensive because the heat for liquefaction is hard to recover and the relative volatility of olefin and paraffin is close to unity. Membrane separation is expected to be a novel energy-saving process for olefin purification from gaseous mixture [1,2]. During the last decades, propylene/propane and ethylene/ethane separation have been tried with various types of membranes on the basis of molecular sieving effect affinity-based separation, as mentioned in Chapter 1.

Polymeric membranes for olefin separation has often been reported. In particular, Ag-containing polymeric membranes were extensively studied and showed superior separation performance by strong interaction between membrane and olefin [3-5]. Ag cations in facilitated transport membranes play as carrier for the transport of olefins.

Whereas these Ag containing polymeric membranes such as liquid phase or solid phase facilitated transport membranes possess great advantage in olefin selectivity, these membranes have difficulty in stability owing to their poor chemical and mechanical strength. In particular, liquid phase-facilitated transport membranes showed high olefin selectivities only in the presence of water and readily lose their olefin selectivity by leakage of carrier.

On the other hand, inorganic membranes, namely, silica, carbon molecular sieving (CMS), metal-organic framework (MOF) and zeolite membranes are expected to have high chemical and pressure resistance, and thus have become recognized as candidates for olefin separation.

Olefin/paraffin separation based on molecular sieving effect by silica, CMS, and MOF have previously been reported [6-10]. In this case, olefins preferentially penetrate through the membranes because of their slightly small sizes.

Zeolites have been attracted attention as membrane material because of their unique molecular sieving and adsorption properties based on their wide variety of crystalline microporous structures. Preparation of FAU-type zeolite membrane and examination of its separation property for the water/2-propanol mixture have been reported [11].

Since zeolite can capture and hold cations as exchanged ion in their microchannels, I aimed at preparing Ag-exchanged X zeolite, a kind of FAU-type zeolite, membrane and investigating its olefin/paraffin separation properties in this chapter. This is the first report about Ag-exchanged zeolite membrane for olefin/paraffin separation in our best knowledge.

2.2. Experimental

Na-X membrane was synthesized by a secondary growth method on a porous α-alumina tubular support (outer diameter, 10 mm; inner diameter, 7 mm; length, 30 mm, Noritake Co. Ltd.). The mean pore diameter of support was ca. 150 nm. The support was seeded by means of a dip coating method with a USY seed slurry, which was prepared from commercially available FAU-type zeolite powder by following protocol. A given amount of FAU powder (Tosoh Co., HSZ 360HUA; SiO_2/Al_2O_3 = 14) was ground with a ball mill. The resultant powder was mixed with an appropriate amount of distilled water, and then the slurry was centrifuged at 4000 rpm for 10 min to remove large particles. After the centrifugation, milky suspension was skimmed and the solid content was adjusted at 2.5 g L^{-1} by adding distilled water. This suspension was used for seeding. The inside of tubular support was plugged with a PTFE rod. The support was dipped in the suspension for 1 min, withdrawn vertically at ca. 3 cm s^{-1}, and then dried at 343 K for 2 h. This process was run twice.

A seeded support was immersed in a synthesis solution for hydrothermal treatment having the molar composition of $80Na_2O:Al_2O_3:9SiO_2:5000H_2O$ [12]. The synthesis solution was prepared as follows. An aluminate solution was prepared by dissolving aluminum hydroxide (Wako Pure Chemical Industries Ltd.) and sodium hydroxide (Wako Pure Chemical Industries Ltd.) in distilled water. Besides, a silicate solution was made using water glass (Kishida Chemical Co. Ltd.) and distilled water. The aluminate solution and the silicate solution were mixed at 343 K for 5 min. After stirring, the solution was poured to a 50 mL polypropylene bottle, and then seeded supports was immersed into the solution. Hydrothermal treatment was carried out at 343 K for 24 h. After the hydrothermal treatment, Na-X membrane obtained was washed with distilled water and dried at 343 K overnight.

Li-X, K-X, Cs-X and Ag-X membranes were prepared by an ion exchange method for Na-X membranes. Nitrate salts were used in the ion exchange methods (i.e. $LiNO_3$ and $AgNO_3$ were used for preparation of Li-X and Ag-X membranes, respectively). Na-X membrane was immersed into the nitrate salt aqueous solution (0.1 – 100 mM) at ambient temperature and degassed under reduced pressure by using an aspirator. After degassing, the membranes was kept while stirring for 1 h. Ion exchanged X membranes were washed with distilled water and dried at 343 K overnight prior to use.

Permeation and separation properties of prepared X membranes were evaluated by using a gas separation apparatus schematically drawn in figure 2.1. Membrane was hold in a membrane module with cylindrical graphite O-rings. Propylene, propane, ethylene and ethane were fed to the outer surface of tubular membrane. The effective surface area of membrane was 6.28 cm^2. Permeated gas was swept by flowing helium. Membrane temperature was controlled in the

range of 303 – 433 K. Each partial pressure in the feed side was adjusted by changing the flow rates of olefin and paraffin in the binary systems. In the unary systems, the partial pressures of hydrocarbons were adjusted by changing the flow rates of dilution gas, helium. Both feed and permeate sides were kept at atmospheric pressure. The permeate gas was analyzed by gas chromatography equipped with the flame ionization detector for its composition. In addition, the flow rate of permeate was calculated by using internal standard gas, methane.

Flux, J, permeance, Π, and separation factor, $\alpha_{A/B}$, were defined as following equations.

$$J\,(\text{mol m}^{-2}\,\text{s}^{-1}) = u\,A^{-1} \quad (1)$$

$$\Pi\,(\text{mol m}^{-2}\,\text{s}^{-1}\,\text{Pa}^{-1}) = J\,\Delta p^{-1} \quad (2)$$

$$\alpha_{X/Y} = Y_A\,Y_B^{-1}\,X_A^{-1}\,X_B \quad (3)$$

where u is permeation flow rate (mol s^{-1}), A is the effective membrane area (m^2) and Δp is the partial pressure difference between the feed and permeate sides (Pa). X_A and X_B are molar fractions of components A and B in the feed. Y_A and Y_B are molar fractions of components A and B in permeate, respectively.

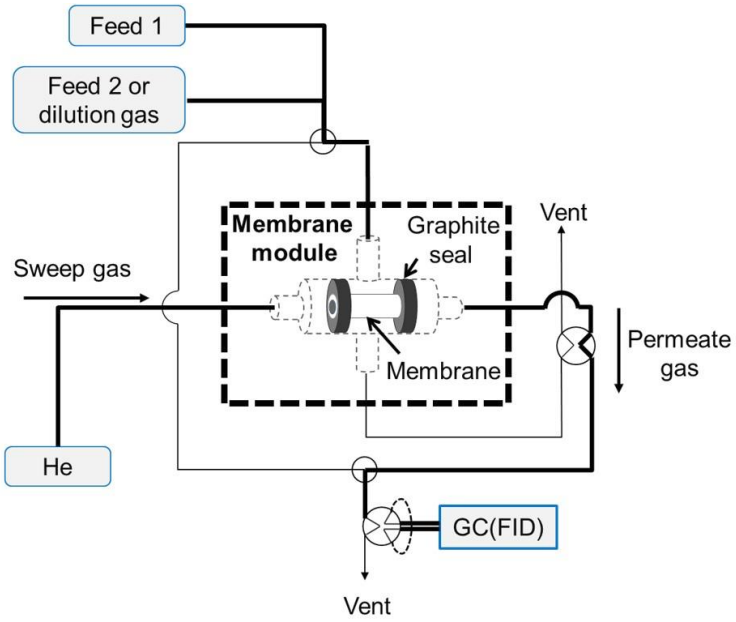

Figure 2.1. Schematic diagram of gas separation apparatus.

2.3. Results and discussion

2.3.1. Membrane synthesis and ion-exchange

Figure 2.2 shows the XRD patterns of Na-FAU and Ag-FAU membranes ion exchanged with the 10 mM $AgNO_3$ solution. The Na-FAU membrane exhibited the typical diffraction pattern of FAU-type zeolite. Si/Al ratio of this membrane were determined by using the

diffraction angle of (111) plane appearing at around $2\theta = 6^{o}$, as follows.

FAU-type zeolite is a cubic crystal and its lattice parameter, *a*, is correlated to the Al content in its framework [13,14]. The lattice parameter is able to be uniquely determined by the diffraction angle of (111) plane. The diffraction angle, 2θ, of (111) plane of Na-FAU membrane prepared was 6.095^{o}, and then the values of the lattice distance of (111) plane, *d*, and *a* were calculated to be 14.5 Å and 25.1, respectively. This value of lattice parameter corresponds to that FAU-type zeolite contains 89 Al atoms in a unit cell having 192 T-atoms, as previously reported [13]. Based on the Al content, I determined Si/Al ratio of this Na-FAU membrane as 1.15. FAU-type zeolites are classified into X-type zeolite having Si/Al of 1.0-1.5 and Y-type having the ratio of 1.5-3.0. It is noteworthy that the prepared membrane was X-type zeolite membrane with high aluminum content.

The XRD pattern of membrane was changed by ion exchange from Na^{+} to Ag^{+}. The peaks coincided with the data reported in the JCPDS standard card (No. 38-233) of Ag-X zeolite. For example, a typical strong reflection peak of (400) around $2\theta = 14^{o}$ was appeared. This result showed that its crystal structure was kept after the ion exchange to Ag-X membrane. In addition, no obvious reflection peaks other than FAU-type zeolite were observed.

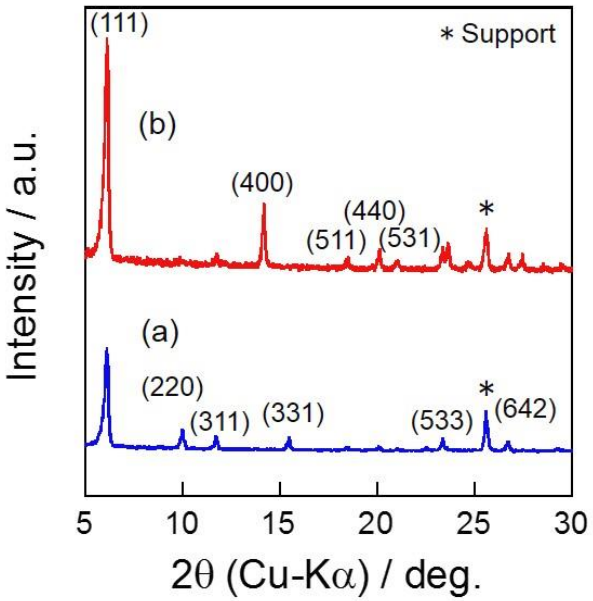

Figure 2.2. XRD patterns of (a) Na-FAU and (b) Ag-FAU membrane ion exchanged with 10 mM $AgNO_3$ solution.

Figure 2.3 shows typical FE-SEM images of Na-X and Ag-X membranes. A crystal layer uniformly covered the surface of support with the thickness of ca. 3.5 μm in both Na-X and Ag-X membranes. Morphological change after the ion exchange was hardly observed in these

FE-SEM views.

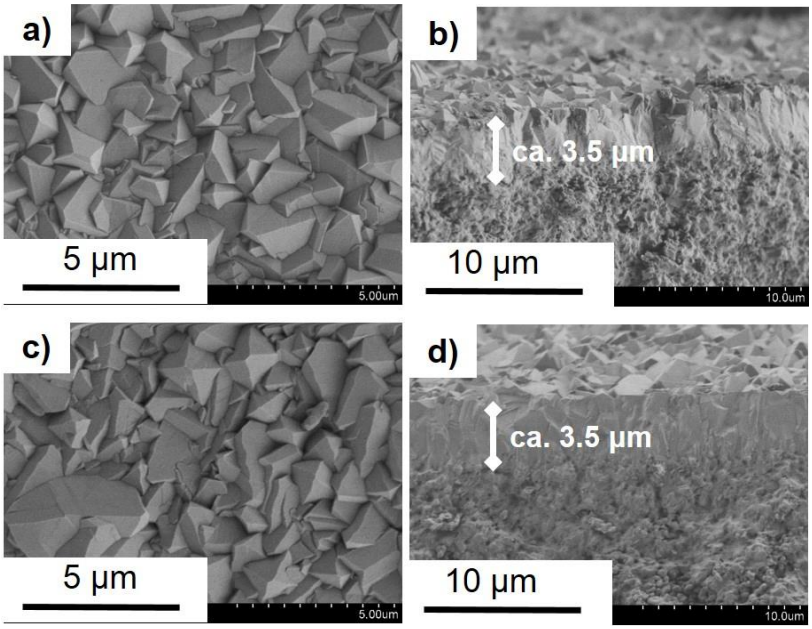

Figure 2.3. Typical FE-SEM images of (a, b) Na-X and (c, d) Ag-X membrane ion exchanged with 10 mM $AgNO_3$ solution.

Ag cation concentration in X membrane was able to be controlled by changing the concentration of $AgNO_3$ aqueous solution used for ion exchange. The ion exchange ratio of Na to Ag cations was calculated using the membrane weights of before and after the ion exchange. The chemical formula for unit cell of Na-X and Ag-X having Si/Al ratio of 1.15 were shown as $Na_{89.3}Al_{89.3}Si_{102.7}O_{384}\cdot_{89.3}H_2O$ and $Ag_{89.3}Al_{89.3}Si_{102.7}O_{384}\cdot_{89.3}H_2O$, respectively. Here, it was assumed that number of adsorbed water molecules was the same as that of cation. Therefore, the weights of these unit cell were calculated as 2.51×10^{-20} and 3.77×10^{-20} g u.c.$^{-1}$. Thus, the ion exchange ratio, *R*, of Ag-X zeolite with Si/Al ratio of 1.15 is able to be calculated by using the membrane weight before and after the ion exchange, as the following equation (4).

$$R(\%) = \left(\frac{W_{ater}}{W_{before}} - 1\right) \div \left(\frac{3.77\times10^{-2}}{2.51\times10^{-2}} - 1\right) \times 100 \quad (4)$$

Where W_{after} and W_{before} represent the membrane weights before and after the ion exchange. Table 2.1 lists the ion exchange ratios of X membranes prepared by using different concentrations of $AgNO_3$ aqueous solution. The exchange ratio of membranes obtained by using 0.10, 1.0, 10 and 100 mM solutions were 20.0, 51.9, 96.9 and 104%, respectively. The exchange ratio increased with increasing concentration of $AgNO_3$ solution and reached about 100% at 10

mM.

Further increase of $AgNO_3$ concentration up to 100 mM gave similar results, that is, full exchange of Na with Ag cations without degradation of crystalline structure. In addition, the reflection peaks corresponding to compounds other than X zeolite were hardly observed in all XRD results, suggesting that Ag metal or oxides were hardly formed even after the ion exchange with 100 mM solution.

Table 2.1. Ag ion exchange ratio

$AgNO_3$ Concentration / mM	Weight increase ratio / g g^{-1}	Exchange ratio / %
0.10	1.10	20.0
1.0	1.26	51.9
10	1.52	96.9
100	1.57	104

2.3.2. Effect of ion-exchange on permeation performance

Figure 2.4 shows the results of propylene/propane separation tests through X membranes with different ion exchange ratios. An equimolar mixture gas of propylene/propane was fed to the membranes at 353 K. The exchange ratio of 0 means Na-X membrane without ion exchange. The propylene and propane permeances through Na-X membrane were 3.68×10^{-7} and 8.35×10^{-8} mol m^{-2} s^{-1} Pa^{-1}, respectively. Whereas both the propylene and propane permeances decreased with ion exchange, particularly the decrease of propane permeance was more evident than that of propylene. As a result, the separation factor was improved accompanied with Ag cation exchange.

For the purposes of comparison, Alkali metal exchanged X-type membranes (Li-X, K-X and Cs-X) were prepared by ion exchange for Na-X membranes. 100 mM of $LiNO_3$ and KNO_3 aqueous solutions were used for preparing Li-X and K-X membranes, respectively. 10 mM of $CsNO_3$ aqueous solution was used for preparing Cs-X membrane. Procedure of ion exchange was the same as in the case of Ag-X membrane. Figure 2.5 shows propylene/propane (50:50) separation properties of alkali metal exchanged X membranes at 353 K. The results with Na-X membrane was also plotted on the figure 2.5 for comparison.

The separation factors of fully exchanged Ag-X membranes prepared with 10 and 100 mM solutions attained above 50 with the propylene permeances of about 4×10^{-8} mol m^{-2} s^{-1} Pa^{-1}.

Ag-X exhibited superior propylene selectivity compared with X membranes exchanged with alkali metal ions, Li-X, K-X and Cs-X. In the following section, I will discuss the reason of the appearance of high propylene selectivity with Ag-X membrane.

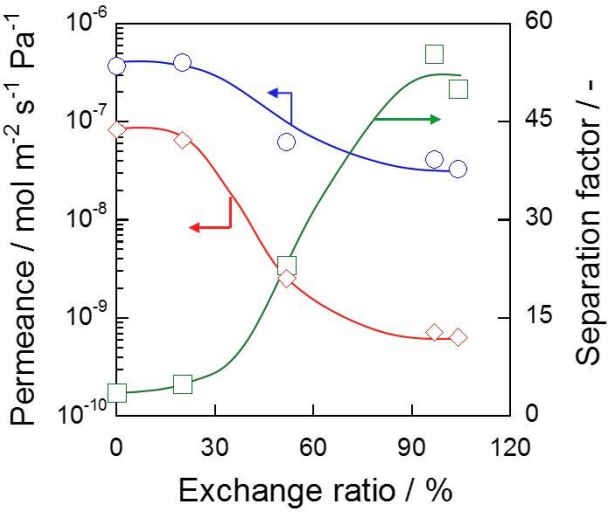

Figure 2.4. Propylene/propane (50:50) separation properties of X membranes at 353 K with different Ag ion exchange ratios. ○, Propylene; ◇, propane; □, separation factor.

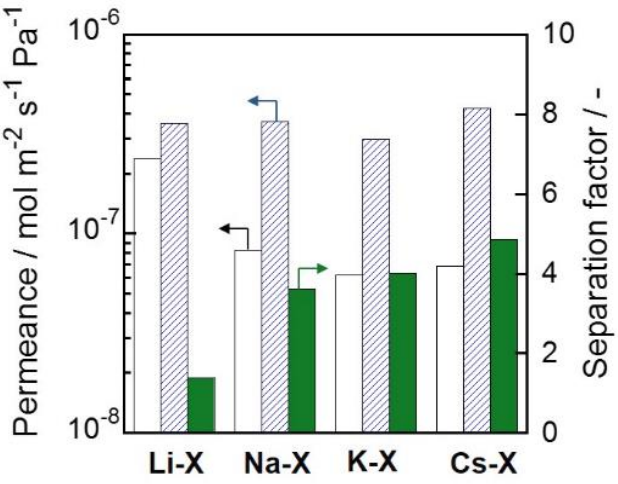

Figure 2.5. Propylene/propane (50:50) separation properties of alkali metal exchanged X membranes at 353 K. Open, shaded and solid bars show propane permeance, propylene permeance and separation factor, respectively.

2.3.3. Comparison of the permselectivity of Ag-X membrane in unary and binary systems

Temperature dependencies of propylene and propane permeances through Ag-X membrane in unary and binary systems were investigated to shed light on its separation mechanism. Ag-X

membrane exchanged by using 10 mM $AgNO_3$ solution was employed in the permeation tests. In the unary systems, the partial pressures of propylene and propane were adjusted at 50 kPa with dilution gas, helium. In the binary system, a propylene and propane equimolar mixture was fed to the membrane.

Figure 2.6 shows the results of the permeation tests. As shown in figure 2.6(a), in the unary systems the propylene permeance increased from 1.11×10^{-8} to 1.02×10^{-7} mol m^{-2} s^{-1} Pa^{-1} with increasing temperature in the range of 313-393 K, and the propane permeance also increased from 1.01×10^{-7} to 3.93×10^{-7} mol m^{-2} s^{-1} Pa^{-1}. Ideal selectivities for propylene were 0.26 – 0.11. In other words, the propane permeance was 4 – 10 times larger than that of propylene in these unary systems.

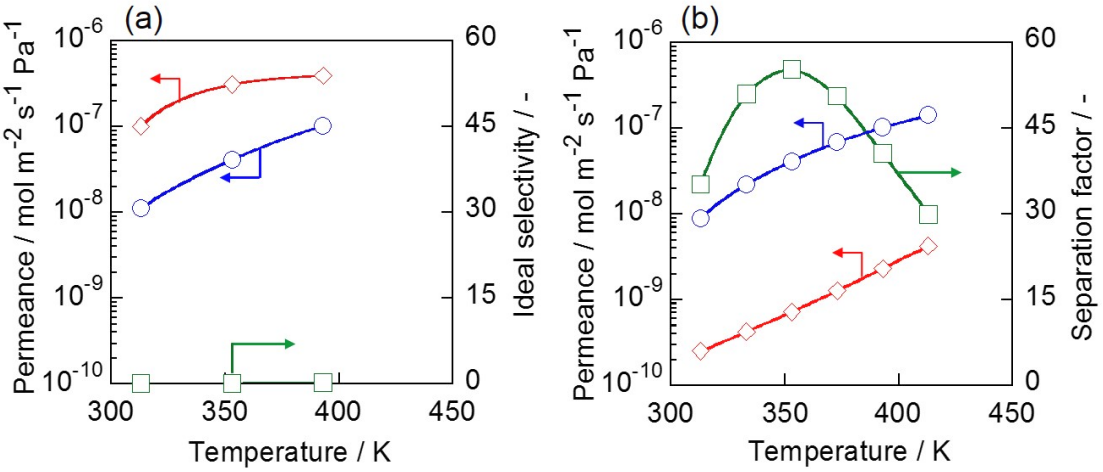

Figure 2.6. Temperature dependencies of propylene/propane (50:50) permeances through Ag-X membrane ion exchanged with 10 mM $AgNO_3$ solution in (a) unary and (b) binary systems, respectively. ○, Propylene; ◇, propane; □, separation factor.

I, however, observed remarkably different permeation behaviors in the binary system, as seen in figure 2.6(b). The propane permeation was strongly inhibited although the propylene permeance was almost the same as that obtained in the unary system. As a result, the propane permeance was a magnitude smaller than that of propylene. In particular, the inhibition of propane permeation with propylene was more effective at lower temperatures. For example, the propane permeance in the binary system was reduced by up to 99.7% compared with that in the unary system at 313 K.

Although propylene permeance gradually increased with increasing temperature up to 413 K, propane permeance steeply rose above 353 K in binary systems. Hence, the separation factor reached a maximum at a given temperature. These results clearly indicated that

propylene/propane separation through Ag-X membrane was not governed by molecular sieving. Coexisting propylene plays an important role for the inhibition of propane permeation.

It is known that Ag cation strongly interacts with olefin's π-electron [15]. The π orbital of olefin overlaps with the vacant 5s orbital of Ag cation and the 4d orbital of Ag cation overlaps with the vacant π* orbital of olefin. I consider that Ag cation occluded in the micropore of FAU-type zeolite predominantly adsorbs propylene. In contrast, propane does not strongly interact with Ag cation and easily diffused in micropore of Ag-X membrane. Thus, the propylene permeance was smaller than that of propane in the unary systems.

On the other hand, in the binary system, such interaction between olefin and Ag cation favors preferential adsorption of propylene against propane in the micropore of Ag-X membrane, possibly leading to blockage of propane permeation. Meanwhile, permeation behavior of propylene were hardly influenced by the propane because the interaction between propane and Ag cation was substantially weak. The propane permeance tended to be strongly hindered at lower temperature in the binary system, as can be noticed by the comparison of figures 2.5(a) and 2.5(b). This behavior would be able to be explained by the adsorbed amount of propylene was larger at lower temperatures, resulting in the stronger inhibition of propane adsorption and permeation.

2.3.4. Effect of propylene concentration in the feed stream on the permselecitivties

Figure 2.7 shows that the effect of propylene concentration in the feed stream on the permeation and separation properties. The mole fraction of propylene was changed from 0.1 to 0.9 and balanced with propane. The permeation test was carried out at 313 K. The propylene permeances through Na-X membrane at the propylene mole fraction of 0.1, 0.5 and 0.9 were 2.29×10^{-7}, 1.05×10^{-7} and 8.21×10^{-8} mol m^{-2} s^{-1} Pa^{-1}, respectively. The propane permeances under the same conditions were 3.21×10^{-8}, 1.98×10^{-8} and 1.48×10^{-8} mol m^{-2} s^{-1} Pa^{-1}, respectively. Both propylene and propane permeances decreased with increasing partial pressure of propylene. As a result, the separation factor slightly decreased from 7.14 to 5.55.

In the case of Ag-X membrane, the propylene permeance and separation factor were markedly influenced by the propylene concentration. The propylene permeance monotonously decreased from 7.74×10^{-8} to 1.50×10^{-8} mol m^{-2} s^{-1} Pa^{-1} with increasing propylene partial pressure. In contrast, the propane permeance was almost constant despite the change of propylene concentration. Consequently, Ag-X membrane showed superior selectivity at lower propylene concentrations. The separation factor at the propylene mole fraction of 0.1 attained 94.2.

I consider the reason of difference in propylene concentration dependency between Na-X

and Ag-X membranes as follows. The amount of propylene adsorbed on Ag-X membrane would be almost saturated even at lower partial pressures because of strong interaction between propylene and Ag cation. In other words, the amount of propylene adsorbed even at the partial pressure of propylene of 10 kPa was almost sufficient to inhibit propane permeation. Therefore, the propane permeance was almost constant at the partial pressure of propylene >10 kPa. For the same reason, the propylene permeance considerably decreased with increasing partial pressure of propylene. In contrast, the amount of propylene adsorbed on Na-X membrane could increase with increasing partial pressure, leading to the decrease of propane permeance.

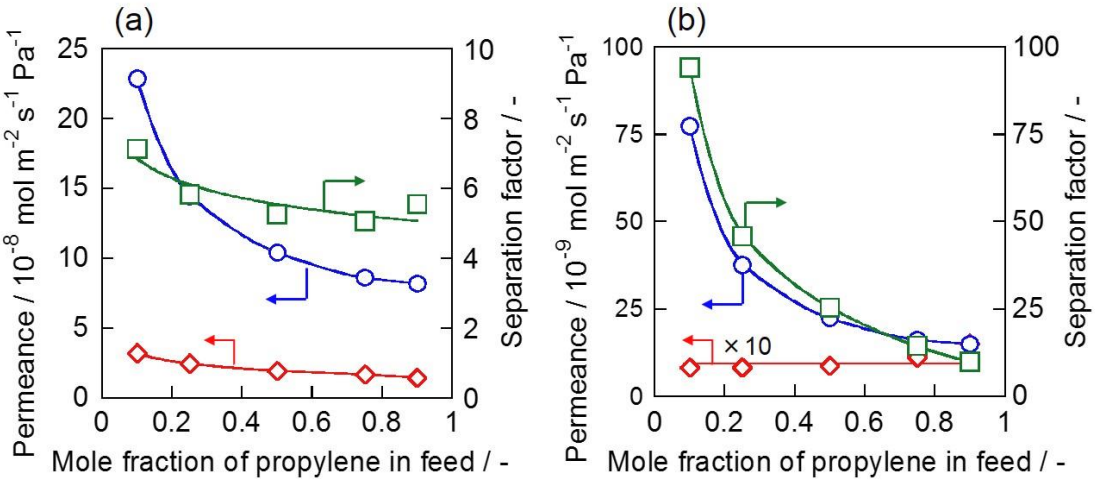

Figure 2.7. Effect of propylene concentration in feed stream on permeation property through (a) Na-X and (b) Ag-X membrane ion exchanged with 10 mM $AgNO_3$ solution at 313 K. ○, Propylene; ◇, propane; □, separation factor.

2.3.5. Durability of Ag-X membrane

Figure 2.8 shows the time course of permeance and separation factor through Ag-X membrane in the propylene/propane binary system. At first, the permeation test was performed at 313 K. After that, the temperature increased every 20 K up to 413 K. Finally temperature decreased to 313 K, and then checked the permeance and separation factor again.

While in the early stage both the propylene and propane permeances changed at every temperature until they stabilized, the permeance and separation factor kept constant with time course once attained stable values. It is notable that the permeances and separation factors at 313 K of first and second measurements were almost the same. Ag-X membrane exhibited stable performance in the temperature range of 313-413 K.

Here, I estimate the long-term durability of Ag-X membrane. Figure 2.9 shows the change of permeances and separation factor for propylene/propane(=50/50 mol%) separation at 353 K

for 10000 h. Propylene permeance is almost the constant during the durability test. In contrast propane permeance slightly increased in the early stage, over the course of initial 2000 hours. After that, propane permeance was constant up to 10000 h. The propylene permeance and separation factor were 5.29×10^{-8} mol m^{-2} s^{-1} Pa^{-1} and 31.7 after the 10000-h permeation test.

As described in Chapter 1, I decided the target performance of Ag-X membrane as the permeance of 3×10^{-8} mol m^{-2} s^{-1} Pa^{-1}, the separation factor of 30, and the life-time of 2 years from the results of simulation studies for propylene/propane separation [16-20]. I conclude that this Ag-X membrane successfully satisfies the required permeance and separation factor, and would satisfy the life-time.

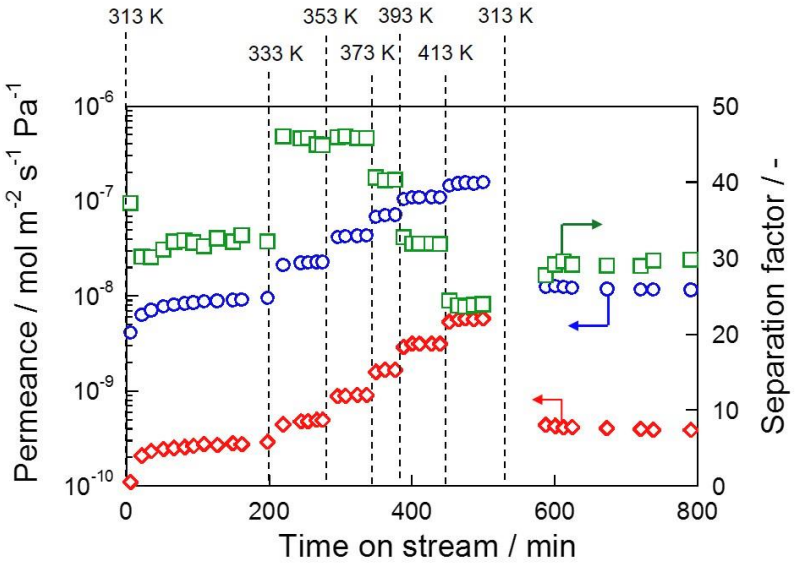

Figure 2.8. Stability of Ag-X membrane ion exchanged with 10 mM $AgNO_3$ solution for propylene/propane (50:50) separation. ○, Propylene; ◇, propane; □, separation factor.

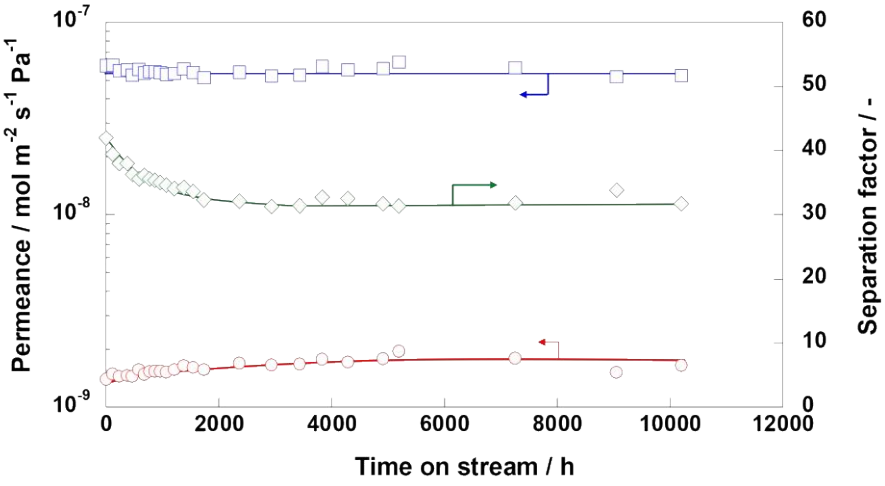

Figure 2.9. Long-term durability of Ag-X membrane for propylene/propane (50:50) separation. □, Propylene; ○, propane; ◇, separation factor.

The long-term durability of Ag-X membrane under argon atmosphere was also evaluated as shown in figure 2.10(a). Ag-X membrane was stored under argon and its separation performance for propylene/propane equimolar mixture was evaluated periodically. As opposed to the case in propylene/propane mixture, propane permeance increased linearly, resulting in that the separation factor became ca. 1 after a lapse of 1000 h. In addition, the same trend was observed in the durability test under propane atmosphere (shown in figure 2.10 (b)). It is well known that Ag cations in zeolite easily migrate and grow to nano-perticles [21]. These results indicates that Ag cations in Ag-X membrane are preserved from sintering by strongly adsorbed propylene. However, the further detail of deterioration mechanism of Ag-X membrane is the subject of future investigation.

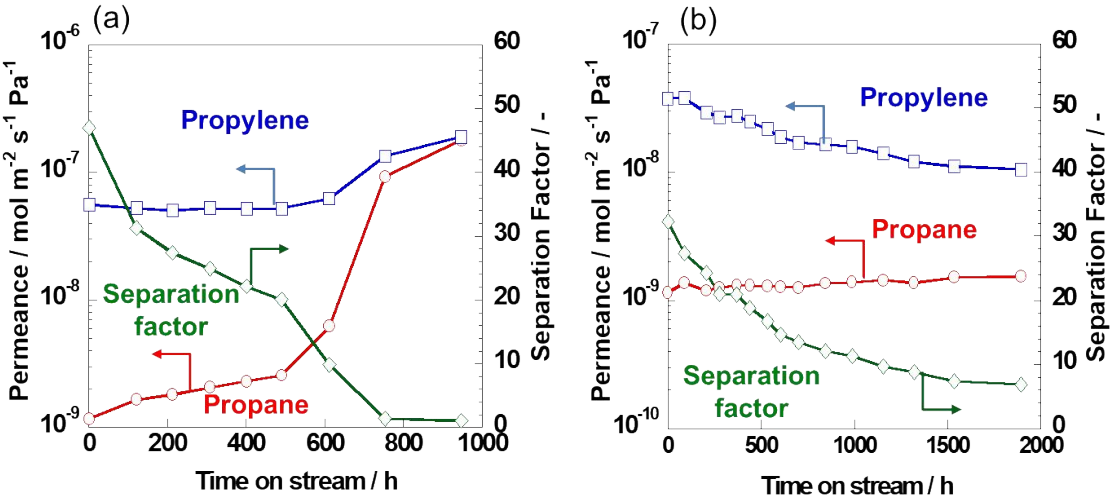

Figure 2.10. The change of separation performance for propylene/propane (50:50) mixture of Ag-X membrane stored under (a) argon and (b) propane atmosphere at 353 K. □, Propylene; ○, propane; ◇, separation factor.

2.3.6. Permselectivity of Ag-X membrane for ethylene/ethane and benzene/cyclohexane separation

Figure 2.11 shows the ethylene and ethane permeation behaviors through Ag-X membrane. The permeation behaviors of ethylene and ethane were very similar to those of propylene and propane shown in figure 2.6, respectively. Ethylene preferentially permeated through Ag-X membrane in the binary system, although the ethane permeance was larger than that of ethylene

in the unary systems. As a result, the ethylene selectivity reached 15.9 with its permeance of 9.04×10^{-8} mol m^{-2} s^{-1} Pa^{-1} at 303 K. The ethane permeance was reduced by up to 93.0% in the binary system at 303 K.

These permeance and selectivity are quite high compared with other membranes previously reported in which referred following section. The decrease of ethane permeance was not obvious compared with the results of propylene/propane binary system. The reasons of smaller selectivity observed for the ethylene/ethane mixture would include the difference of molecular sizes in two systems and adsorption properties of olefins. It seems to be more difficult to inhibit ethane permeation with adsorbed ethylene because ethylene and ethane were smaller than propylene and propane. In addition, ethylene adsorption would be rather weak because of physical factors such as its smaller relative pressure and its small sectional area of molecule in comparison with propylene.

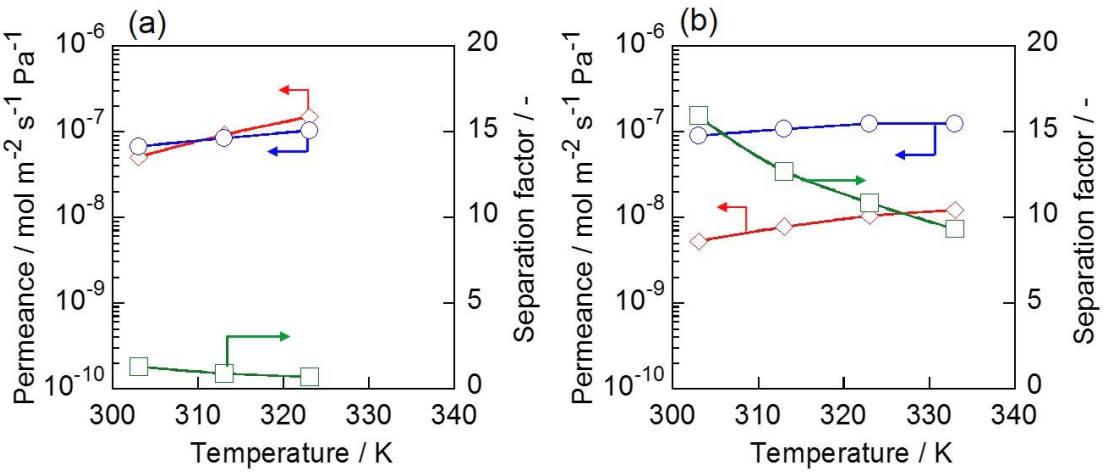

Figure 2.11. Temperature dependencies of ethylene/ethane (50:50) permeances through Ag-X membrane ion exchanged with 10 mM $AgNO_3$ solution in (a) unary and (b) binary systems, respectively. ○, Ethylene; ◇, Ethane; □, separation factor.

Figure 2.12 shows the separation performances of Na-X and Ag-X membranes for benzene/cyclohexane(=50/50 mol%) mixture. As in the cases of propylene/propane and ethylene/ethane, separation performance increased by an ion-exchange. This result suggested that the Ag-X membrane is useful for not only olefin/paraffin but also aroma/naphthene separations.

2.3.7. Positioning of Ag-X membrane in inorganic membranes

I discuss olefin/paraffin separation properties of Ag-X membrane prepared in this study with

those of other types of membranes previously reported, such as CMS, ZIF-8, silica, mixed matrix, alumina, and polymeric membranes. Ag-X membrane developed in this study successfully separated C_2 and C_3 olefin/paraffin mixtures with relatively high permeances and high separation factors. Ag-X membrane exhibited the maximum propylene selectivity of 94.2 with the permeance of 7.74×10^{-8} mol m^{-2} s^{-1} Pa^{-1} at 313 K. It also exhibited the maximum ethylene selectivity of 15.9 with the permeance of 9.04×10^{-8} mol m^{-2} s^{-1} Pa^{-1} at 303 K.

Figure 2.13 compares the permeances and separation factors of various types of membranes in propylene/propane [4,7-10,22-28] and ethylene/ethane [3,6,29-32] separation. In figure 2.13, I only plotted the results in binary systems and did not adapt the ideal selectivities and permeances in unary systems. Ag-X membrane exhibited superior permeance and selectivity for both propylene/propane and ethylene/ethane separation compared with other inorganic membranes previously reported. Although some facilitated transport polymeric membranes using ionic liquid or $AgNO_3$ solution as carrier overwhelm Ag-X membrane, these membrane have difficulty in stability as described in introduction. These Robeson plots suggested that Ag-X is one of the most feasible membrane materials having high permeances and selectivities for olefin/paraffin separation.

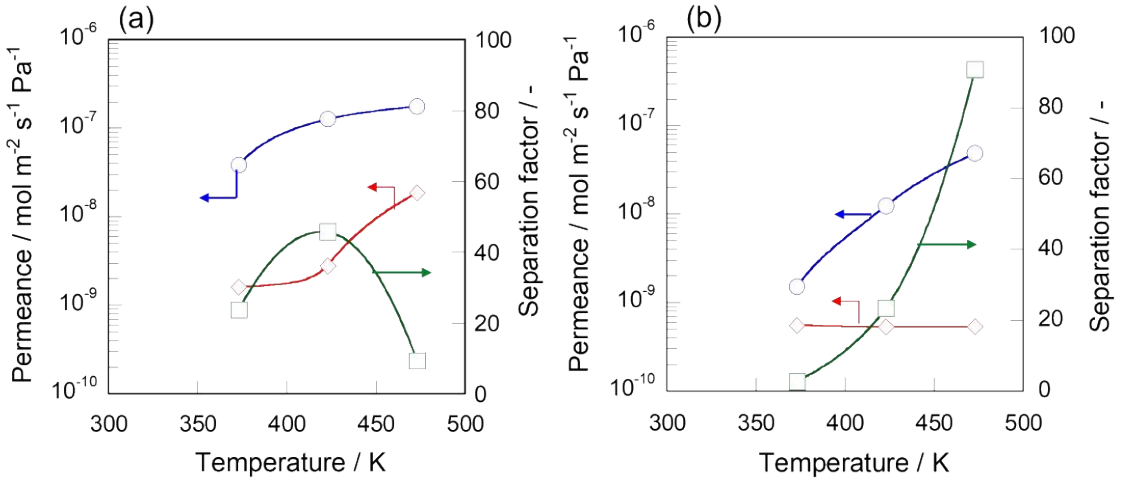

Figure 2.12. Temperature dependencies of benzene/cyclohexane (50:50) permeances through (a) Na-X, (b) Ag-X membrane in binary systems, respectively. ○, Benzene; ◇, Cyclohexane; □, separation factor.

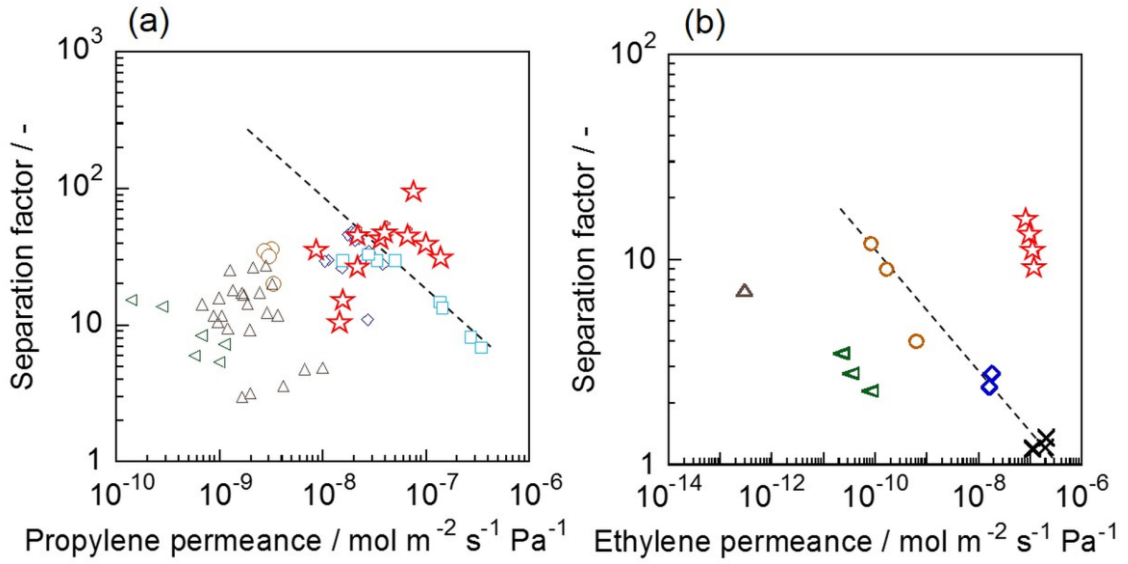

Figure 2.13. Robeson plots of (a) propylene/propane and (b) ethylene/ethane separation. ○, CMS; ◇, ZIF-8; □, silica; △, mixed matrix; ◁, polymer; X, alumina; ☆, Ag-X (this study).

2.4. Conclusions

Tubular Ag-X membrane was prepared by an ion exchange method for Na-X membrane using $AgNO_3$ solution. I performed propylene/propane and ethylene/ethane separation by Ag-exchanged X-type membrane.

Ion exchange from Na-X to Ag-X improved propylene selectivity from 3.63 to 55.4 for propylene/propane separation at 353 K in the binary system. Selective permeation of olefin was probably based not on molecular sieving effect but on strong interaction between olefin and Ag cation. I consider that preferentially adsorbed olefin inhibited paraffin adsorption, and then paraffin permeance was strongly hindered by adsorbed olefin.

Ag-X membrane exhibited superior and stable performance for propylene/propane separation in the temperature range of 313-413 K. In addition, the propylene permeance and separation factor after the 10000-h permeation test. From the result of durability test successfully satisfies the required performance which is assumed in simulation studies for propylene/propane separation described in Chapter 1. Ag-X would be one of the most promising membrane materials for olefin/paraffin separation.

References

[1] Benali, M.; Aydin, B. Ethane/Ethylene and Propane/Propylene Separation in Hybrid Membrane Distillation Systems: Optimization and Economic Analysis. *Sep. Purif. Technol.*

2010, 73, 377-390.

[2] Caballero, J.A.; Grossmann, I.E.; Keyvani, M.; Lenz, E.S. Design of Hybrid Distillation – Vapor Membrane Separation System. *Ind. Eng. Chem. Res.* **2009**, 48, 9151-9162.

[3] Ryu, J.H.; Lee, H.; Kim, Y.J.; Kang, Y.S.; Kim, H.S. Facilitated Olefin Transport by Reversible Olefin Coordination to Silver Ions in a Dry Cellulose Acetate Membrane. *Chem. Eur. J.* **2001**, 7, 1525-1529.

[4] Wang, Y.; Ren, J.; Deng, M. Ultrathin Solid Polymer Electrolyte PEI/Pebax2533/$AgBF_4$ Composite Membrane for Propylene/Propane Separation. *Sep. Purif. Technol.* **2011**, 77, 46-52.

[5] Fallanza, M.; Ortiz, A.; Gorri, D.; Ortiz, I. Experimental Study of Separation of Propane/Propylene Mixtures by Supported Ionic Liquid Membranes Containing Ag^+-RTILs as Carrier. *Sep. Purif. Technol.* **2012**, 97, 83-89.

[6] Xu, L.; Rungta, M.; Koros, W.J. Matrimid® Derived Carbon Molecular Sieve Hollow Fiber Membranes for Ethylene/Ethane Separation. *J. Membr. Sci.* **2011**, 380, 138-147.

[7] Hayashi, J.; Mizuta, H.; Yamamoto, M.; Kusakabe, K.; Morooka, S.; Suh, S.-H. Separation of Ethane/Ethylene and Propane/Propylene Systems with a Carbonized BPDA-pp'ODA Polyimide Membrane. *Ind. Eng. Chem. Res.* **1996**, 35, 4176-4181.

[8] Kanezashi, M.; Shazwani, W.N.; Yoshioka, T.; Tsuru, T. Separation of Propylene/Propane Mixtures by Bis(triethoxysilyl) methane (BTESM)-Derived Silica Membranes Fabricated at Different Calcination Temperatures. *J. Membr. Sci.* **2012**, 415-416, 478-485.

[9] Liu, D.; Ma, X.; Xi, H.; Lin, Y.S. Gas Transport Properties and Propylene/Propane Separation Characteristics of ZIF-8 membranes. *J. Membr. Sci.* **2014**, 451, 85-93.

[10] Pan, Y.; Li, T.; Lestari, G.; Lai, Z. Effective Separation of Propylene/Propane Binary Mixtures by ZIF-8 Membranes. *J. Membr. Sci.* **2012**, 390-391, 93-98.

[11] Sawamura, K.; Furuhata, T.; Sekine, Y.; Kikuchi, E.; Subramanian, B.; Matsukata, M. Zeolite Membrane for Dehydration of Isopropylalcohol-Water Mixture by Vapor Permeation. *ACS Appl. Mater. Interfaces* **2015**, 7, 13728-13730.

[12] Kumakiri, I.; Yamaguchi, T.; Nakao, S. Preparation of Zeolite A and Faujasite Membranes From Clear Solution. *Ind. Eng. Chem. Res.* **1999**, 38, 4682-4688.

[13] Hiraiwa, M.Y.; Hongo, T.; Hayashi, H.; Takaishi, T.; Nakata, S.; Yamazaki, A. Phase Transition and Thermal Behavior Change of Low Silica X Zeolite at [Al] = 90. *Chem. Lett.* **2010**, 39, 1242-1244.

[14] Takaishi, T. Ordered Distribution of Al Atoms in the Framework of Faujasite Type and a Chiral Y. *J. Phys. Chem.* **1995**, 99, 10982-10987.

[15] Carter, J.L.; Yates, D.J.C.; Lucchesi, P.J.; Elliott, J.J.; Kevorkian, V. The Adsorption of Ethylene on a Series of Near-Faujasite Zeolites Studied by Infrared Spectroscopy and

Calorimetry. *J. Phys. Chem.* **1966**, 70, 1126-1136.

[16] Zarca, R.; Ortiz, A.; Gorri, D.; Biegler, L.T.; Ortiz, I. Optimization of multistage olefin/paraffin membrane separation processes through rigorous modeling. *AIChE J.* **2019**, 65, e16588.

[17] Takane, K.; Suzuki, K.; Matsuda, K.; Yamaki, T.; Endo, A. Design and Economic Evaluation of the Separation Processes using Inorganic Membrane Technology. *MEMBRANE* **2019**, 44, 163-168.

[18] Yamaki, T.; Yoshimune, M.; Hara, N.; Negishi, H. Design and Economic Evaluation of the Separation Processes using Inorganic Membrane Technology. *J. Jpn. Petrol. Inst.* **2019**, 62, 80-86.

[19] Zarca, R.; Ortiz, A.; Gorri, D.; Biegler, L.T.; Ortiz, L. Optimized distillation coupled with state-of-the-art membranes for propylene purification. *J. Membr. Sci.* **2018**, 556, 321-328.

[20] Amedi, H.R.; Aghajani, M. Economic Estimation of Various Membranes and Distillation for Propylene and Propane Separation. *Ind. Eng. Chem. Res.* **2018**, 57, 4366-4376.

[21] Monpezat, A.; Topin, S.; Thomas, V.; Pagis, C.; Aouine, M.; Burel, L.; Cardenas, L.; Tuel, A.; Malchere, A.; Epicier, T.; Farrusseng, D.; Roiban, L.; Migration and Growth of Silver Nanoparticles in Zeolite Socony Mobil 5 (ZSM-5) Observed by Environmental Electron Microscopy: Implications for Heterogeneous Catalysis. *ACS Appl. Nano Mater.* **2019**, 2, 6452-6461.

[22] Liu, D.; Ma, X.; Xi, H.; Lin, Y.S. Gas Transport Properties and Propylene/Propane Separation Characteristics of ZIF-8 Membranes. *J. Membr. Sci.* **2014**, 451, 85-93.

[23] Kwon, H.T.; Jeong, H.-K. In situ Synthesis of Thin Zeolitic-Imidazolate Framework ZIF-8 Membranes Exhibiting Exceptionally High Propylene/Propane Separation. *J. Am. Chem. Soc.* **2013**, 135, 10763-10768.

[24] Xu, L.; Rungta, M.; Brayden, M.K.; Martinez, M.V.; Stears, B.A.; Barbay, G.A.; Koros, W.J. Olefins-Selective Asymmetric Carbon Molecular Sieve Hollow Fiber Membranes for Hybrid Membrane-Distillation Processes for Olefin/Paraffin Separations. *J. Membr. Sci.* **2012**, 423-424, 314-323.

[25] Das, M.; Koros, W.J.; Performance of 6FDA-6FpDA Polyimide for Propylene/Propane Separations. *J. Membr. Sci.* **2010**, 365, 399-408.

[26] Ma, X.; Lin, B.K.; Wei, X.; Kniep, J.; Lin, Y.S. Gamma-Alumina Supported Carbon Molecular Sieve Membrane for Propylene/Propane Separation. *Ind. Eng. Chem. Res.* **2013**, 52, 4297-4305.

[27] Sun, H.; Ma, C.; Wang, T.; Xu, Y.; Yuan, B.; Li, P.; Kong, Y. Preparation and Characterization of C_{60}-Filled Ethyl Cellulose Mixed-Matrix Membranes for Gas Separation of

Propylene/Propane. *Chem. Eng. Technol.* **2014**, 37, 611-619.

[28] Askari, M.; Chung, T.-S. Natural Gas Purification and Olefin/Paraffin Separation Using Thermal Cross-Linkable co-Polyimide/ZIF-8 Mixed Matrix Membranes. *J. Membr. Sci.* **2013**, 444, 173-183.

[29] Bux, H.; Chmelik, C.; Krishna, R.; Caro, J. Ethene/Ethane Separation by the MOF Membrane ZIF-8: Molecular Correlation of Permeation, Adsorption, Diffusion. *J. Membr. Sci.* **2011**, 369, 284-289.

[30] Lin, Y.S.; Ji, W.; Wang, Y.; Higgins, R.J. Cuprous-Chloride-Modified Nanoporous Alumina Membranes for Ethylene-Ethane Separation. *Ind. Eng. Chem. Res.* **1999**, 38, 2292-2298.

[31] Ploegmakers, J.; Japip, S.; Nijmeijer, K. Mixed Matrix Membranes Containing MOFs for Ethylene/Ethane Separation Part A: Membrane Preparation and Characterization. *J. Membr. Sci.* **2013**, 428, 445-453.

[32] Ilinich, O.M.; Zamaraev, K.I. Separation of Ethylene and Ethane over Polyphenyleneoxides Membranes: Transient Increase of Selectivity. *J. Membr. Sci.* **1993**, 82, 149-155.

Chapter 3 The adsorption properties of olefin and paraffin on Ag-X membrane

3.1. Introduction

Membrane separation has attracted attention as a novel energy-saving process for propylene and ethylene purification. Sholl and Lively pointed out that purification of propylene and ethylene requires as much as 0.3% of global energy use and suggested that membrane-based separation should be introduced for olefin purification [1]. Hence, many types of membranes have been reported previously for propylene separation.

Understanding adsorption and diffusion phenomena in micropores is essential for an understanding of the separation mechanism using membranes made of microporous materials such as zeolites and MOFs. Permeation phenomena were explained generally by an adsorption-diffusion model in which the permeation selectivity can be expressed as the product of adsorption and diffusion selectivities [2-4]. In other words, permeation selectivity is mainly governed by adsorption selectivity when diffusion selectivity is low, and vice versa.

Following studies of the ZIF-8 membrane for propylene/propane separation by Lai *et al.* [5,6], ZIF-8 membranes have been researched extensively [7-11]. ZIF-8 membranes have great potential for propylene/propane separation on the basis of diffusion selectivity [10,11]. Li *et al.* studied the adsorption and diffusion properties of propylene and propane in the micropores of ZIF-8 [10]. It was pointed out that although the heats of adsorption and adsorption capacities for propylene and propane are similar, the diffusion coefficient of propylene is 125 times greater than that of propane. The slightly smaller size of propylene contributes to a larger diffusion rate in the micropores of ZIF-8 compared with propane.

It is also known that separation performance appears due to adsorption selectivity other than the molecular sieving effect described above. A membrane made of silicalite-1, all-silica zeolite with the MFI topology, showed ethanol-selective permeation from an ethanol/water mixture due to its strong hydrophobicity [2,12,13]. Sano et al. were the first to report that silicalite-1 membrane exhibited a high ethanol permselectivity [12,13]. Nomura et al. investigated the transport mechanism of ethanol and water through silicalite-1 membrane [2]. They reported that the water permeance decreased in the presence of ethanol. While the diffusion coefficients of ethanol and water in silicalite-1 membrane are almost the same, the amount of ethanol adsorbed was approximately 10 times larger than that of water, resulting in a membrane with high ethanol selectivity. This selective permeation of ethanol from an aqueous solution by hydrophobic zeolite membrane was the study that triggered research on zeolite membranes utilizing adsorption selectivity.

Almost all porous membranes for propylene/propane separation previously reported show propylene selectivity based on molecular sieving that led to the appearance of diffusion selectivity as described above [5-11]. On the other hand, propylene/propane separation membranes using unique adsorption property of zeolite have also been reported [14,15]. Caro *et al.* reported Na-X membrane grown on an alumina support modified with 3-aminopropyltriethoxysilane [14]. Their membrane showed the separation factor of 3.3 for propylene/propane mixture on the basis of the adsorption selectivity.

In Chapter 2, I have developed X-type zeolite membrane for propylene/propane separation, and found that the ion-exchange from Na to Ag cations markedly enhanced the propylene selectivity, likely due to strong interaction between Ag cation in zeolite and olefins. I also found that propane permeation through Ag-X membrane was inhibited by the presence of propylene in the feed as in the case of ethanol separation through silicalite-1 membrane. In Ag-X membrane, preferentially adsorbed propylene would play an important role for the inhibition of propane permeation and contribute to a high selectivity. However, details of the adsorption behavior of propylene and propane on Ag-X membrane is still open question.

In this chapter, I shed light on the adsorption properties of propylene and propane on Ag-X membrane. I quantitatively investigated the relationship between adsorption properties and separation performance based on the isotherms of propylene and propane on Ag-X membranes.

3.2. Experimental

3.2.1. Membrane preparation

X-type membrane, containing Na^+ as counter cation, was synthesized by a secondary growth method as described in Chapter 1. Na-X membrane was prepared on the outer surface of a tubular support. A porous α-alumina (o.d. = 10 mm, i.d. = 7 mm, length = 30 mm, average pore size = 150 nm, Noritake Co. Ltd.) was used as the support. The Si/Al ratio of the prepared membrane was determined to be 1.15 via an X-ray diffraction (XRD) technique, using the diffraction angle of the (111) plane appearing at around $2\theta = 6°$ described in Chapter 2.

Ag-X membrane was prepared by ion-exchange of the Na-X membrane. Na-X membrane was immersed in 10 mM $AgNO_3$ aqueous solution and degassed under reduced pressure using an aspirator. After degassing, the membrane was held in the solution while stirring for 1 h. Then, the membrane was washed with distilled water and dried at 343 K overnight prior to use. The ion-exchange ratio was calculated as ca. 97% using the membrane weights before and after ion-exchange.

3.2.2. Permeation and separation test

The permeation and separation properties of a propylene/propane mixture were evaluated according to a method described in Chapter 1. The molar fraction of propylene was adjusted from 0.0005 to 0.9 by changing the flow rates of propylene and propane. Both the feed and permeate sides were kept at atmospheric pressure. The permeate side was swept with flowing helium. The separation tests were carried out at 313 K.

The permeate gas was analyzed by gas chromatography for its composition. In addition, the flow rate of permeate was calculated by using an internal standard of methane gas. Flux, J [mol m^{-2} s^{-1}], permeance, Π [mol m^{-2} s^{-1} Pa^{-1}], and separation factor, $\alpha_{A/B}$ [-], are defined by following equations:

$$J = u\,A^{-1} \qquad (1)$$

$$\Pi = J\,\Delta p^{-1} \qquad (2)$$

$$\alpha_{X/Y} = Y_A\,Y_B^{-1}\,X_A^{-1}\,X_B \qquad (3)$$

where u is the permeation flow rate [mol s^{-1}], A is the effective membrane area of 6.28×10^{-4} [m^2] and Δp is the partial pressure difference between the feed and permeate sides [Pa]. X_A and X_B are molar fractions of components A and B in the feed. Y_A and Y_B are molar fractions of components A and B in permeate, respectively.

3.2.3. Adsorption test

The adsorption isotherms of propylene and propane on Na- and Ag-X membranes were evaluated using a non-destructive volumetric adsorption method. The measurement was carried out using a BELSORP-max (MicrotracBEL Corp.) instrument with a specially designed sample holder that I developed. To determine accurate isotherm by volumetric method, this sample holder and measurement system enabled us to insert the whole membrane without destruction with a minimized dead-volume, leak, and exact control of temperature as follows.

A photograph of special sample holder is shown in Figure 3.1. An outer diameter of α-alumina support is 10 mm and an inner diameter of the sample holder is 11 mm. Therefore, this sample holder enabled insertion of the whole of membrane without sample destruction.

Some ideas are employed in the home-made sample holder to obtain veracious information about adsorption property. To determine accurate isotherm by volumetric method, minimizing a leak and exact control of temperature are necessary. A VCR gasket face seal is adopted to minimize a leak from a joint of sample holder and the body.

There are two strategies for exact control of sample temperature. One of them is reducing heat-transfer and radiation from isotherm bath located upper side of the sample holder. Another one is improvement of heat-transfer from liquid nitrogen bath located around the sample holder. An aluminum pixy hat and a red glass rod are placed on a membrane sample to reduce

heat-transfer and radiation, respectively. In addition, a glass rod plays a role for reduction of dead-volume in sample holder. On the other hand, aluminum balls are stuffed around a membrane for improvement of heat-transfer rate from liquid nitrogen bath.

The membrane sample was outgassed at 373 K for 36 h under vacuum prior to the adsorption tests. Adsorption measurements were performed at 313 K, the same temperature for separation tests.

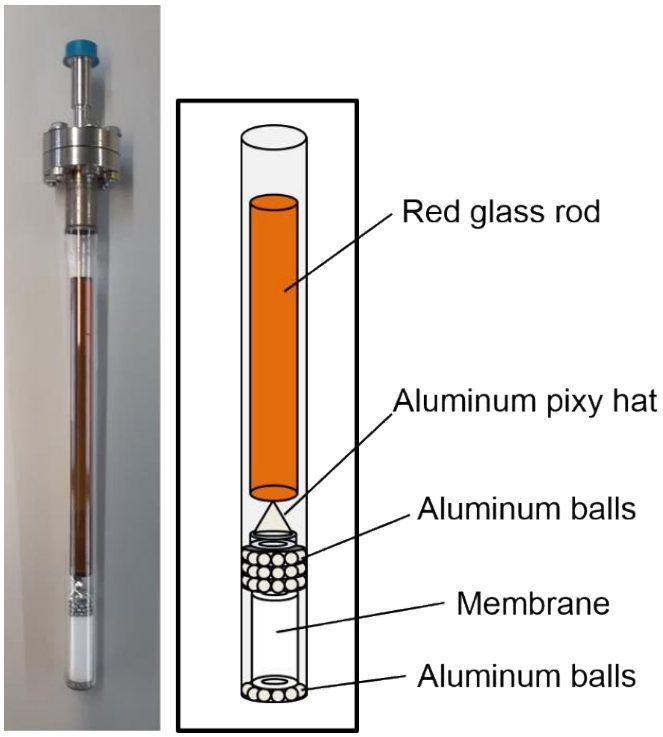

Figure 3.1 A photograph of sample holder for N_2 adsorption measurement.

3.3. Results and discussion

3.3.1. Permeation and separation properties for propylene/propane mixture of Ag-X membrane

Figure 3.2 shows the permeation behavior of Ag-X membrane for propylene/propane mixtures at 313 K. The molar fraction of propylene in the mixture was varied from 0.0005 to 0.9 balanced with propane in a step-wise manner. Because the feed side was kept at atmospheric pressure, the partial pressures of propylene and propane were both 50.5 kPa, respectively, at a propylene molar fraction of 0.5. In addition, the propylene purity on the permeation side, $C_{C3}^{=}$, is defined by the following equation:

$$C_{C3}^{=}\,[-] = J_{propylene}\,(J_{propylene} + J_{propane})^{-1} \qquad (4)$$

The Ag-X membrane showed excellent separation performance, in particular at lower propylene partial pressures. For example, the membrane exhibited a separation factor of 95.9 for

propylene with a permeance of 1.92×10^{-7} mol m^{-2} s^{-1} Pa^{-1} at 0.01 of the molar fraction of propylene.

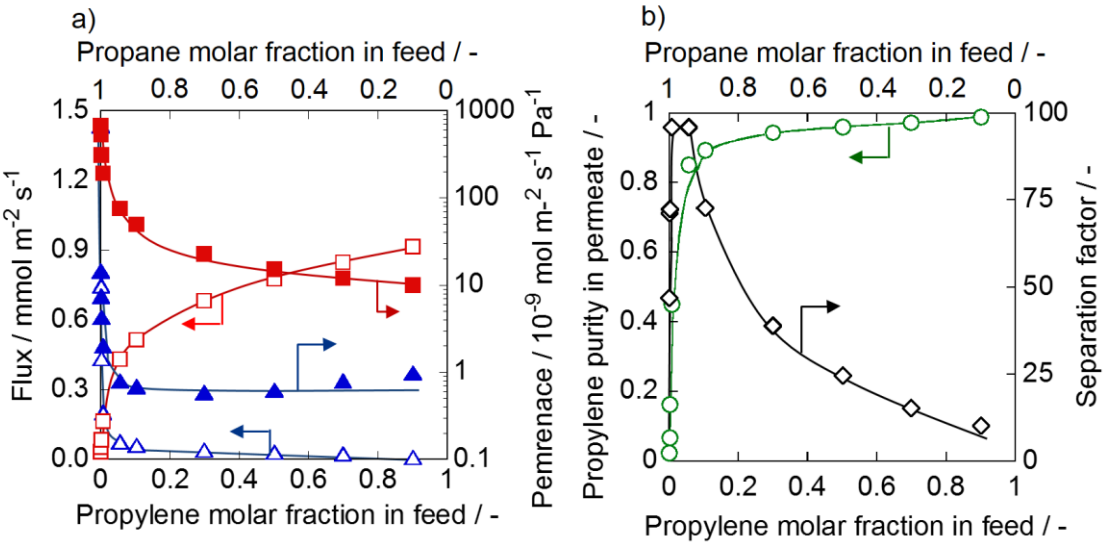

Figure 3.2 Separation properties of Ag-X membrane for propylene/propane mixture at 313 K. Effect of propylene molar fraction in feed on a) flux or permeance and b) propylene purity in permeate or separation factor. □, propylene; △, propane (Open symbol, flux; Closed symbol, permeance); ○, propylene purity in permeate; ◇, separation factor.

While propylene exhibited higher fluxes with increasing molar fraction of propylene, its permeance gradually decreased with increasing propylene composition in the feed. The propylene permeances at molar compositions of 0.005 and 0.9 were 6.76×10^{-7} and 1.02×10^{-8} mol m^{-2} s^{-1} Pa^{-1}, respectively. When the partial pressure of propylene was increased by a factor of 180, its flux was enhanced by only 28 times, leading to a decrease in permeance to about one-sixth as much.

In contrast, the permeation behavior of propane differed from that of propylene. The propane flux increased as the propane partial pressure increased. In particular, the propane flux steeply increased at a propane molar fraction > 0.9. The fluxes at propane molar fractions of 0.1, 0.9, and 0.9995 were 9.69×10^{-3}, 6.18×10^{-2}, and 1.43 mmol m^{-2} s^{-1}, respectively. As a result, the propane permeance increased with increasing partial pressure of propane contrary to the propylene permeation behavior.

Here, I discuss the differences in permeation behavior between propylene and propane through the Ag-X membrane on the basis of the permeation mechanisms. Flux through micropores in a zeolite membrane is generally dominated by both the adsorbed amount and the diffusivity of the molecule [2-4]. In general, at lower partial pressures, the adsorbed amount

linearly increases with increasing partial pressure in accordance with Henry's law; consequently, flux also increases linearly. Therefore, the permeance should be constant despite differences in partial pressure. When the adsorbed amount approaches the saturation level at higher partial pressures, the adsorbed amount becomes difficult to proportionally increase, resulting in a flux is similarly difficult to increase. In this case, the permeance decreases with increasing partial pressure.

As shown in figure 3.2, the propylene flux showed an upward convex curve and its permeance decreased as the partial pressure of propylene increased, implying that the adsorbed amount of propylene tended to saturate at higher partial pressure. Hence, I propose that propylene permeation through Ag-X membrane can be explained qualitatively by an adsorption-diffusion model.

On the other hand, propane showed permeation behavior that is opposite to that of propylene. Because coexisting propylene strongly inhibited propane permeation through the Ag-X membrane [16], we consider that the apparently unnatural permeation behavior of propane was possibly explained by competitive adsorption of propylene and propane. The adsorbed amount of propane might be strongly influenced not only by the partial pressure of propane but also by that of propylene.

I also studied the effect of moisture in feed gas. Figure 3.3 shows the separation performance for the propylene/propane equimolar mixture with and without 3000 ppm of water vapor. The relative humidity, RH, changed from 4.1 to 0.30% by changing the membrane temperature from 313 to 373 K. As clearly shown in figure 3.3, the propylene permeances with and without water vapor are almost the same. In addition, the separation factor did not deteriorate by moisture as well. I, thus, concluded that Ag-X membrane does not lose its separation property even in the presence of a small content of water.

Here, I discuss the reason of a good resistance of Ag-X membrane against humid. Previously, the effects of humidity on the permselectivity through zeolite membranes were reported for gas separations, particularly CO_2 purification. Dong *et al.* studied the effect of water vapor on the separation performance of Na-FAU zeolite membrane for CO_2/N_2 separation [17]. The CO_2 permeance and separation factor decreased by the existence of 2.64 kPa of water vapor below 353 K (RH > 6.5%). Dutta *et al.* also reported the influence of a trace amount of water on the permselectivity of Na-FAU/polymer composite membrane for CO_2/N_2 [18]. Although the CO_2 permeance and separation factor declined in the presence of 46 ppm of water at 298 K (RH = 0.15%), a higher humidity tolerance was observed at a higher temperature of 348 K (RH = 0.012%).

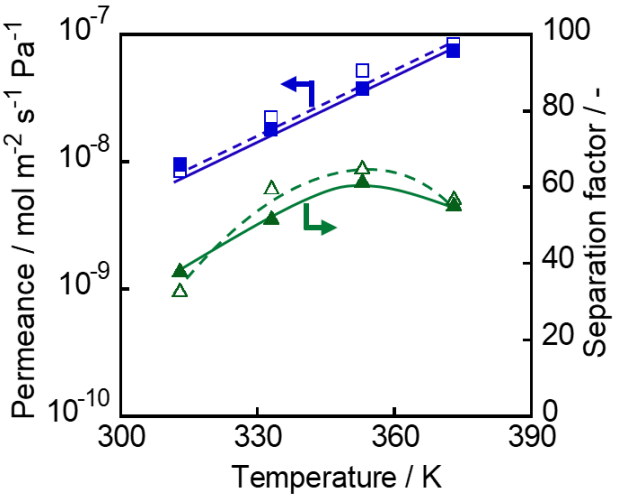

Figure 3.3 Permeation and separation performance of Ag-X membrane for an equimolar mixture of propylene/propane mixture with and without 3000 ppm of water vapor. □, propylene; △, separation factor. Open and closed symbols represent the results under dry and wet conditions, respectively.

The adsorption property of CO_2 and water on FAU-type zeolite were investigated in both experimental and theoretical approaches [19-21]. Smit *et al.* calculated that the desorption enthalpy of water (52 kJ mol^{-1}) on Na-X was larger than that of CO_2 (40 kJ mol^{-1}) [21]. They also pointed out that water is likely adsorbed, and that the adsorbed water dramatically reduces the available adsorption sites for CO_2 in a mixture of CO_2 and water.

In this study, the separation and permeation performance of Ag-X membrane for the propylene/propane mixture was hardly influenced even in the presence of 3000 ppm of water, as described above. I consider that a strong interaction of olefin with Ag-X zeolite might be a reason of a high humidity tolerance in this study, while the relatively small value of RH (0.30 - 4.1%) would cause the negligible influence of water vapor. Tsapatsis *et al.* similarly reported that the adsorption amount of H_2S on Ag-FAU was hardly influenced by water vapor (RH = 0.41%) [22]. They calculated the adsorption heats of H_2S (66 kJ mol^{-1}) and water (57 kJ mol^{-1}) on Ag-FAU and considered that a relatively large adsorption heat of H_2S contributed to a high adsorption capacity for H_2S even under humid conditions. Besides, it have been reported that the adsorption heats of ethylene and water on Ag-X were 76 kJ mol^{-1} and 57 kJ mol^{-1}, respectively [22,23]. Therefore, I consider that the high permselectivity of Ag-X membrane was retained in the presence of water vapor due to a large deference of adsorption heat between olefin and water as well.

3.3.2. Adsorption properties of propylene and propane on Ag-X membrane

Because adsorption properties strongly affect permeation behavior as described above, I investigated the adsorption properties of propylene and propane in unary systems. Figure 3.4 shows the adsorption isotherms of propylene and propane on (a) Na- and (b) Ag-X membranes at 313 K. According to figure 3.4(a), the amount of propylene adsorbed on the Na-X membrane was larger than that of propane over the whole pressure range measured, likely due to interaction between propylene and the Na cation. The adsorbed amount of propylene, 3.09 cm^3 (STP) g^{-1} at 10^{-2} kPa, was approximately 26 times larger than that of propane at the same pressure. In addition, the amount of propylene adsorbed surpassed that of propane even at 100 kPa; the amounts of propylene and propane adsorbed were 92.7 and 68.5 cm^3 (STP) g^{-1}, respectively.

As shown in figure 3.4(b), the amount of propylene adsorbed on the Ag-X membrane at lower pressures increased dramatically compared with that on the Na-X membrane. Specifically, the adsorbed amount of propylene, 39.0 cm^3 (STP) g^{-1}, at 10^{-2} kPa, was approximately 90 times larger than that of propane at the same pressure. The adsorbed amount precipitously increased at very low pressure, ~10^{-3} kPa, and then almost saturated at 10 kPa. It is known that Ag cations strongly interact with the π-electron of olefins [23,24], resulting in Ag-X membrane that was readily saturated with propylene at lower propylene partial pressures.

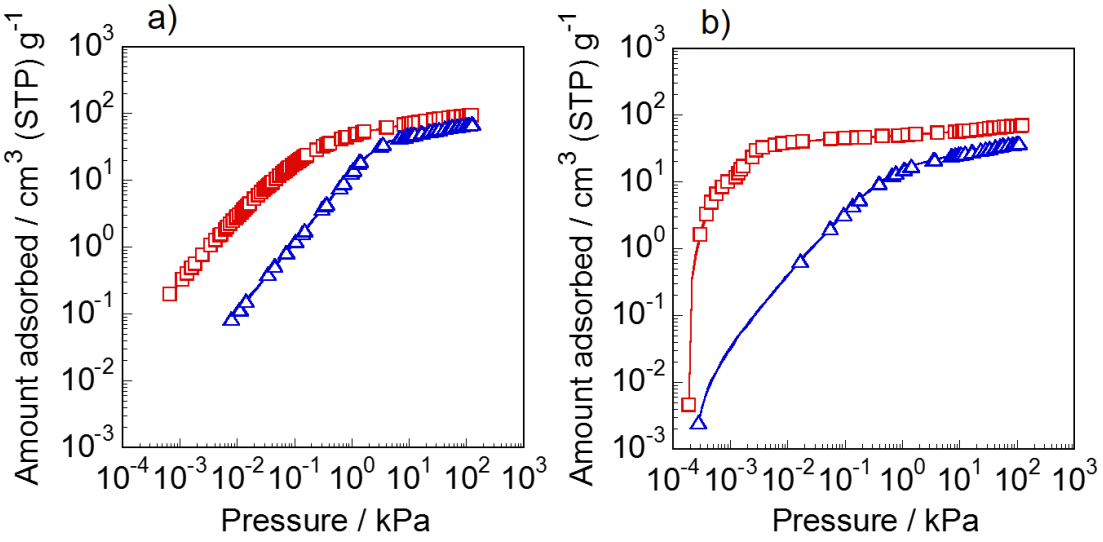

Figure 3.4 Adsorption isotherms for propylene and propane on (a) Na- and (b) Ag-X membranes at 313 K. □, propylene; △, propane.

Also, the adsorbed amounts of propylene were 57.8 and 68.5 cm^3(STP) g^{-1} at 10 and 90 kPa, respectively, showing the difficulty of increasing the amount adsorbed with partial pressure when the adsorbed amount was already nearly saturated at a pressure of 10 kPa. This would be

one of the reasons why propylene permeance decreased with increasing partial pressure in this range, as shown in figure 3.2(a).

Although the adsorption properties of zeolite X for propylene markedly changed by ion-exchange from Na to Ag cations, the adsorption isotherm of propane on Na- and Ag-X membranes scarcely changed, possibly because of weak interaction between propane and these cations. As a result, I consider that the significant difference in the adsorbed amounts on Ag-X between propylene and propane was the reason for the enhancement of separation performance by the ion-exchange from Na to Ag cations that I recently reported [16].

It should be noted that not only the saturated adsorption amount but also the steep rise of isotherm at lower pressure was important to discuss the separation properties of Ag-X membrane. As shown in figure 3.4, the uptakes appeared at very low pressure < 0.1 kPa were clearly observed on each membrane, and thus I can discuss quantitatively a contribution of the adsorption property to the separation property in the following section.

3.3.3. Evaluation of adsorption properties of propylene and propane in a binary system

Quantitative discussion of the adsorbed amount in a binary system is required to understand the contribution of adsorption property to the separation performance of a membrane for a binary mixture. To estimate adsorbed amounts in a binary system, I adopted the Langmuir adsorption model and the Markham–Benton approach in the following section.

When the adsorption isotherm is plotted as $P\,V^{-1}$ vs. P to show a linear relationship, it can be analyzed according to the Langmuir adsorption model by using the following equations:

$$V = V_S\,K\,P\,(1+K\,P)^{-1} \qquad (5)$$

Equation (5) can be modified as follows:

$$P\,V^{-1} = P\,V_S^{-1} + K^{-1}\,V_S^{-1} \qquad (6)$$

where V [cm^3(STP) g^{-1}] is the adsorbed amount at a certain pressure, and P [Pa]. K [Pa^{-1}] and V_S [cm^3(STP) g^{-1}] are the adsorption equilibrium constant and the saturated adsorption amount, respectively. All isotherms drawn in Fig. 3.4 exhibit linear relationships between $P\,V^{-1}$ and P, as shown in figure 3.5. Therefore, the values of V_S and K are able to be calculated from the slope and the intercept, respectively.

Table 3.1 lists the calculated values of K and V_S. As can be seen, the values of K for propylene and propane on the Na-X membrane were 3.18×10^{-3} and 1.83×10^{-4}, respectively. These values increased to 1.74×10^{-1} and 8.93×10^{-4} by the ion-exchange from Na to Ag. Thus, the ratio of $K_{\text{propylene}}$ to K_{propane} on Na- and Ag-X membrane increased from 17.4 to 195 by ion-exchange, emphasizing the remarkable preferential adsorption of propylene.

When the two components, A and B, adsorbed in accordance with the Langmuir equation in

each unary system, each adsorbed amount in a binary system, V_A and V_B [cm^3(STP) g^{-1}], can be evaluated by the Markham–Benton approach, as follows [25]:

$$V_A = K_A V_{SA} P_A (1+K_A P_A+K_B P_B)^{-1} \quad (7)$$

$$V_B = K_B V_{SB} P_B (1+K_A P_A+K_B P_B)^{-1} \quad (8)$$

Each adsorbed amount was calculated from the saturated adsorption amount and the equilibrium constant was determined from the $P V^{-1}$ vs. P plots shown in figure 3.5.

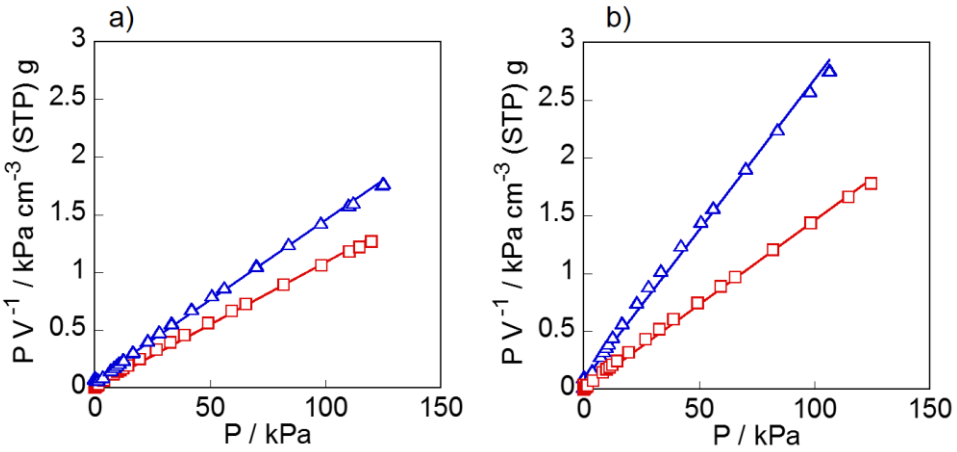

Figure 3.5 $P V^{-1}$ vs. P plots for propylene and propane on (a) Na- and (b) Ag-X membrane at 313 K. □, propylene; △, propane.

Table 3.1 Langmuir constants and saturated adsorption amounts on Na- and Ag-X membranes at 313 K

	Langmuir constant / 10^{-3} Pa		Saturated amount of adsorption / cm^3 (STP) g^{-1}	
	Propane	Propylene	Propane	Propylene
Na-X	0.183	3.18	72.5	92.6
Ag-X	0.893	174	37.3	67.6

To discuss the packing state of micropores in the membrane, the volumetric occupancy, O_V [vol%], was calculated by the following equation:

$$O_V = V_F (N B)^{-1} \times 100 \quad (9)$$

where V_F [m^3 u.c.$^{-1}$] is the free volume in X-type zeolite per unit cell, N [u.c.$^{-1}$] is the numbers of adsorbed molecules per unit cell, and B [m^3] is the volume of a molecule.

I assumed that V_F is the product of unit cell volume of 14.4288 nm^3 and accessible volume of 27.42% [26]. Propylene and propane were assumed to be spheres with diameters of 0.45 and

0.43 nm,[3] and N was calculated from the adsorbed amount [cm^3(STP) g^{-1}] and the weight of the unit cell. The weight of unit cell was determined by the compositions of Na- and Ag-X, $Na_{88}Al_{88}Si_{104}O_{384}$ and $Ag_{88}Al_{88}Si_{104}O_{384}$, respectively. The composition of unit cell was determined from the Si/Al ratio and Ag/Al ratio. Tables 3.2 and 3.3 list the values of N and O_V for Na-X and Ag-X membranes, respectively.

Table 3.2 Numbers of adsorbed molecules in a unit cell of Na-X zeolite and their occupancy on Na-X membrane at 313 K in binary system evaluated by the Markham–Benton approach

$X_{propylene}$ / -	Amount adsorbed / u.c.$^{-1}$		Occupancy / vol%		Propylene molar fraction in adsorbed phase / -
	Propane	Propylene	Propane	Propylene	
0.0010	35.4	7.92	37.3	9.54	0.183
0.010	15.5	34.7	16.3	41.8	0.691
0.10	14.4	35.4	15.9	44.8	0.711
0.25	6.27	46.3	6.91	58.6	0.881
0.50	2.32	51.6	2.57	65.3	0.957
0.75	0.804	53.7	0.888	67.9	0.985
0.90	0.271	54.4	0.299	68.8	0.995

Table 3.3 Numbers of adsorbed molecules in a unit cell of Ag-X zeolite and their occupancy on Ag-X membrane at 313 K in binary system evaluated by the Markham–Benton approach

$X_{propylene}$ / -	Amount adsorbed / u.c.$^{-1}$		Occupancy / vol%		Propylene molar fraction in adsorbed phase / -
	Propane	Propylene	Propane	Propylene	
0.0010	11.7	38.8	12.3	46.8	0.768
0.010	1.68	56.0	1.77	67.5	0.971
0.10	1.52	59.5	1.82	80.4	0.975
0.25	0.522	61.3	0.623	83.9	0.992
0.50	0.176	61.8	0.209	84.7	0.997
0.75	0.0587	62.2	0.0700	85.0	0.999
0.90	0.0195	62.3	0.0233	85.1	0.999

The results listed in Tables 3.2 and 3.3 clearly indicated that the adsorption selectivity of X membrane was enhanced by the ion-exchange from Na to Ag. For example, the ratio of

adsorption amounts of propylene to propane on Na- and Ag-X membranes at a propylene molar ratio of 0.5 are 22.2 and 351, respectively. The occupancies of propylene and propane in the micropores of Ag-X membrane under the same conditions were 84.7 and 0.209 vol%, being equal to ca. 62.2 and 0.176 molecules in a unit cell, respectively. In other words, the micropores in Ag-X membrane would be almost filled with propylene even in the atmosphere of an equimolar mixture of propane and propylene.

3.3.4. Relationship between adsorption property and separation performance

Figure 3.6 shows the relationship of propylene molar fraction between the adsorbed phase and the gas phase evaluated using the Markham–Benton approach. To compare the results of the adsorption test with that of the separation test shown in figure 3.2(b), the purity of propylene on the permeation side of the Ag-X membrane is also plotted.

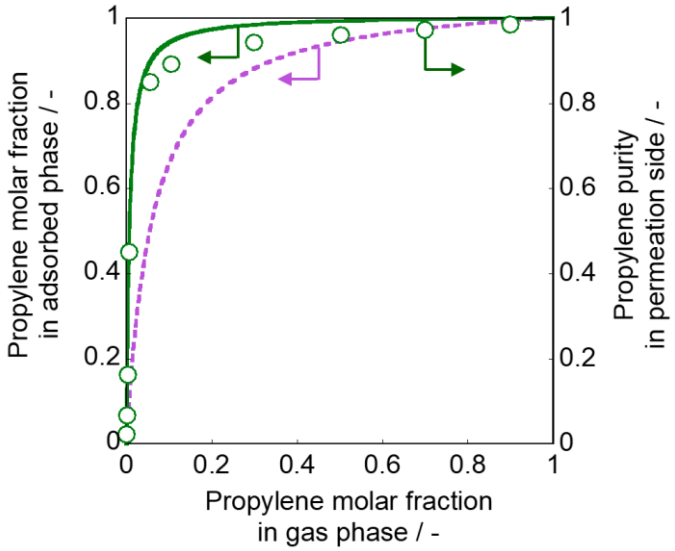

Figure 3.6 Relationship of propylene molar fractions between adsorbed phase on Na- and Ag-X membranes and gas phase. Solid line, adsorbed phase on Ag-X; dashed line, adsorbed phase on Na-X; ○, propylene purity on permeation side.

The difference in propylene molar fraction in the adsorbed phase between Na-X and Ag-X tended to be greater at a smaller propylene fraction in the gas phase. Micropores in Ag-X are easily occupied by propylene above 0.1 propylene fraction in the gas phase owing to a strong interaction between Ag cations and olefins. In contrast, the propylene fraction in the adsorbed phase decreased at a propylene molar fraction < 0.1 in the gas phase. This result is in good agreement with the permeation behavior of propane, as shown in figure. 3.2: the propane flux

and permeance increased with decreasing propylene concentrations at a propylene molar fraction < 0.1.

It is worth noting that the calculated molar fraction in the adsorbed phase in the binary system almost agrees with the results of the permeation test. As described in the introduction, separation by porous membranes was able to be classified as follows: diffusion dominated, adsorption dominated, or both. According to the discussion above, the results of separation and adsorption tests strongly suggest that the permeation selectivity of the Ag-X membrane for a propylene/propane mixture was dominated by adsorption selectivity, which can be estimated from each isotherm in unary systems.

The purity of propylene measured in the permeate by separation tests was somewhat less than that calculated in the adsorbed phase. I consider that a small amount of defect exists in a membrane, which slightly decrease the separation performance. In other words, the purity in the permeate and the adsorbed phase would be equal in the case of an ideal defect-free Ag-X membrane.

3.3.5. Evaluation of adsorption species and heats of propylene and propane on the basis of BET theory

Repetitive adsorption tests of propylene and propane on Ag-X membrane were carried out to evaluate the adsorption species. After the first adsorption test mentioned in 3.3.2, Ag-X membrane was degassed at 313 K for 2 h under vacuum condition. The second adsorption test were taken place for degassed sample at the same conditions to the first time. Figure 3.7 shows results of repetitive adsorption tests of propylene and propane on Ag-X membrane at 313 K. There is a big difference between the adsorption amounts of propylene in the first and second time, indicating that strongly adsorbed propylene was not able to be desorbed by vacuuming. The amount of strongly adsorbed propylene was 30 cm^3 (STP) g^{-1} at 100 kPa. In contrast, the adsorbed amounts of propane were almost the same in the first and second time, suggesting that physically adsorbed propane was easily desorbed.

Adsorption heats of strongly adsorbed propylene and propane were calculated on the basis of BET theory. Figure 3.8 shows that BET plot of propylene and propane. Adsorption heat was calculated by following equations,

$$\text{The slope of BET plot} = (C\text{-}1)(v_m\, C)^{-1} \qquad (10)$$

$$\text{The intercept of BET plot} = (v_m\, C)^{-1} \qquad (11)$$

$$C = \exp((Q_1\text{-}Q_L)(R\, T)^{-1}) \qquad (12)$$

where v_m, C, Q_1 and Q_L are adsorbed amount of single layer, adsorption constant, adsorption heat and condensation heat, respectively.

The calculated adsorption heats of propylene nd propane were 63.0 and 37.0 kJ mol^{-1}. The huge difference of adsorption heat would contributes to high separation of Ag-X membrane discussed in above section.

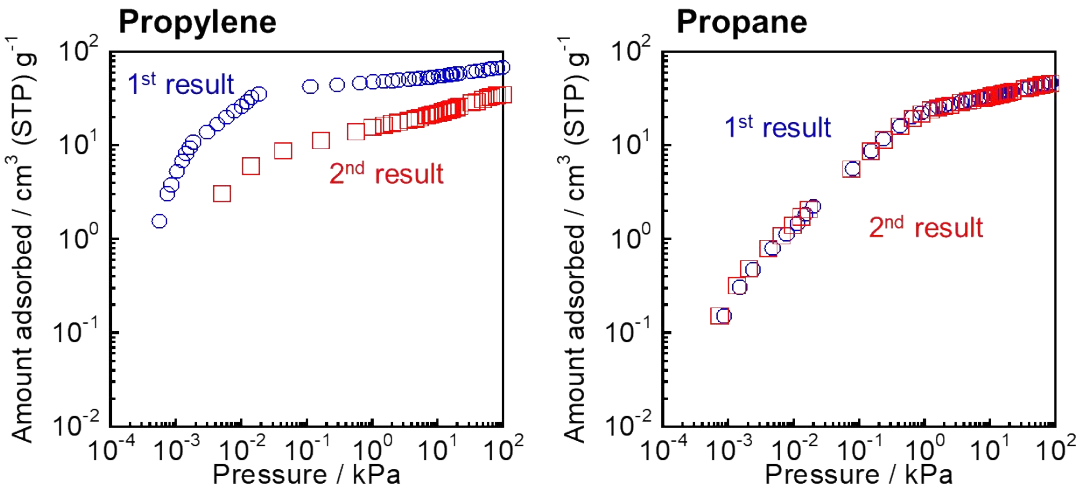

Figure 3.7 Results of repetitive adsorption tests of propylene and propane on Ag-X membrane at 313 K.

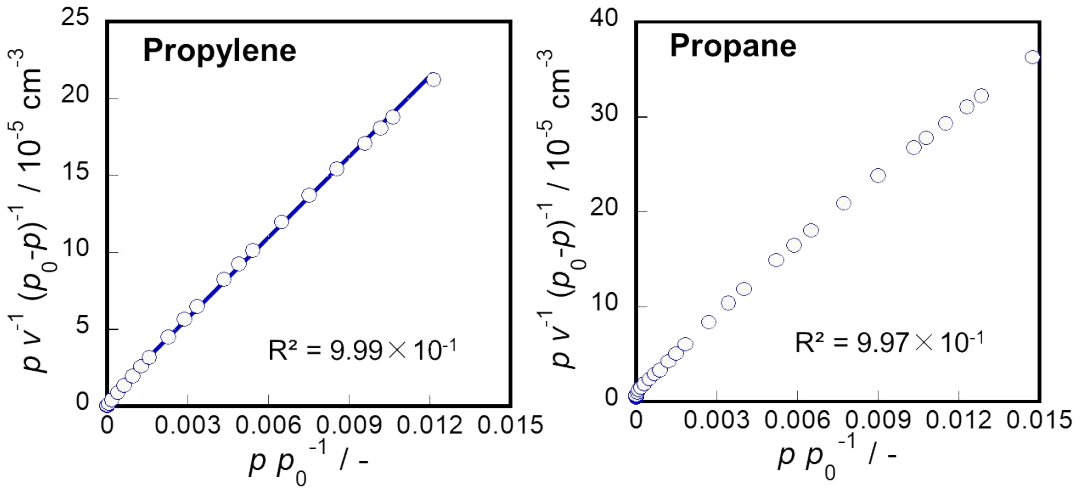

Figure 3.8 BET plot of propylene and propane on Ag-X membrane at 313 K.

3.3.6. Observation of permeation behavior in Ag-X membrane by using mass-spectrograph

The strongly adsorbed propylene which hardly desorbed by 2-h vacuuming was observed by repetitive adsorption tests as mentioned above. Here we studied the permeation behavior of propylene in Ag-X membrane at 313 K by mass-spectrograph (MS).

Feed gas was switched as C_3D_6, Ar and C_3H_6, sequentially. Permeate was swept by Ar and detected by MS. At first, C_3D_6 was fed enough period. Then, the feeding of C_3D_6 stopped and Ar

was fed to a membrane. When the signal of C_3D_6 became negligibly small, C_3H_6 was finally fed to a membrane. Figure 3.9 shows the procedure of this experiment. If strongly adsorbed C_3D_6 is able to be diffuse in Ag-X membrane by the feeding of C_3H_6, the signal of C_3D_6 should be observed.

Figure 3.10 shows the changes of the flow rates of C_3D_6 and C_3H_6 detected by MS. First, we confirmed the saturation of C_3D_6 flow rate and disappear of C_3D_6 signal by the feeding of Ar. After that, the signal of C_3D_6 was clearly observed as soon as supplying C_3H_6 and decreased with time. The amount of C_3D_6 permeated after the supplying of C_3H_6 was calculated as 30.8 cm^3 (STP) g^{-1} from the area surrounded by the signal and baseline. This amount permeated have good agreement with the amount of strongly adsorbed propylene as shown in 3.3.5. From these results, we concluded that strongly adsorbed propylene is able to diffuse and permeate through Ag-X membrane under the conditions of permeation test. The large adsorption heat which is necessary for the desorption of propylene may be supplied by the adsorption of next molecule.

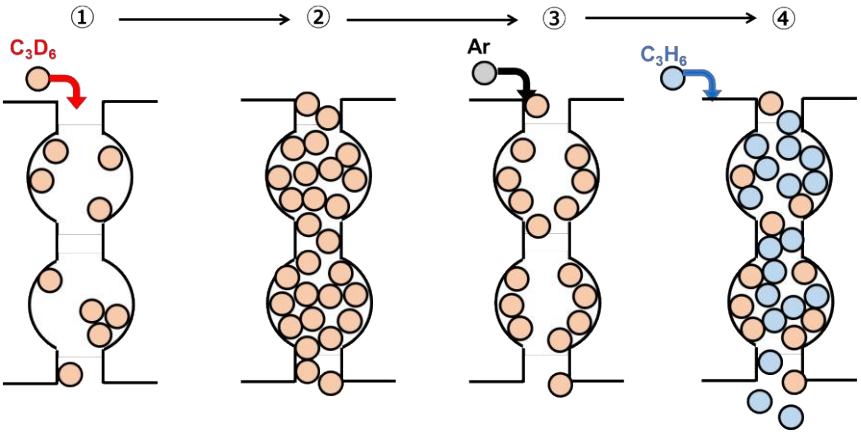

Figure 3.9 The procedure of permeation behavior observation by MS.

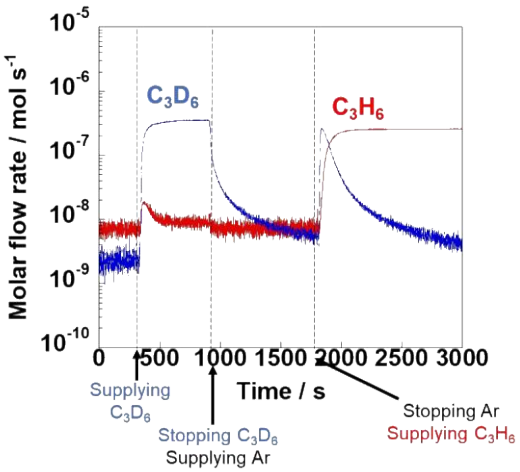

Figure 3.10 The changes of the flow rates of C_3D_6 and C_3H_6 detected by MS.

3.3.7. Evaluation of ideal selectivity of Ag-X membrane by pressurization on permeation side

To evaluate the ideal separation performance of Ag-X membrane which has no defects, I carried out propylene/propane separation test with pressurization on permeation side. The pressure of feed side is kept at atmosphere. Because the effect of flow in inter-crystalline pathway would be negligible by pressurization on permeation side, I can estimate the ideal selectivity of Ag-X membrane without defects.

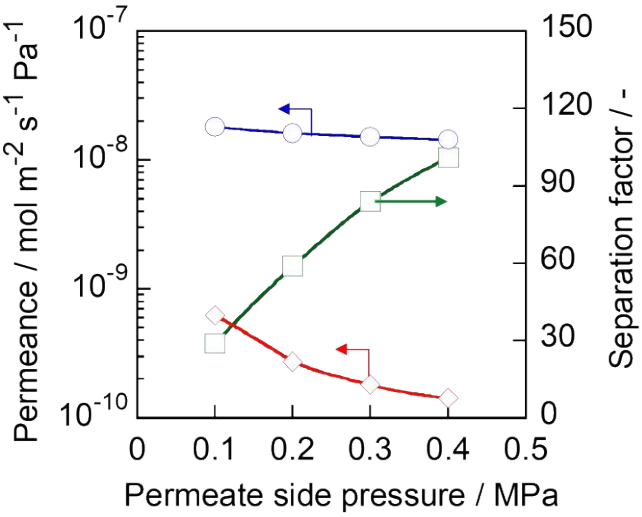

Figure 3.11 Separation test for propylene/propane (=50:50 mol%) mixture at 313 K with the pressure of permeate side at 0 - 0.4 MPa. ○, propylene; ◇, propane; □, separation factor.

Figure 3.11 shows the separation test for propylene/propane (=50:50 mol%) mixture at 313 K with the pressure of permeate side at 0 - 0.4 MPa. Separation factor increased with increasing the pressure of permeate side; the separation factor of 101 at 0.4 MPa, and then the separation factor will reach the ceiling of ca. 150 at higher pressure. This result suggests that Ag-X membrane has a potential for separation factor of ca. 150 for propylene/propane mixture at 313 K if the membrane without defect is prepared.

Similar evaluation was taken place with deferent temperature of 353 K. Figure 3.12 shows the separation test for the equimolar mixture of propylene/propane at 353 K with the pressurization of permeation side up to 0.4 MPa. As in the case of figure 3.11, Separation factor increased with increasing a pressure. The separation factor at 353 K will reach the ceiling of ca. 200 at higher pressure.

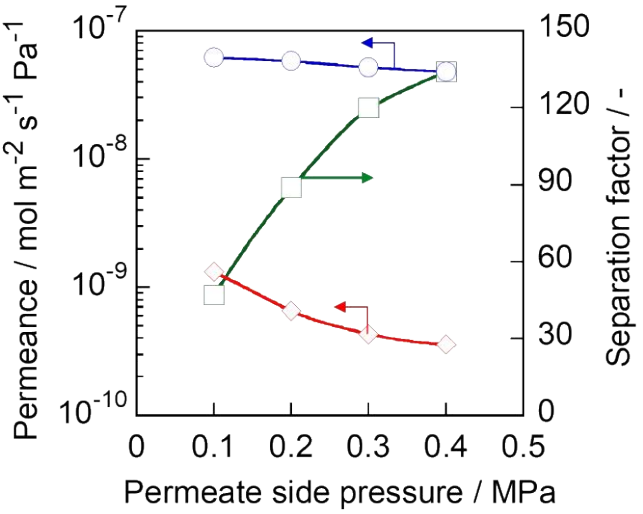

Figure 3.12 Separation test for propylene/propane (=50:50 mol%) mixture at 353 K with the pressure of permeate side at 0 - 0.4 MPa. ○, propylene; ◇, propane; □, separation factor.

3.3.8. Selectivity of Ag-X membrane for various C_1-C_3 hydrocarbon mixtures

Ag-X membrane was used for olefin separation in various C_1-C_3 hydrocarbon mixtures. In this measurement, the equimolar binary mixtures of C_1-C_3 hydrocarbons were used as feed components. Two kinds of component were chosen from methane, ethane, ethylene, propane and propylene. The permeances of each hydrocarbon in unary systems were also evaluated for comparison.

Figure 3.13 shows the permeances of C_1-C_3 hydrocarbons through Ag-X membrane in unary and binary systems at 313 K. In unary systems, the order of permeances was as follows; methane > ethane > ethylene > propane > propylene. This result suggested that molecular size strongly effects on the permeability and olefins' diffusivity reduced by an interaction with Ag cation.

All olefin permeances were magnitude larger than those of paraffins in all cases of olefin/paraffin binary mixtures, such as methane/ethylene, methane/propylene, ethane/ethylene, ethane/propylene, propane/ethylene and propane/propylene. These results showed that Ag-X membrane is able to exhibit the affinity-based separation performance for olefins/paraffin mixtures even in the presence of smaller paraffins. In these cases, olefin permeances in binary systems were almost the same as the values in unary systems. In contrast, paraffin permeances drastically decreased by the existence of olefins.

Larger molecules preferentially penetrated through Ag-X membrane in the case of separation for binary mixtures of paraffins, such as methane/ethane, methane/propane, ethane/propane. These selectivities may be dominated by the difference of interaction between

Ag-X membrane and paraffins in similarly with olefin/paraffin separation. Although there are no significant affinity between membrane and paraffins, the adsorption heat of paraffins strongly depends on a carbon number. In general, longer-chain paraffin has larger adsorption heat on micropore because the sectional area which interacts with the wall of micropore tends to be large. Myers *et al.* and Lercher *et al.* reported the adsorption heats of *n*-paraffin on FAU- and MFI-type zeolites increased with ca. 7 and 10 kJ mol^{-1} by increasing each carbon number [27,28].

In ethylene/propylene separation, Ag-X membrane exhibited propylene selectivity as well. The reason why larger molecules preferentially penetrated should be the same as the paraffin/paraffin separation.

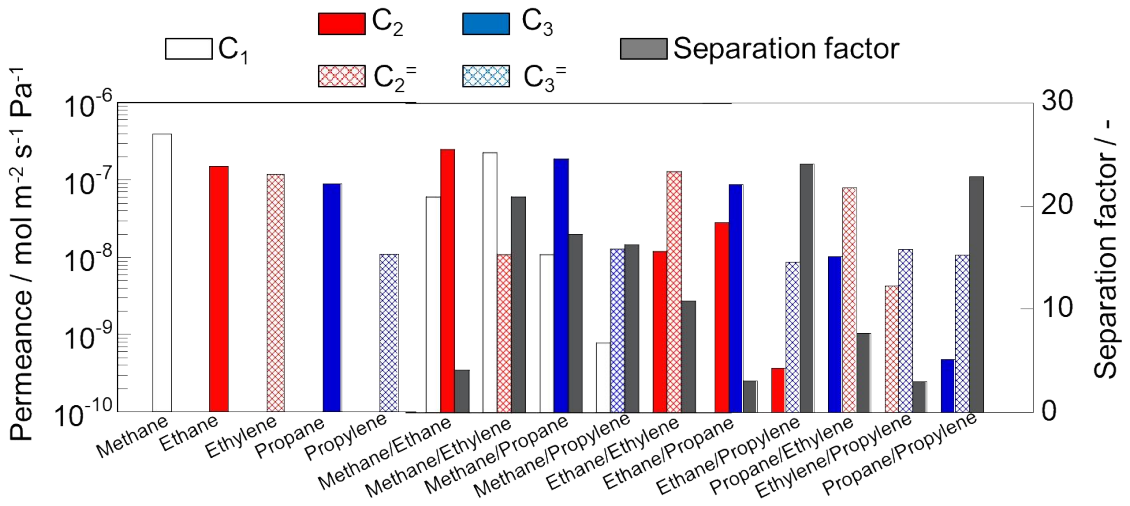

Figure 3.13 Permeances of C_1-C_3 hydrocarbons through Ag-X membrane in unary and binary systems at 313 K.

3.3.9. Relationship between ion-exchange ratio and separation performance

Figure 3.14 show the relationship between ion-exchange ratio and separation performance. I prepared 16 Ag-X membranes with various ion-exchange ratio by the method mentioned in Chapter 2. These separation performances were almost the same in the range of 0-60% of Ag-exchange ratio. The separation factor clearly increased by increasing Ag-exchange ratio above 60%. This phenomenon can be explained by percolation model as follows.

Here we assume the model of three-dimensional site-percolation for diamond lattice. The supercage in FAU-type zeolite is connected to neighboring four supercages through 12-membered channels as shown in figure 3.14(b). This structure can be drawn as diamond lattice model which has four-coordinated structure. In figure 3.14(c), the atoms and bonds of

diamond lattice represent the supercages and 12-membered channels of FAU, respectively.

The white spheres in figure 3.14(c) mean the Na-X domains in which propane is able to penetrate. In contrast, black spheres represent the Ag-X domains in which propane is not able to permeate. When white spheres create the cluster which traverse longitudinally, propane become penetrates though the membrane. In this model, critical percolation probability is known as 0.428, indicating that pathways for propane is open below the Ag-exchange ratio of 0.572 (=1-0.428). This value has good agreement with the relationship between ion-exchange ratio and separation performance.

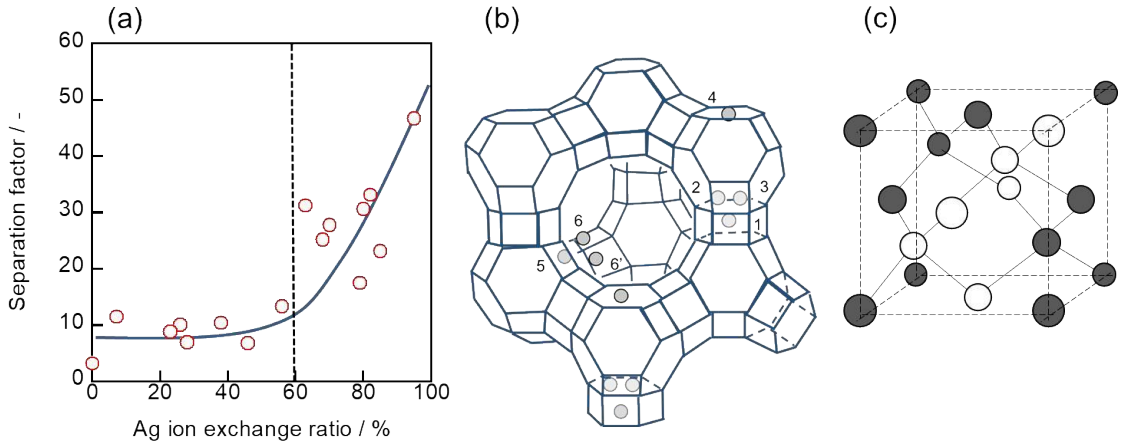

Figure 3.14 Relationship between ion-exchange ratio and separation performance. (a) Results of separation test at 373 K with Ag-X membrane having various Ag-exchange ratio. (b) Model of X-type zeolite structure. (c) Model of three-dimensional site-percolation for diamond lattice.

Table 3.4 lists the critical percolation probability of some other three-dimensional site-percolation model having different coordination number [29]. Simple cubic, body-centered cubic and face-centered cubic lattices have the coordination numbers of 6, 8 and 12, respectively. The lattice having higher coordination number required high ion-exchange ratio to block propane permeation. In other words, propane could easily penetrate through the lattice with high coordination number even at high ion-exchange ratio because there existed many detour path. Such calculated ion-exchange ratio differed from the results of separation tests as shown in figure 3.14(a).

Table 3.4 Critical percolation probabilities of three-dimensional site-percolation models

Lattice	Coordination number / -	Critical percolation probability [29] / -	Required ion-exchange ratio / -
Diamond	4	0.428	0.572

Simple cubic	6	0.312	0.688
Body-centered cubic	8	0.246	0.754
Face-centered cubic	12	0.198	0.812

3.4. Conclusions

I explored the adsorption properties of propylene and propane on Na- and Ag-X membranes in order to understand the contribution of adsorption selectivity to propylene/propane separation through Ag-X membrane. The amount of propylene adsorbed on Ag-X membrane at lower pressures markedly increased compared with that on Na-X membrane, leading to the occurrence of excellent separation by Ag-X membrane.

Molar fractions of propylene in the adsorbed phase in the binary system were calculated and compared with the results of permeation tests. The calculated propylene purity in the adsorbed phase showed good agreement with propylene purity on the permeation side of the Ag-X membrane. Therefore, I conclude that the permeation selectivity of Ag-X membrane for propylene/propane mixture is mainly governed by adsorption selectivity, which can be estimated by using each isotherm in unary systems.

References

[1] Sholl, D.S.; Lively, R.P. Seven Chemical Separations to Change the World. *Nature* **2016**, 532, 435-437.

[2] Nomura, M.; Yamaguchi, T.; Nakao, S. Ethanol/Water Transport through Silicalite Membranes. *J. Membr. Sci.* **1998**, 144, 161-171.

[3] Bux, H.; Chmelik, C.; Krishna, R.; Caro, J. Ethene/Ethane Separation by the MOF Membrane ZIF-8: Molecular Correlation of Permeation, Adsorption, Diffusion. *J. Membr. Sci.* **2011**, 369, 284-289.

[4] Krishna, R. Describing the Diffusion of Guest Molecules inside Porous Structures. *J. Phys. Chem. C* **2009**, 113, 19756-19781.

[5] Pan, Y.; Lai, Z. Sharp Separation of C2/C3 Hydrocarbon Mixtures by Zeolitic Imidazolate Framework-8 (ZIF-8) Membranes Synthesized in Aqueous Solutions, *Chem. Commun.* **2011**, 47, 10275-10277.

[6] Pan, Y.; Li, T.; Lestari, G.; Lai, Z. Effective Separation of Propylene/Propane binary mixtures by ZIF-8 membranes, *J. Membr. Sci.* **2012**, 390-391, 93-98.

[7] Kwon, H.T.; Jeong, H.-K. In Situ Synthesis of Thin Zeolitic-Imidazolate Framework ZIF-8 Membranes Exhibiting Exceptionally High Propylene/Propane Separation. *J. Am. Chem. Soc.* **2013**, 135, 10763-10768.

[8] Ma, X.; Kumar, P.; Mittal, N.; Khlyustova, A.; Daoutidis, P.; Mkhoyan, K.A.; Tsapatsis, M. Zeolitic Imidazolate Framework Membranes Made by Ligand-Induced Permsectivation. *Science* **2018**, 361, 1008-1011.

[9] Rashidi, F.; Leisen, J.; Kim, S.J.; Rownaghi, A.A.; Jones, C.W.; Nair, S. All-Nanoporous Hybrid Membranes: Redefining Upper Limits on Molecular Separation Properties. *Angew. Chem. Int. Ed.* **2019**, 58, 236-239.

[10] Hara, N.; Yoshimune, M.; Negishi, H.; Haraya, K.; Hara, S.; Yamaguchi, T. Diffusive Separation of Propylene/Propane with ZIF-8 membranes. *J. Membr. Sci.* **2014**, 450, 215-223.

[11] Li, K.; Olson, D.H.; Seidel, J.; Emge, T.J.; Gong, H.; Zeng, H.; Li, J. Zeolitic Imidazolate Frameworks for Kinetic Separation of Propane and Propene. *J. Am. Chem. Soc.* **2009**, 131, 10368-10369.

[12] Sano, T.; Yanagishita, H.; Kiyozumi, Y; Kitamoto, D.; Mizukami, F. Separation of Ethanol/Water Mixture by Silicalite Membrane. *Chem. Lett.* **1992**, 21, 2413-2414.

[13] Sano, T.; Yanagishita, H.; Kiyozumi, Y; Mizukami, F.; Haraya, K. Separation of Ethanol/Water Mixture by Silicalite Membrane on Pervaporation. *J. Membr. Sci.* **1944**, 95, 221-228.

[14] Mundstock, A.; Wang, N.; Friebe, S.; Caro, J. Propane/Propene Permeation through Na-X membranes; The Interplay of Separation Performance and Pre-synthetic Support Functionalization. *Microporous Mesoporous Mater.* **2015**, 215, 20-28.

[15] Shrestha, S.; Dutta, P. K.; Modification of a Continuous Zeolite Membrane Grown within Porous Polyethersulfone with Ag(I) Cations for Enhanced Propylene/Propane Gas Separation. *Microporous Mesoporous Mater.* **2019**, 279, 178-185.

[16] Sakai, M.; Sasaki, Y.; Tomono, T.; Seshimo, M.; Matsukata, M. Olefin Selective Ag-Exchanged X-Type Zeolite Membrane for Propylene/Propane and Ethylene/Ethane Separation. *ACS Appl. Mater. Interfaces* **2019**, 11, 4145-4151.

[17] Gu, X.; Dong, J.; Nenoff, T.M. Synthesis of Defect-Free FAU-Type Zeolite Membranes and Separation for Dry and Moist CO_2/N_2 Mixtures. *Ind. Eng. Chem. Res.* **2005**, 44, 937-944.

[18] Wang, B.; Dutta, P. K. Influence of Cross-Linking, Temperature, and Humidity on CO_2/N_2 Separation Performance of PDMS Coated Zeolite Membranes Grown within a Porous Poly(ethyl sulfone) Polymer. *Ind. Eng. Chem. Res.* **2017**, 56, 6065-6077.

[19] Li, G.; Xiao, P.; Webley, P.A.; Zhang, J.; Singh, Ranjeet. Competition of CO_2/H_2O in Adsorption Based CO_2 Capture. *Energy Procedia* **2009**, 1, 1123-1130.

[20] Shirono, K.; Endo, A.; Daiguji, H. Molecular Dynamics Study of Hydrated Faujasite-Type Zeolites. *J. Phys. Chem. B* **2005**, 109, 3446-3453.

[21] Joos, L.; Swisher, J.A.; Smit, B. Molecular Simulation Study of the Competitive

Adsorption of H_2O and CO_2 in Zeolite 13X. *Langmuir* **2013**, 29, 15936-15942.

[22] Kumar, P.; Sung, C.-Y.; Muraza, O.; Cococcioni, M.; Hashimi, S.A.; McCormick, A.; Tsapatsis, M. H_2S Adsorption by Ag and Cu Ion Exchanged Faujasites. *Microporous Mesoporous Mater* **2011**, 146, 127-133.

[23] Carter, J.L.; Yates, D.J.C.; Lucchesi, P.J.; Elliott, J.J.; Kevorkian, V. The Adsorption of Ethylene on a Series of Near-Faujasite Zeolites Studied by Infrared Spectroscopy and Calorimetry. *J. Phys. Chem.* **1966**, 70, 1126-1136.

[24] Choi, E.Y.; Kim, S.Y.; Kim, Y.; Seff, K. Crystal Structure of an Ethylene Sorption Complex of Fully Dehydrated, Fully Oxidized, Fully Ag^+-exchanged zeolite X. *Microporous Mesoporous Mater* **2003**, 62, 201-210.

[25] Markham, E.C.; Benton, A.F. The Adsorption of Gas Mixtures by Silica. *J. Am. Chem. Soc.* **1931**, 53, 497-507.

[26] "FAU: Framework Type", 1. Apr. 2019. http://asia.iza-structure.org/IZA-SC/framework.php?STC=FAU

[27] Savitz, S.; Siperstein, F.; Gorte, R.J.; Myers, A.L. Calorimetric Study of Adsorption of Alkanes in High-Silica Zeolites. *J. Phys Chem. B* **1998**, 102, 6865-6872.

[28] Eder, F.; Lercher, J.A. Alkene sorption in molecular sieves: The contribution of ordering, intermolecular interactions, and sorption on Bronsted acid sites. *Zeolites* **1997**, 18, 75-81.

[29] Odagaki, T. Percolation no Kagaku. *Shokabo* **1993**.

Chapter 4 Preparation of *BEA-type zeolite membrane with high aluminium content

4.1. Introduction

In Chapters 2 and 3, I developed the Ag-exchanged X-type zeolite membrane and investigated its permselectivity for olefin/paraffin mixtures. In olefin separation by using Ag-X membrane, preferentially adsorbed olefins strongly inhibited the adsorption and permeation of paraffins. There is strong interaction between olefins and Ag cations because the π orbital of olefin overlaps with the vacant 5s orbital of Ag cation and the 4d orbital of Ag cation overlaps with the vacant π* orbital of olefin.

Here I consider that Ag-exchanged zeolite membrane other than X-type zeolite can exhibit olefin selectivity by an affinity-based separation as well. *BEA-type zeolite which is a kind of large pore zeolites similar to X-type zeolite and is often used as catalyst. Recently, the seed-assisted synthetic method of *BEA without using OSDA was reported [1-4]. *BEA powdery crystal synthesized by the seed-assisted method had a specific feature, large ion-exchange capacity. I expect that such *BEA membrane having large ion-exchange capacity is suitable membrane material for olefin separation.

*BEA crystal can be obtained with absence of organic structure-directing agent (OSDA). Tetraethyl ammonium (TEA) cation is generally used as organic structure directing agent (OSDA). However, zeolite synthesis using OSDAs presents both economic and environmental concerns. As such, the seed-assisted synthetic method have been developed in recent years. In these reports, *BEA crystals were grown in a TEA^+-free synthesis gel in which homogeneous nucleation did not occur.

OSDA-free synthesis for membrane requires no calcination step to remove OSDA. Indeed, zeolite membranes prepared using OSDAs are often damaged in this calcination step, thereby hindering their size exclusion ability [5,6]. It was reported that membrane breakage was caused by the large differences in thermal expansion coefficients between support and membrane and/or by the volume change in the zeolite crystal followed by removal of OSDA. Preparation of zeolite membrane in the absence of OSDA would therefore address the above issues. Lin *et al.* reported that the MFI-type zeolite membrane synthesized without OSDA exhibited a high separation performance as a consequence of omitting the calcination step [7,8].

Matsukata *et al.* also previously reported that MOR and ZSM-5 membranes having good molecular sieving properties were formed by the secondary growth method using seed crystals in the absence of OSDA [9]. Zhang *et al.* reported that an organic template-free route for synthesizing *BEA membrane [10]. They have pointed out that the template-free route was able

to avoid the defects formation in the course of calcination. Formation process of *BEA membrane under OSDA-free conditions is still open question.

In this chapter, I report OSDA-free synthesis of *BEA-type zeolite to membrane preparation. The membrane formation process is carefully observed, and the role of seed crystals on the support surface for the formation of the *BEA membrane is studied.

4.2. Experimental

4.2.1. Membrane preparation

*BEA membranes were prepared by a secondary growth method. More specifically, a *BEA seed crystal was supported on a surface of a support by a dip coating method. A porous tubular α-alumina (o.d. = 10 mm, i.d. = 7 mm, length = 30 mm, average pore size = 150 nm, supplied from Noritake Co. Ltd.) was used as the support. A seeded support was then immersed in synthesis gel in the absence of OSDA and crystallized for the desired period.

*BEA seed crystal was prepared by conventional hydrothermal treatment using OSDA based on the previous report [11]. The composition of the synthesis gel was $200SiO_2$:$1Al_2O_3$:$18Na_2O$:60TEAOH:$2905H_2O$. Colloidal silica (ST-S, Nissan Chemical), sodium hydroxide (Kanto Chemical), sodium aluminate (Kanto Chemical), tetraethylammonium hydroxide (TEAOH, 35 wt%, Aldrich), and distilled water were used as the raw materials. A silica solution was prepared by mixing of colloidal silica and the half amount of TEAOH. While, an aluminum solution was prepared by mixing of distilled water, sodium hydroxide, sodium aluminate and the half amount of TEAOH. Both solutions were stirred for 20 min prior to mixing, and the resulting mixture was shaken vigorously for 30 min. Subsequently, the synthesis gel was aged by stirring at 298 K for 24 h. The aged synthesis gel was poured into a PTFE-lined autoclave and crystallized at 373 K for 7 days. After the crystallization, solid product was filtered and washed with distilled water prior to drying overnight at 383 K. The dried crystals were dispersed in a given amount of distilled water to prepare a seed slurry, the concentration of which was adjusted to 5 g L^{-1}.

OSDA-free *BEA membranes were prepared as follows. Tubular α-alumina support was immersed in the seed slurry for 1 min then dried at 343 K for 2 h. This process was repeated twice. The seeded support was then calcined at 803 K for 6 h to remove OSDA occluded in the micropore of seed crystals and to chemically bind the seeds onto the support surface. Following calcination, the seeded support was set in a PTFE-lined autoclave with the synthesis gel (40 g) and crystallized for a given period in an air oven at 393 K.

According to the previously reported procedure [2], the parent gel with the composition of $100SiO_2$:$1Al_2O_3$:$30Na_2O$:$2000H_2O$ was prepared by mixing of colloidal silica (ST-S, Nissan

Chemical), sodium hydroxide (Kanto Chemical), sodium aluminate (Kanto Chemical) and distilled water. Colloidal silica was added in a drop-wise manner to a mixture of the other components, and the resulting mixture was aged while stirring at 333 K for 4 h prior to use. After crystallization, obtained membrane was washed with boiling water and dried overnight.

4.2.2. Characterization of seed crystals and membrane

The obtained seed crystal and membranes were observed by field-emission electron microscope (FE-SEM, S-4800, Hitachi). Silicon and aluminum concentrations of the prepared membrane were analyzed by using an energy dispersive X-ray spectrometry (EDS, X-max, Oxford Instruments) coupled with FE-SEM.

Composition of seed crystal was determined by inductance coupling plasma spectra spectroscopy (ICP, SPECTROCIROS CCD, Rigaku). Seed crystals were dissolved in a 1 wt% KOH solution upon heating under microwave irradiation for 1 h prior to measurement.

Micropore volume of *BEA membrane was evaluated using a non-destructive N_2 adsorption method. The measurement was performed by using a BELSORP-max (MicrotracBEL Corp.) instrument with a special sample holder developed in-house. This sample holder enabled insertion of the whole of membrane without sample destruction. The photograph of sample holder is shown in the supplementary material. The membrane sample was outgassed at 623 K for 8 h under vacuum prior to the adsorption tests. Adsorption measurements were carried out at 77 K.

4.2.3. Permeation measurements

Vapor permeation tests in unary systems were performed to evaluate molecular-sieving property of the prepared membrane. Three molecules of different molecular sizes, namely *n*-hexane, cyclohexane, and 1,3,5-trimethylbenzene, were employed. The hydrocarbon vapor was fed to the outer surface of the membrane at 101 kPa in the absence of a dilution gas. Permeate side, inside of tubular support, was swept with argon and both the feed and permeate sides were kept at atmospheric pressure. Thus, permeation occurred based on concentration gradient. Membrane temperature was increased from 473 to 623 K in a stepwise manner.

In the permeation measurements, the fraction of hydrocarbon in the permeate was evaluated using a gas chromatograph equipped with a flame ionization detector (GC-FID, GC-8A, Shimadzu). The hydrocarbon permeation flow rate was determined using methane as an internal standard gas. The permeation flux, J, was calculated using Eq (1);

$$J\ (\mathrm{mol\ m^{-2}\ s^{-1}}) = u\,A^{-1} \qquad (1)$$

where u is the flow rate ($\mathrm{mol\ s^{-1}}$) and A is the membrane area ($\mathrm{m^2}$). Permeance, P, was then

determined using Eq. (2);

$$\Pi\,(\text{mol m}^{-2}\ \text{s}^{-1}\ \text{Pa}^{-1}) = J\,\Delta p^{-1} \qquad (2)$$

where Δp is partial pressure difference between the feed and permeate sides (Pa).

4.3. Results and discussion

4.3.1. Formation process of OSDA-free *BEA membrane

Figure 4.1 shows typical FE-SEM images of seeded support and membranes prepared at 393 K for different crystallization periods. All samples were washed with boiling water and dried overnight prior to observation. Before hydrothermal treatment, spherical seed crystals measuring 200–400 nm uniformly covered the outer surface of a support. Indeed, a seed crystal layer ~1 μm thick was observed in the cross-sectional view. However, following hydrothermal treatment, clear morphological changes were observed in the seed crystals, where partial dissolution took place over the initial 2 days, and an amorphous layer was formed on the surface of seed layer after 1 day. Although seed crystals close to the surface mainly dissolved, the cross-sectional view indicated that particles still partially remained.

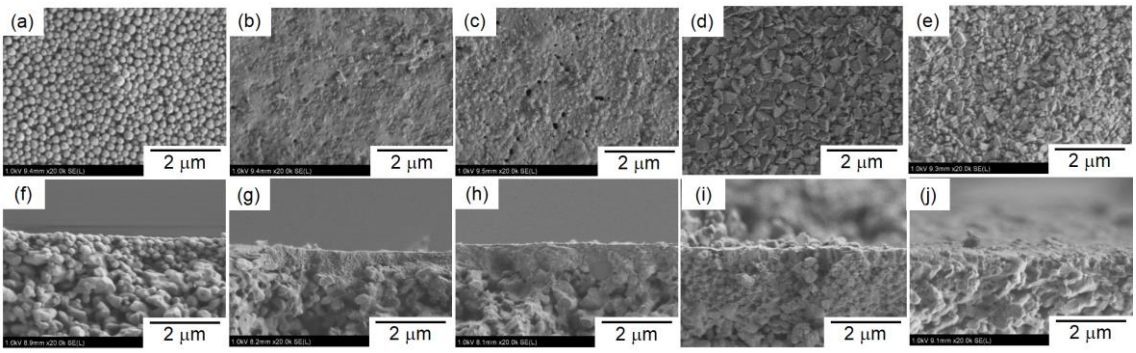

Figure 4.1 Typical FE-SEM images of (a, f) a seeded support and *BEA membranes crystallized for (b, g) 1, (c, h) 2, (d, i) 5, and (e, j) 7 days.

After 2 days of crystallization, the amorphous layer also remained on the surface, and angular crystals were observed in this amorphous layer. In contrast, distinguishing octahedral crystals uniformly covered the support surface after 5 and 7 days, and neither the spherical seeds or the amorphous layer were present in any great quantities. The thicknesses of the original seeded layer and the grown membrane were similar, ca. 1 μm. A thin membrane was successfully prepared by the secondary growth method without using OSDA.

The crystal with truncated octahedral morphology seems to be very similar to typical *BEA crystals synthesized by the OSDA-free method. Sasaki *et al.* reported a hypothesis for formation process of the characteristics morphology in *BEA crystal synthesized in the absence of OSDA

[12]. It was found that the Si/Al ratio of a membrane crystallized for 7 days was ~5.1 (determined by EDX), thereby indicating that the membrane contains a large quantity of aluminum compared to the seed crystals (ca. 19) and the synthesis gel (50). Such a high aluminum content is a common characteristic of *BEA crystals grown under OSDA-free conditions. Okubo *et al.* reported *BEA powder synthesis under OSDA-free condition by using a synthesis gel (Si/Al = 50) and seed crystal (Si/Al = 12) [2]. The obtained *BEA powder showed a lower Si/Al ratio of 6.6. Mintova *et al.* also reported well-shaped Al-rich octahedral *BEA crystals (Si/Al = ca. 5), which were obtained through seed-assisted synthesis without an OSDA [1].

Figure 4.2 shows the XRD patterns of seeded support and membranes at 393 K. No obvious reflection peaks other than those corresponding to the *BEA-type zeolite and support, α-alumina, were observed for any of the samples. The intensity of a typical diffraction peak appearing at approximately $2\theta = 7.5°$ decreased in the early stages of hydrothermal treatment, prior to increasing once again when the synthesis period was prolonged. The change in intensity was consistent with the results of microscopic observations made by FE-SEM.

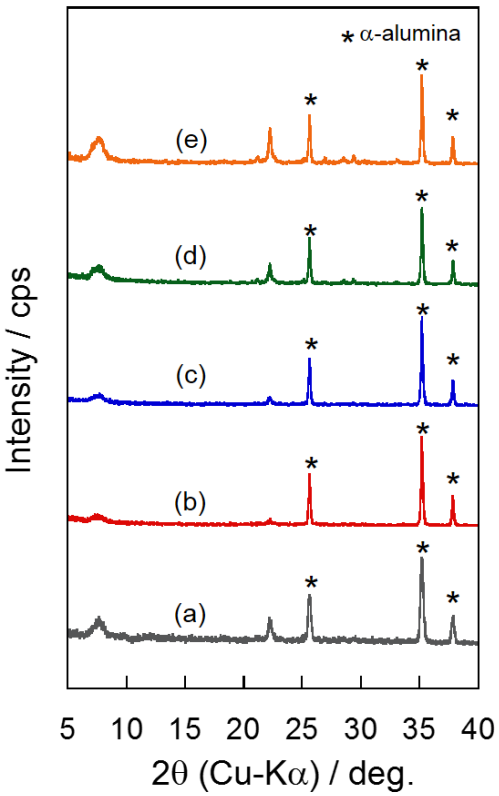

Figure 4.2 XRD patterns of (a) a seeded support and *BEA membranes crystallized for (b) 1, (c) 2, (d) 5, and (d) 7 days.

N_2 adsorption measurements were carried out to evaluate the changes in the micropore volume, an index of crystallinity, during the course of membrane formation. Figure 4.3 shows the N_2 adsorption isotherms for the seed crystals and the membranes crystallized over different periods. In addition, the changes in the micropore volume calculated using the Saito-Foley (S-F) method are plotted in Figure 4.4 [13,14].

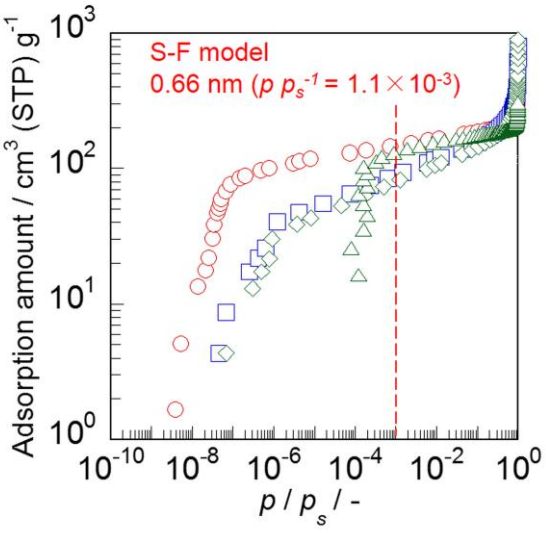

Figure 4.3 Results of non-destructive N_2 adsorption isotherm. △, Seed crystal; membranes crystallized for ◇, 1; □, 2; ○, 7 days.

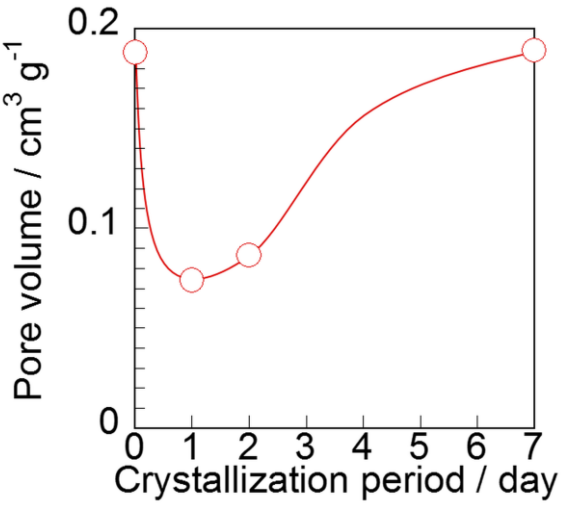

Figure 4.4 Pore volume change during hydrothermal treatment calculated from N_2 adsorption isotherm.

The volume of zeolitic pores in membrane was calculated as follows. N_2 adsorbed amount at

$p\,p_s^{-1} = 1.1 \times 10^{-3}$ was adopted as the adsorbed amount at saturation in zeolite pore because this quantity represents the adsorbed amount required for the saturation of a cylindrical pore with a diameter 0.66 nm, which is a comparable pore size to the *BEA-type zeolite, as determined using the S-F method.

Seed crystals had a micropore volume of 0.188 $cm^3\ g^{-1}$ before the hydrothermal treatment to form membrane. The micropore volume in membrane was reduced by ~50% in the early stages of hydrothermal treatment, with a volume of 0.086 $cm^3\ g^{-1}$ being calculated after 2 days. This was attributed to partial dissolution of seed crystals and the formation of amorphous and/or crystals with poor crystallinity.

In contrast, the micropore volume of the sample increased in the later stage of treatment, with the membrane crystallized for 7 days giving a volume of 0.189 $cm^3\ g^{-1}$. As a result, the micropore volume of the membrane exceeded that of the seed crystals obtained with prolonged crystallization, thereby suggesting that the crystals generated and grown in the later stage possessed a high crystallinity. In other words, the entire membrane consisted of well-crystallized *BEA following hydrothermal treatment for 7 days. These changes in the micropore volume during the secondary growth were in good agreement with the FE-SEM and XRD results.

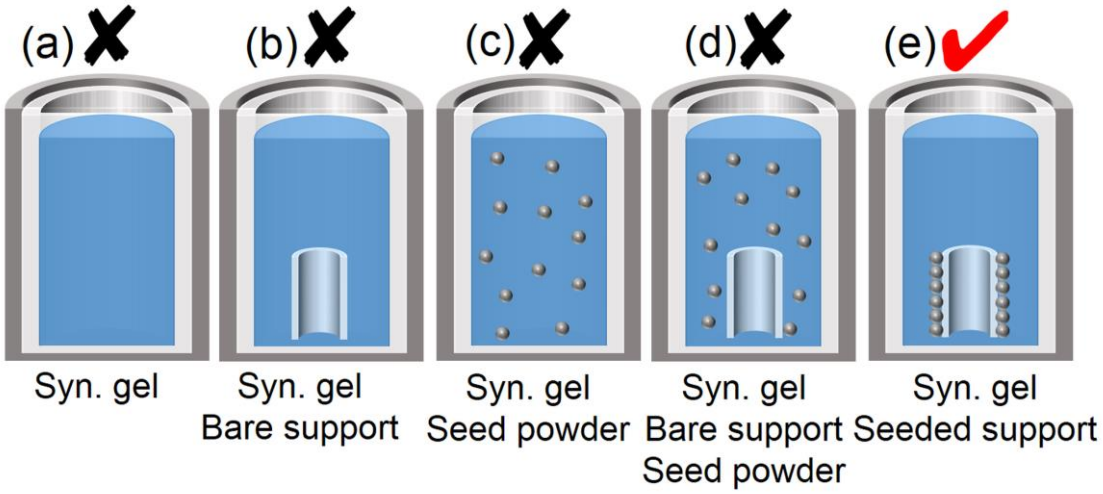

Figure 4.5 Success and failure of *BEA growth under various conditions. (a) only synthesis gel, (b) gel + bare support, (c) gel + *BEA powder, (d) gel + bare support + *BEA powder, and (e) gel + seeded support.

I also wished to shed light on the role of seed crystals during *BEA membrane formation under OSDA-free conditions. Thus, the solid phases formed in the bulk solution in the autoclave and on the support surface were examined under 5 different conditions. More specifically, crystallization was performed at 393 K for 7 days for: (a) only synthesis gel, (b) gel + bare

support, (c) gel + *BEA powder, (d) gel + bare support + *BEA powder, and (e) gel + seeded support, as shown in Figure 4.5. The quantity of added *BEA powder was adjusted to be equal to that seeded on the support for membrane preparation, i.e., 5 mg. The quantity of SiO_2 in this 5 mg seed crystal was approximately 1.0×10^{-3} wt% of that in the synthesis gel.

Figure 4.6 shows the XRD patterns of these products. Figures 4.6(a) and (c) shows the XRD patterns of solid phases formed in the bulk solution. Figures 4.6(b), (d) and (e) shows the XRD patterns of solid phase formed on the support. As a result, *BEA membrane layer formed on the support surface only in the case using seeded support, as shown in (e). In contrast, amorphous were formed in bulk solution and on supports in the other cases, (a), (b), (c) and (d). These results strongly suggest that the growth of a *BEA membrane under such OSDA-free conditions occurred only when the seed layer was attached to the support.

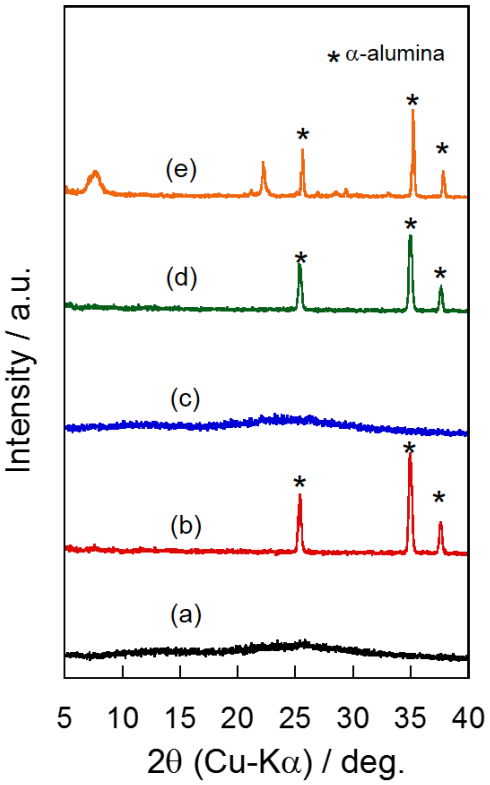

Figure 4.6 XRD pattern of solid products formed under 5 kinds of conditions. (a) only synthesis gel, (b) gel + bare support, (c) gel + *BEA powder, (d) gel + bare support + *BEA powder, and (e) gel + seeded support.

In many previously reported cases, the required seed amount for OSDA-free synthesis of the *BEA crystal was ≥ 1 wt% [2]. In contrast, I herein successfully prepared an OSDA-free *BEA membrane using a very small quantity of the seed crystal, ca. 1.0×10^{-3} wt%. I therefore

considered that the densely supported seed layer induced the formation of a local high concentration in the vicinity of the support surface, leading to crystal formation and growth.

The effect of the Si/Al ratio of seed crystals on membrane formation were evaluated. Figure 4.7 shows XRD patterns and FE-SEM images of *BEA membranes prepared with seed crystals with different Si/Al ratio of 32.0, 19.2, 5.1. Seed crystal having the Si/Al ratio of 5.1 and 32.0 were prepared according to previous reports [2,11], respectively.

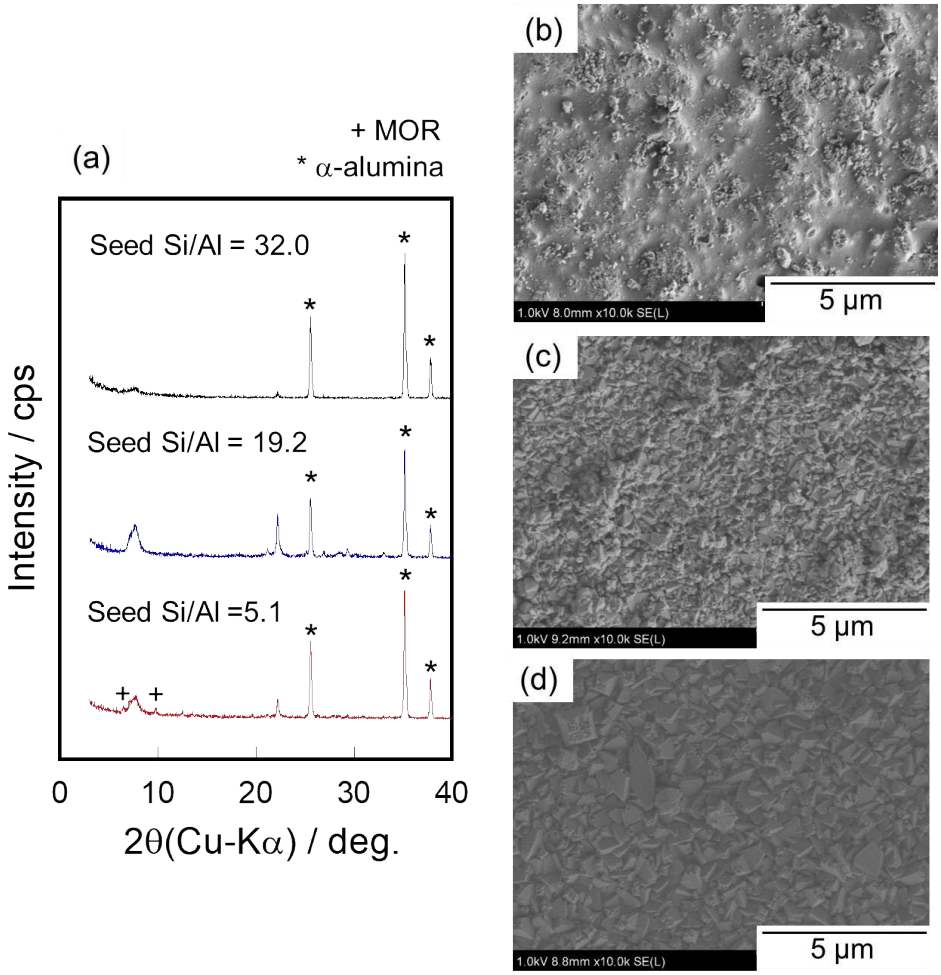

Figure 4.7 XRD patterns (a) and FE-SEM images of *BEA membranes prepared with seed crystals with different Si/Al ratio of 32.0 (b), 19.2 (c), 5.1 (d).

The membranes prepared by using seed crystal with low Si/Al ratio had the mixed phase of *BEA and MOR-type zeolites. This result indicated that seed crystal with low Si/Al ratio had insufficient effect for structure-directing because of the difficulty of dissolution. In contrast, the membranes synthesized by using seed crystal with high Si/Al ratio has low crystallinity. Amorphous layer was observed from the FE-SEM image of the surface of the membrane,

suggesting that seed crystal with high Si/Al ratio was unavailing because of the high dissolubility. We can conclude that the seed crystal having appropriate dissolubility conduces to compact *BEA membrane.

Consequently, I was able to summarize the formation process for an OSDA-free *BEA membrane, as shown in Figure 4.8. After dip-coating, the seed crystals were uniformly ordered on the outer surface of the support (Figure 4.8(a)). In the early stages of secondary growth, the ordered seeds partially dissolved, and small quantities of seeds remained in the amorphous layer (Figure 4.8(b)). Subsequently, crystal growth of the remaining crystals and heterogeneous crystallization from the amorphous layer occurred. In the secondary growth step, such a densely supported seed layer was found to play an important role in the formation of a continuous *BEA layer of typical octahedral crystals on the support surface (Figure 4.8(c)).

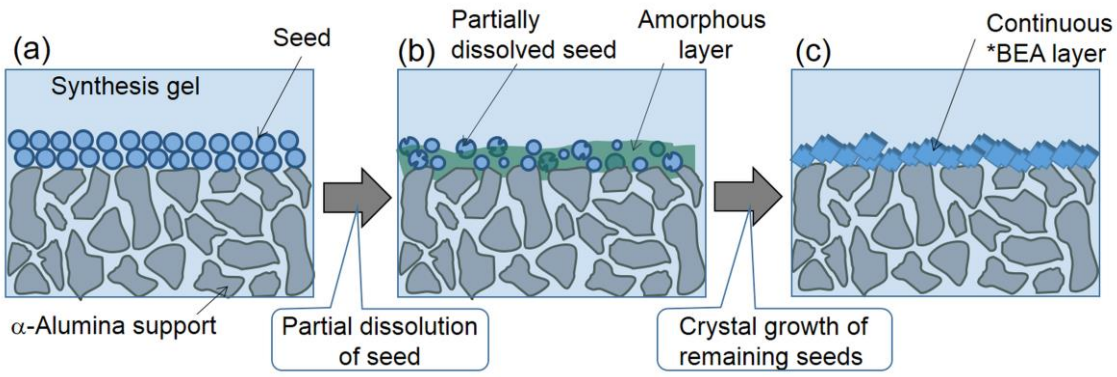

Figure 4.8 Schematic diagram of formation process of OSDA-free *BEA membrane.

4.3.2. Permeation and separation properties

Figure 4.9 shows the results of vapor permeation tests in unary systems for evaluation of the molecular sieving property of prepared OSDA-free *BEA membrane. It was found that the *n*-hexane and cyclohexane permeances increased upon increasing the membrane temperature, likely due to the diffusivities of these molecules increasing in the *BEA membrane micropores at higher temperatures. In contrast, the permeance of 1,3,5-trimethylbenzene (TMB) was two orders of magnitude smaller than those of *n*-hexane and cyclohexane. At 623 K, the permeances of *n*-hexane and cyclohexane were 1.1×10^{-7} and 1.0×10^{-7} mol m^{-2} s^{-1} Pa^{-1}, respectively. As a result, the ideal selectivities of *n*-hexane/TMB and cyclohexane/TMB were 107 and 100.

It is known that the dimensions of a molecule are important to understand size exclusion in zeolites [15]. Thus, at least two dimensions of the molecule should be smaller than the diameter of the cylindrical pore of *BEA, ca. 0.66 nm, to allow it to enter the pore. The smallest and

second-smallest dimensions of *n*-hexane, cyclohexane and TMB are 0.401 × 0.454, 0.498 × 0.658, and 0.406 × 0.818 nm, respectively [16]. Therefore, *n*-hexane and cyclohexane permeate easily through *BEA membrane, while TMB is not able to enter the micropores due to its bulky size. Accordingly, the small TMB permeance observed indicated that the *BEA membrane had very few defects that allowed TMB permeation. In other words, *BEA membrane exhibited superior molecular sieving property over a wide temperature range up to 623 K.

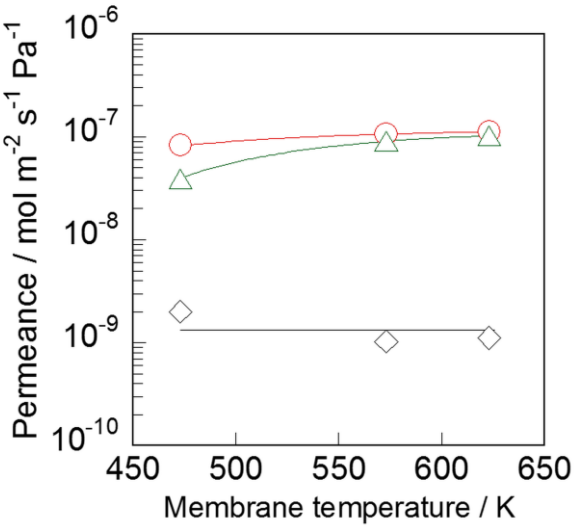

Figure 4.9 Temperature dependencies of hydrocarbon permeances in unary systems. ○, *n*-hexane; △, cyclohexane; ◇, 1,3,5-trimethylbenzene.

In Table 4.1, I compare our results with previous reports on the permeation and separation properties of *BEA membranes, where the previously reported examples were prepared using TEA^+ as OSDA [17-19]. It was found that the permeances of a large molecule, ca. 1,3,5-triisopropylbenzene (TIPB), were one magnitude larger than that of TMB through the membrane prepared under OSDA-free conditions. I believe that the low permeance of TMB through our OSDA-free *BEA membrane was probably attributed to fewer defects within the membrane. Moreover, the high separation performance of the prepared OSDA-free *BEA membrane possibly resulted from omission of the undesirable calcination step that often damages membrane quality.

4.4. Conclusions

A thin *BEA membrane was successfully synthesized by a secondary growth method under OSDA-free conditions. I found that in the early stages of hydrothermal treatment, the seed crystals partially dissolved and an amorphous phase appeared. Subsequently, crystal growth of

the remaining seeds and heterogeneous crystallization from the amorphous layer occurred. Finally, a well-crystallized membrane was produced. The OSDA-free *BEA membrane prepared exhibited a high ideal selectivity for *n*-hexane/TMB and cyclohexane/TMB mixtures due to molecular sieving effect. Large molecule such as cyclohexane was able to penetrate *BEA membrane with a relatively high permeance, suggesting that this membrane could be considered a novel class of material for the separation of large hydrocarbons.

Table 4.1 Results of hydrocarbon permeation tests for various *BEA membranes

Components	PV or VP	Temperature / K	Permeance[(a)] / 10^{-8} mol m^{-2} s^{-1} Pa^{-1}	Separation factor or ideal selectivity / -	Ref.
n-Hexane /2,2-dimethylbutane	VP	473	20	5.0	f5
Trans/ cis-1,4-dimethylcyclohexane	VP	373	21	2.1	f5
1,3,5-Trimethylbenzene	PV	303	8.3[(b)]	-	f5
2-Methylpentane /2,2-dimethylbutane	PV	303	0.17[(b)]	1.5	f6
1,3,5-Trimethylbenzene	PV	298	26[(b)]	-	f26
n-Hexane /1,3,5-Trimethylbenzene	VP	623	11	107	This work
Cyclohexane /1,3,5-Trimethylbenzene	VP	623	10	100	This work

(a) Permeances of the preferentially penetrated components are shown in cases of binary systems.

(b) Permeances are calculated from dividing the flux by the saturated vapor pressure.

References

[1] Majano, G.; Delmotte, L.; Valtchev, V.; Mintova, S. Al-Rich Zeolite Beta by Seeding in the Absence of Organic Template. *Chem. Mater.* **2009**, 21, 4184-4191.

[2] Kamimura, Y.; Chaikittislip, W.; Itabashi, K.; Shimojima, A.; Okubo, T. Critical Factors in the Seed-Assisted Synthesis of Zeolite Beta and "Green Beta" from OSDA-Free Na+-Aluminosilicate Gels. *Chem. Asian J.* **2010**, 5, 2182-2191.

[3] Kamimura, Y.; Tanahashi, S.; Itabashi, K.; Sugawara, A.; Wakihara, T.; Shimojima, A.; Okubo, T. Crystallization Behavior of Zeolite Beta in OSDA-Free, Seed-Assisted Synthesis. *J.*

Phys. Chem. C. **2011**, 115, 744-750.

[4] Xie, B.; Song, J.; Ren, L.; Ji, Y.; Li, J.; Xiao, F.-S. Organotemplate-Free and Fast Route for Synthesizing Beta Zeolite. *Chem. Mater.* **2008**, 20, 4533-4535.

[5] Choi, J.; Jeong, H.-K.; Snyder, M.A.; Storger, J.A.; Masel, R.I.; Tsapatsis, M. Grain Boundary Defect Elimination in a Zeolite Membrane by Rapid Thermal Processing. *Science,* **2003**, 325, 590-593.

[6] Dong, J.; Lin, Y.S.; Hu, M.Z.-C.; Peascoe, R.A.; Payzant, E.A. Template-removal-associated microstructural development of porous-ceramic-supported MFI zeolite membranes. *Micropor. Mesopor. Mater.* **2000**, 34, 241-253.

[7] Pan, M.; Lin, Y.S. Template-free secondary growth synthesis of MFI type zeolite membranes. *Micropor. Mesopor. Mater.* **2001**, 43, 319-327.

[8] Yuan, W.; Lin, Y.S.; Yang, W. Molecular Sieving MFI-Type Zeolite Membranes for Pervaporation Separation of Xylene Isomers. *J. Am. Chem. Soc.* **2004**, 126, 4776-4777.

[9] Li, G.; Kikuchi, E.; Matsukata, M. The control of phase and orientation in zeolite membranes by the secondary growth method. *Micropor. Mesopor. Mater.* **2003**, 62, 211-220.

[10] Tang, Y.; Liu, X.; Nai, S.; Zhang, B. Template-free synthesis of beta zeolite membranes on porous α-Al_2O_3 supports. *Chem. Commun.* **2014**, 50, 8834-8837.

[11] Schoeman, B.J.; Babouchkina, E.; Mintova, S.; Valtchev, V.P.; Sterte, J. The Synthesis of Discrete Colloidal Crystals of Zeolite Beta and their Application in the Preparation of Thin Microporous Films. *J. Porous Mater.* **2001**, 8, 13-22.

[12] Sasaki, Y.; Yoshida, Y.; Fisher, C.A.J.; Ikeda, T.; Itabashi, K.; Okubo, T. Polytype distributions in low-defect zeolite beta crystals synthesized without an organic structure-directing agent. *Micropor. Mesopor. Mater.* **2016**, 225, 210-215.

[13] Saito, A.; Foley, H.C. Curvature and Parametric Sensitivity in Models for Adsorption in Micropores. *AIChE J.* **1991**, 37, 429-436.

[14] Saito, A.; Foley, H.C. Argon porosimetry of selected molecular sieves: experiments and examination of the adapted Horvath-Kawazoe model. *Microporous Mater.* **1995**, 3, 531-542.

[15] Csicsery, S.M. Shape-selective catalysis in zeolites. *ZEOLITES* **1984**, 4, 202-213.

[16] Webster, C.E.; Drago, R.S.; Zerner, M.C. Molecular Dimensions for Adsorptives. *J. Am. Chem. Soc.* **1998**, 120, 5509-5516.

[17] Tuan, V.A.; Weber, L.L.; Falconer, J.L.; Noble, R.D. Synthesis of B-Substituted β-Zeolite Membranes. *Ind. Eng. Chem. Res.* **2003**, 42, 3019-3021.

[18] Maloncy, M.L.; van der Berg, A.W.C.; Gora, L.; Jansen, J.C. Preparation of zeolite beta membranes and their pervaporation performance in separating di- from mono-branched alkanes. *Micropor. Mesopor. Mater.* **2005**, 85, 96-103.

[19] Chen, Y.; Zhu, G.; Peng, Y.; Yao, X.; Qiu, S. Synthesis and characterization of (*h0l*) oriented high-silica zeolite beta membrane. *Micropor. Mesopor. Mater.* **2009**, 124, 8-14.

Chapter 5 Permeation and separation property Ag-*BEA membrane for olefin recovery

5.1. Introduction

In Chapters 2 and 3, I showed that Ag-X membrane shows high permeation and separation performance for olefin/paraffin mixtures. To study possibility of olefin recovery by using Ag-exchanged zeolite membrane other than X-type zeolite, I have developed *BEA-type zeolite which is a kind of large pore zeolites similar to X-type zeolite in Chapter 4. The *BEA membrane synthesized under OSDA-free conditions had a specific feature, large ion-exchange capacity. I expect that such *BEA membrane having large ion-exchange capacity is suitable membrane material for olefin separation. In this chapter, I prepared Ag-*BEA membrane and investigated the olefin separation and permeation performance.

5.2. Experimental

5.2.1. Preparation procedure of Ag-*BEA membrane

OSDA-free *BEA membrane, containing Na^+ as counter cation, was prepared by a seed assisted method. The synthesis procedure was described in Chapter 4. OSDA-free Na-*BEA membrane formed on the outer surface of support. A porous tubular α-alumina (o.d. = 10 mm, i.d. = 7 mm, length = 30 mm, average pore size = 150 nm) was used as a support.

Ag-*BEA membrane for propylene/propane and ethylene/ethane separation was prepared by the ion-exchange of OSDA-free Na-*BEA membrane with 10 mM of silver nitrate aqueous solution. The membrane was immersed in $AgNO_3$ aqueous solution for 1 h at 353 K while stirring. Then, *BEA membrane was washed with distilled water and dried at 343 K overnight prior to use.

5.2.2. Separation measurement

Permeation and separation properties for olefin/paraffin mixtures were evaluated, as follows. A mixture of ethylene/ethane, propylene/propane, propylene/N_2, ethylene/N_2, or ethylene/ethane/propylene/propane was fed to the outer surface of tubular support. The permeate side, the inside of tubular support, was swept with argon and both of feed and permeate sides were kept at atmospheric pressure.

In the permeation and separation measurements, the permeation flow rate was determined by a gas chromatography equipped with a flame ionization detector (GC-FID, GC-8A, Shimadzu) by using internal standard gas, methane. Permeation flux, *J*, was calculated as follows.

J_X (mol m^{-2} s^{-1}) = $u_X A^{-1}$ (2)

u_X is the flow rate (mol s^{-1}) of component X and A is the membrane area (m^2). And then, permeance, Π, and separation factor $\alpha_{X/Y}$ were determined using the following equations (3) and (4);

Π_X (mol m^{-2} s^{-1} Pa^{-1}) = $J\,\Delta p_X^{-1}$ (3)

$\alpha_{X/Y}$ (−) = $Y_A\,Y_B^{-1}\,X_A^{-1}\,X_B$ (4)

where X_A and X_B are molar fractions of components A and B in the feed. Y_A and Y_B are molar fractions of components A and B in permeate, respectively.

5.3. Results and discussion

5.3.1. Propylene/propance and ethylene/ethane separation performance

Figures 5.1(a) and (b) shows the photos of Na-*BEA and Ag-*BEA membrane prepared, respectively. The Ag-*BEA membrane was prepared by ion-exchange with $AgNO_3$ aqueous solution for Na-*BEA. By ion-exchange, the color of membrane surface changed from white to light gray. A thin and compact layer of Ag-*BEA crystals synthesized on the outer surface of support are observed in typical FE-SEM images, as shown in figures 5.1(c) and (d).

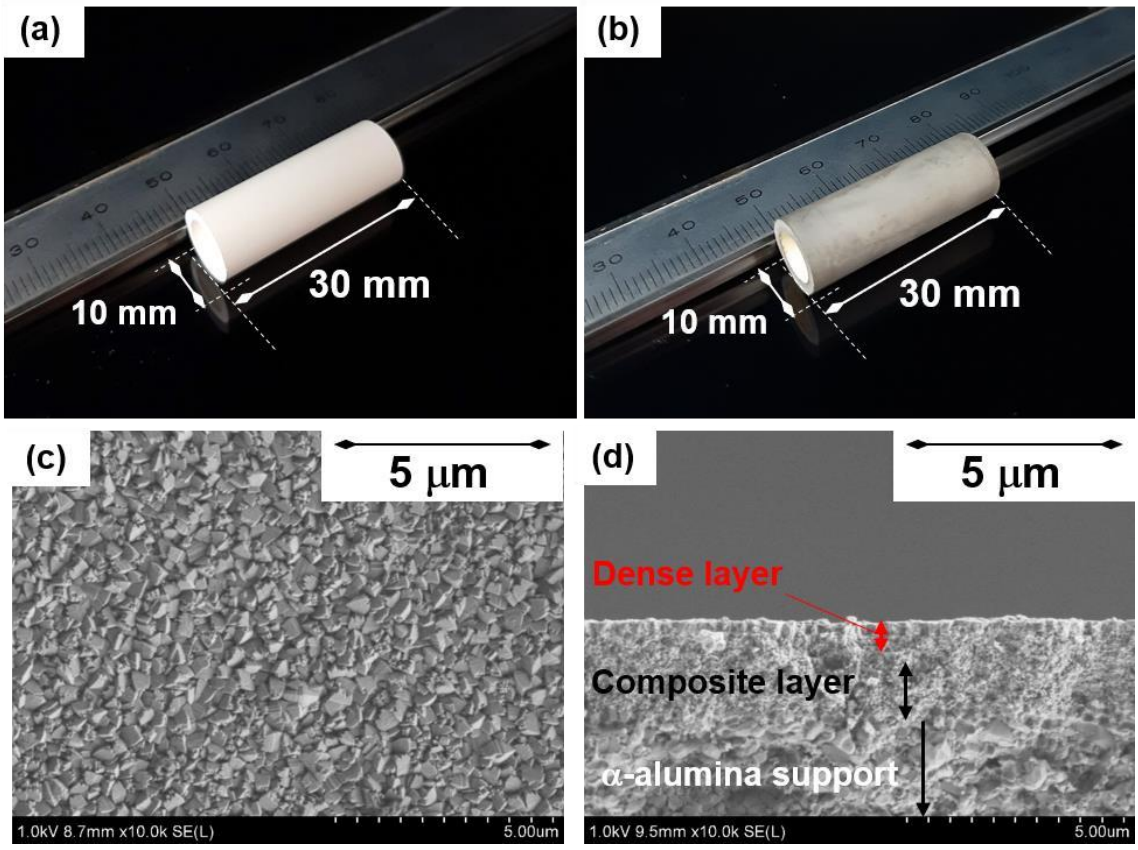

Figure 5.1 Photos of (a) Na-, (b) Ag-*BEA membrane synthesized on α-alumina support.

Typical FE-SEM images of (c) surface and (d) cross-section of Ag-*BEA membrane.

I investigated the effect of Ag cation introduction on the permeation and separation properties. Figure 5.2 shows the results of separation tests for an equimolar ethylene/ethane mixture through (a) Na- and (b) Ag-*BEA membranes. The ethane permeance markedly decreased to less than a tenth by changing cation from Na to Ag cations, resulting in that the separation factor of ethylene/ethane drastically increased from around 2 to above 60 by the ion-exchange. For example, the separation factor for ethylene through Ag-*BEA membrane at 333 K was 77.1 with its permeance of 1.04×10^{-7} mol m^{-2} s^{-1} Pa^{-1}. The ethylene permeances through both membranes increased with increasing temperature, possibly because the diffusivities of ethylene in these membranes improved at elevated temperature.

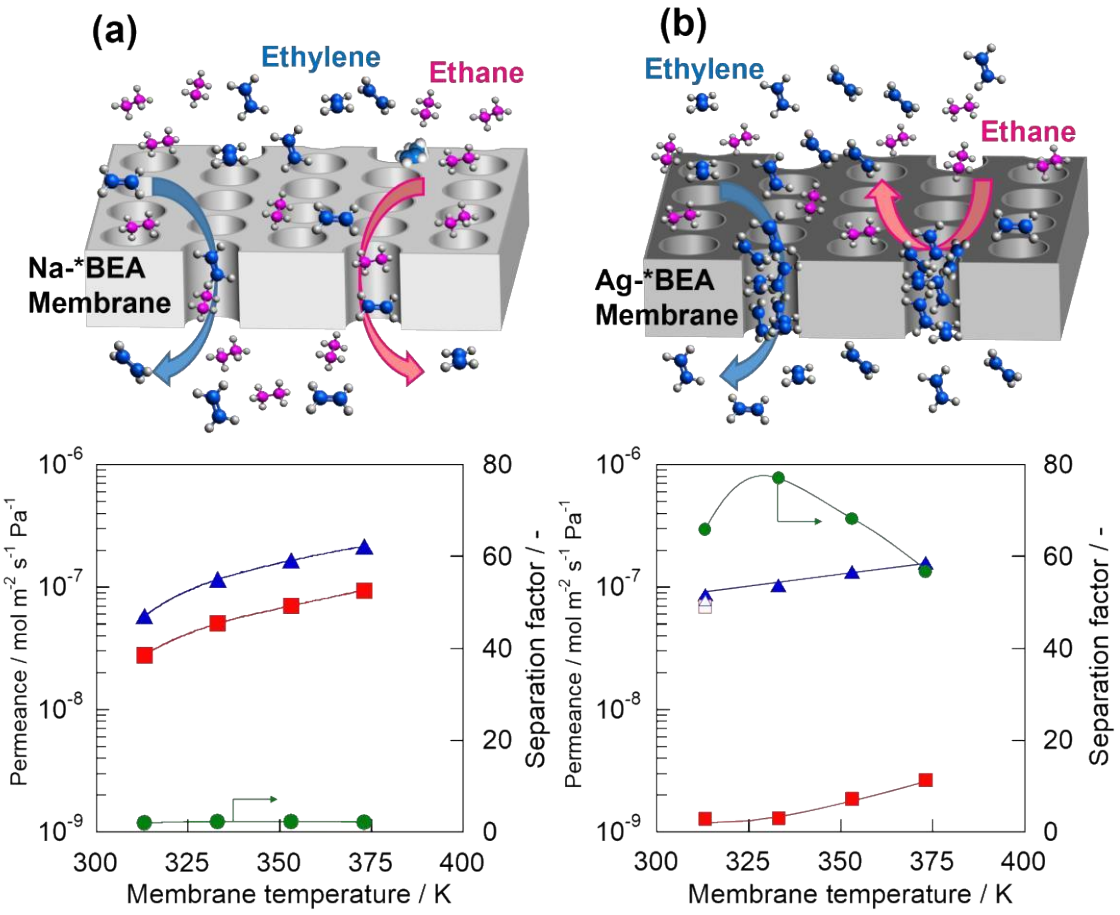

Figure 5.2 Results of separation tests for ethylene/ethane equimolar mixture through (a) Na-, (b) Ag-*BEA membrane. △, ethylene; □, ethane; ○, separation factor. Closed symbol, binary system; open symbol, unary system.

Figure 5.2 compares the permeances in the unary and binary systems. The permeances of ethylene and ethane in the unary systems at 313 K through Ag-*BEA membrane were plotted as open symbols in Figure 5.2 (b): The ethane permeance in the unary system was 10 times larger than that in the binary system. This phenomenon is similar to that observed with Ag-X membrane as described in Chapter 3. I consider that the remarkable reduction of ethane permeance in the binary system was caused by the filling of zeolite micropore with ethylene, as schematically drawn in figure 5.2 (b).

It is noted that the separation ability of Ag-*BEA for the ethylene/ethane mixture was much superior to that of Ag-X membrane which I previously reported, 15.9 at 303 K. A relatively smaller pore size of *BEA-type zeolite, 0.66 nm, may contribute to blocking of ethane permeation by ethylene compared with that of X-type zeolite, 0.74 nm.

Figure 5.3 shows the separation properties of (a) Na-, (b) Ag-*BEA membranes for an equimolar propylene/propane mixture. The permeation behaviors of propylene and propane were almost the same as those observed in the ethylene/ethane separation. The propylene permeance through Ag-*BEA membrane was several times smaller than that of ethylene: The separation factor at 373 K was 82.9 with the propylene permeance of 3.57×10^{-8} mol m^{-2} s^{-1} Pa^{-1}. Ethylene would have a larger diffusivity in micropore because of its small size compared with propylene, resulting in its larger permeance.

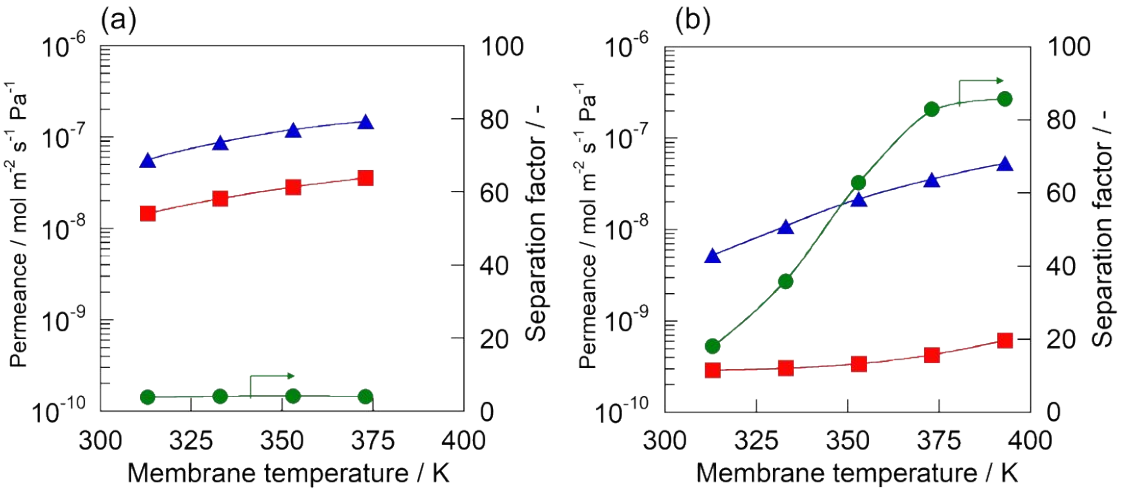

Figure 5.3 Results of separation tests for propylene/propane equimolar mixture through (a) Na-, (b) Ag-*BEA membrane. △, propylene; □, propane; ○, separation factor.

5.3.2. Adsorption properties of olefins and paraffins on Ag-*BEA membrane

I herein studied the adsorption properties of ethylene, ethane, propylene, and propane on Ag-*BEA membrane, as shown in figure 5.4. Each isotherm was evaluated at 313 K in the

unary systems. To obtain precise isotherms, a sample holder and measurement equipment that I specially designed enabled us to insert the whole membrane without destruction with a minimized dead-volume, leak, and accurate control of temperature. It is noteworthy that the adsorbed amounts of ethylene and propylene on Ag-*BEA membrane markedly increased at very low pressures at around 10^{-3} kPa.

The adsorption equilibrium constants, K (Pa^{-1}) were calculated from the isotherms according to the Langmuir's equation as follows.

$$P\,V^{-1} = P\,Vs^{-1} + K^{-1}\,Vs^{-1} \qquad (5)$$

where P is the pressure (Pa), V is the amount adsorbed (cm^3(STP) g^{-1}), and V_S is the saturated adsorption amount (cm^3(STP) g^{-1}). Therefore, the values of V_S and K are calculated from the slope and the intercept of $P\,V^{-1}$ vs. P plot. As a result, $K_{propylene}$ (1.78) and $K_{ethylene}$ (0.845) were much greater than $K_{propane}$ (0.475) and K_{ethane} (0.188).

I considered that Ag-*BEA membrane showed the high olefin selectivity based on such differences of affinity with Ag cation between olefin and paraffin. As in the case of Ag-X membrane, adsorption of olefins on Ag-*BEA membrane play an important role for expression of olefin selectivity.

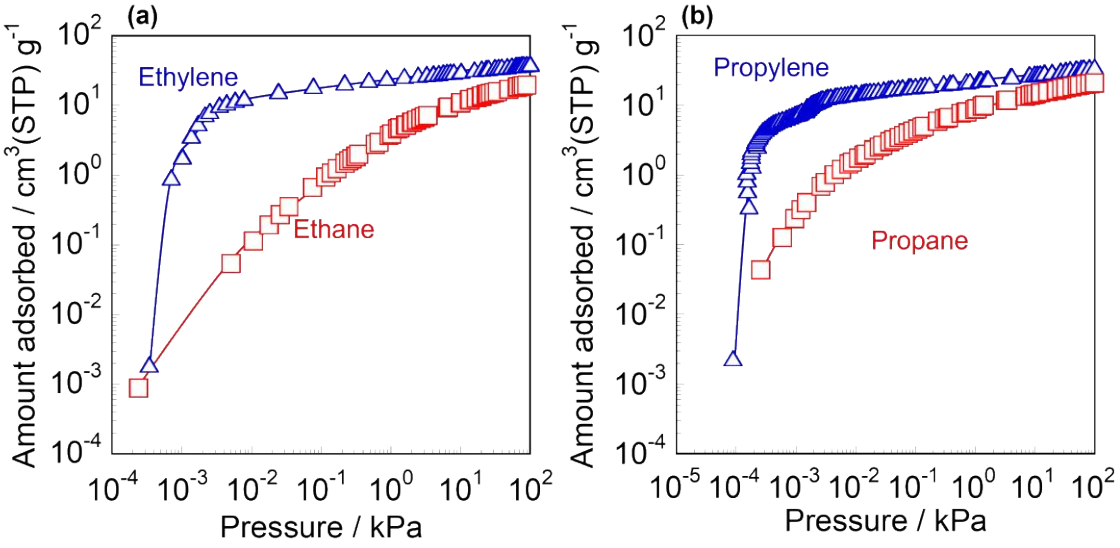

Figure 5.4 Adsorption isotherms on Ag-*BEA membrane at 313 K. (a) △, ethylene and □, ethane. (b) △, propylene and □, propane.

As shown in figures 5.2 and 5.3, Ag-*BEA membrane exhibited superior separation performance for both ethylene/ethane and propylene/propane mixtures. Although many studies about molecular sieving membranes for the propylene/propane or ethylene/ethane separation have been reported as described above, these molecular sieving membranes have shown a high

selectivity for either ethylene or propylene. Suitable pore sizes for ethylene/ethane and propylene/propane separation by molecular sieving are different. In other words, individual membranes have to be used for each separation system. For example, it was reported that a separation factor of ZIF-8 membrane for propylene/propane exceeded 100 [1], whereas that for ethylene/ethane was only 2.0 [2], suggesting that ZIF-8 is a promising membrane material for propylene/propane separation by size. Its pore size is, however, too large to separate ethylene/ethane.

I compared the performance of Ag-*BEA membrane to those of other (a) propylene [1,3-11] and (b) ethylene [2,12-18] selective inorganic membranes previously reported, as shown in Figure 5.5. These Robeson plots clearly show that Ag-*BEA membrane is promising owing to the larger permeance and superior selectivity to olefin for the separation of olefin/paraffin mixture. In particular, the separation and permeation properties of Ag-*BEA membrane for ethylene/ethane overwhelms those of other membranes. The ethylene permeance was four orders of magnitude larger than that those through membranes showing similar separation factors like CMS; The separation factor was about 30-times greater than those through membranes showing the subequal permeances like ZIF-8.

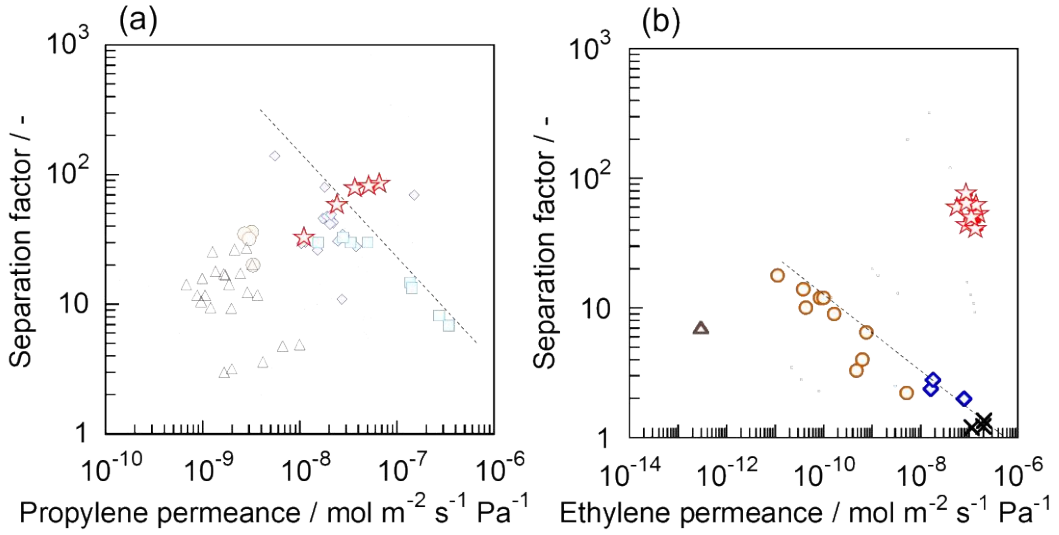

Figure 5.5 Robeson plots of (a) propylene/propane and (b) ethylene/ethane separations. ○, CMS; ◇, ZIF-8; □, silica; △, mixed matrix; ×, alumina; ☆, Ag-*BEA (this study).

5.3.3. Comparing of Ag-X and Ag-*BEA membranes

Here I discuss the differnce of separation properties of Ag-*BEA and Ag-X membranes. The separation performance could be influenced by pore size, Si/Al ratio and defect amount in membrane. As mentioned above, the smaller pore size of *BEA (0.66 nm) compared to X (0.74

nm) may contribute the high separation performance because preferentially adsorbed molecule have to block the permeation of other molecules in the case of affinity-based separation. In contrast, the high Si/Al ratio of *BEA (ca. 5) relative to that of X (1.5) may not feasible for olefin separation. Unfortunately, I am not able to clear the quantitative effect of these factors on separation performance.

The amount of non-zeolitic pathway through Ag-*BEA and Ag-X membranes were evaluated by using nano-permporometry. Nano-permporometry was performed by using Porometer nano-6 (MicrotracBEL Corp ., Japan BEL, Japan Inc .). Permeate flow rate of inert gas through the membrane was measured while the relative pressure of vapor was increased in a step-wise manner. In this process, pores in the membrane were plugged by condensation of vapor in the order of pore size from smallest to largest, and then permeate flow rate of inert gas decreased. Pore size distribution could be calculated by a relationship between the relative pressure of vapor and flow rate. In the measurement, *n*-hexane and helium were used as condensable vapor nad inert gas, respectively. Membrane temperature was fixed at 333 K.

We defined a ratio of the non-zeolitic pathway to all pathways for quantitative discussion about the effect of the non-zeolitic pathway on molecular sieving ability. The ratio of the non-zeolitic pathway was calculated as dividing helium permeance at $p\ ps^{-1}$ of 0.1 by the permeance at $p\ ps^{-1}$ of 0 according to a previous report by Hedlund *et al.* [19]. Helium permeance at $p\ ps^{-1}$ of 0 means the permeance through all pathways. Besides, helium permeance at $p\ ps^{-1}$ of 0.1 means through non-zeolitic pathway having more than ca. 1 nm of diameter determined based on the Kelvin equation. Therefore, the ratio of the non-zeolitic pathway was larger than 1 nm to all pathways can be evaluated.

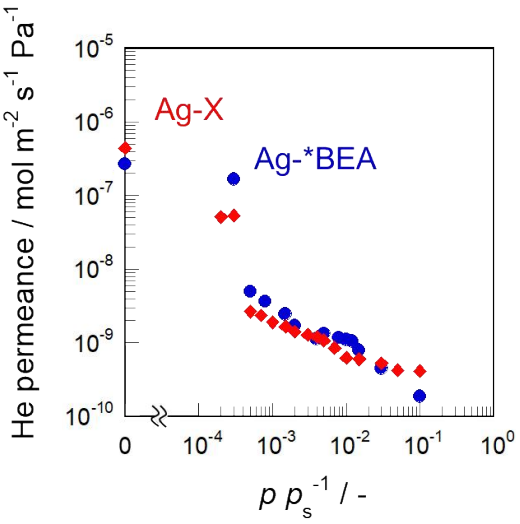

Figure 5.6 The results of nano-permporometry tests for Ag-*BEA and Ag-X membranes

Figure 5.6 shows the results of nano-permporometry tests for Ag-*BEA and Ag-X membranes. From the results of nano-permporometry tests, the ratio of non-zeolitic pathways through Ag-*BEA and Ag-X membranes were 0.068 and 0.093 %, respectively. This results strongly suggested that the small amount of defects in Ag-*BEA membrane contributed to its separation performance. When I assume that the separation factor of permeation flow through non-zeolitic pathways are 1, ideal permeances without defect can be estimated as follows. Permeance without defect was calculated by taking difference between the original permeance in separation test and helium permeance at $p\,ps^{-1}$ of 0.1 in nano-permporometry test.

Table 5.1 shows the calculated permeances and separation factors based on the results of nano-permporometry. Here, the permeances of ethylene, ethane, propylene and propane at 333 K in figures 2.11 and 2.6 were used as original permeance through Ag-X membrane. In the same manner, these permeances at 333 K shown in figures 5.2 and 5.3 were used for Ag-*BEA membrane. The calculated separation factors by ignoring the effect of defect overwhelmed original separation factors. For example, the separation factors for propylene/propane through Ag-X and Ag-*BEA membranes increased from 52.5 and 35.9 to 597 and 93.1, respectively. I can concluded that the high separation performance of Ag-*BEA membrane shown in Chapter 5 was based on the relatively high compactness. In addition, the separation performances of Ag-X and Ag-*BEA are able to increase by reducing defects. These results agreed with the results shown in figures 3.7 and 3.8.

Table 5.1 Calculated ideal permeances and separation factors based on the results of nano-permporometry

(a) Ethylene/ethane separation

	[A]	[B]		[B]-[A]		Ideal
	He permeance at $p\,ps^{-1}$ = 0.1 / 10^{-9} mol m^{-2} s^{-1} Pa^{-1}	Original permeance / 10^{-9} mol m^{-2} s^{-1} Pa^{-1}		Ideal permeance / 10^{-9} mol m^{-2} s^{-1} Pa^{-1}		Separation factor
		ethylene	ethane	ethylene	ethane	
Ag-*BEA	0.189	104	1.31	104	1.12	92.6
Ag-X	0.412	126	12.2	126	11.8	10.7

(b) Propylene/propane separation

	[A]	[B]	[B]-[A]	Ideal
	He permeance at	Original permeance / 10^{-9}	Ideal permeance / 10^{-9}	Separation

	$p\ ps^{-1} = 0.1 / 10^{-9}$	mol m^{-2} s^{-1} Pa^{-1}		mol m^{-2} s^{-1} Pa^{-1}		factor
	mol m^{-2} s^{-1} Pa^{-1}	Propylene	propane	propylene	propane	
Ag-*BEA	0.189	10.9	0.304	10.7	0.115	93.1
Ag-X	0.412	23.7	0.451	23.3	0.039	597

5.3.4. Other applications of Ag-*BEA membrane

I would like to propose a possible new purification process for olefin production by using olefin-selective Ag-*BEA membrane. Currently, ethylene and propylene were purified from a mixture of C_1-C_4 hydrocarbons by a series of distillations [20] shown in figure 5.7(a). In this process, methane was removed by the first distillation tower, and then ethylene and ethane were separated from the remained C_2-C_4 mixture. C_4 hydrocarbons were, then, separated from C_3-C_4 mixture. The obtained mixture of ethylene/ethane and propylene/propane were fed to distillation towers for ethylene and propylene purifications, respectively. These distillation towers for ethylene and propylene purification consume most of the energy of the whole purification system mainly because of a small deference of boiling points at low temperature and a high reflux ratio (Δb.p. of ethylene and ethane, 15 K; Δb.p. of propylene and propane, 5.6 K).

Taking the advantage of affinity-based olefin separation, I would like to propose a novel olefin purification process to reduce the energy cost and number of distillation tower (shown in figure 5.7(b) in supporting information). After removing methane in the first distillation tower, the mixture of C_2-C_4 is fed to a membrane unit for separating olefins and paraffins. In this system, a mixture of ethylene, propylene, and butenes would be recovered from the permeate side and that of ethane, propane, and butanes remained in the retentate side, respectively. Each mixture of C_2-C_4 which have large differences of boiling points (Δb.p. of ethylene and propylene, 56 K; Δb.p. of propylene and 1-butene, 41 K) can be separated easily by a distillation with low energy consumption.

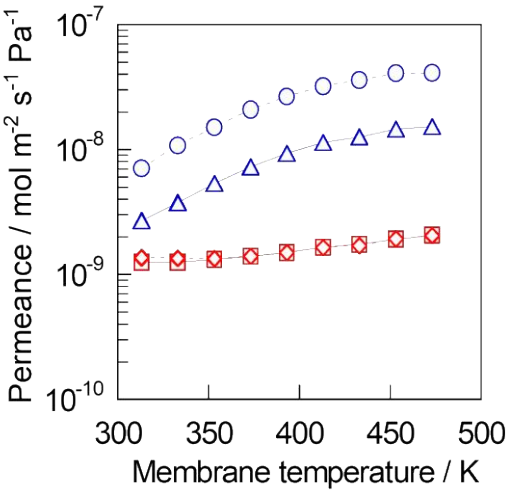

Figure 5.7 Results of separation tests for ethylene/ethane/propylene/propane equimolar mixture through Ag-*BEA membrane. △, ethylene; □, ethane; ○, propylene; ◇, propane.

Figure 5.8 shows the separation performance of Ag-*BEA membrane for an equimolar mixture of ethylene/ethane/propylene/propane. As expected, both propylene and ethylene selectively permeated from the ternary mixture through Ag-*BEA membrane.

Affinity-based membrane separation found in this study would have a pottential to innovate the purification processes in olefin production process such as naphsa cracking and fluid catalytic cracking. The separation property shown in figure 5.8 suggeted that olefin purity in the permeate reached above 93% from 50% in the feed.

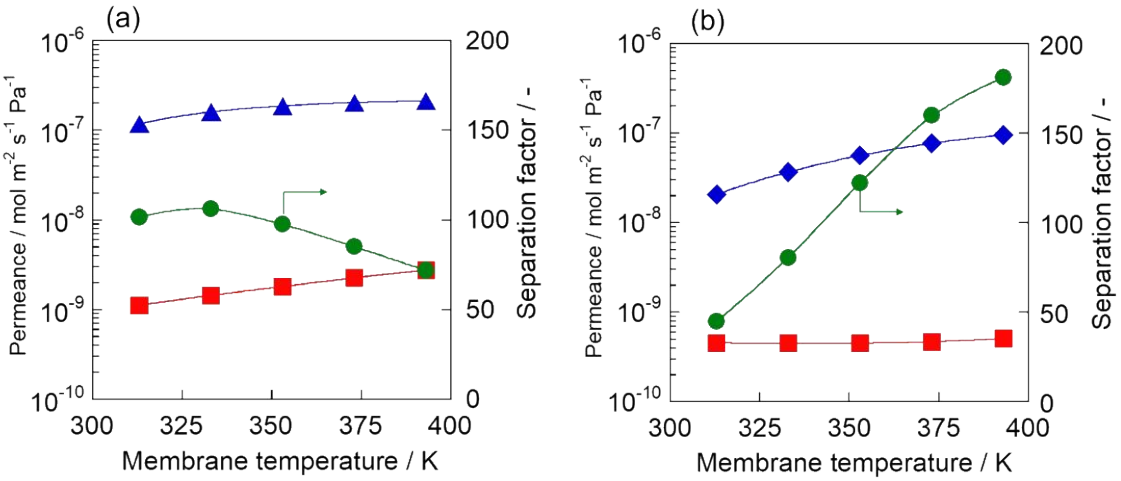

Figure 5.8 Results of separation tests for olefin/N_2 mixture through Ag-*BEA membrane. (a) $C_2^=/N_2$. (b) $C_3^=/N_2$. △, olefins; □, N_2; ○,separation factor.

In addition, I found that Ag-*BEA membrane exhibited high olefin selectivities in olefin/N_2

separation tests (olefin/N_2 = 15/85 kPa), as shown in figure 5.9. Whereas N_2 is smaller than both ethylene and propylene, Ag-*BEA membrane showed excellent ethylene and propylene selectivities of 106 at 333 K and 181 at 393 K, respectively.

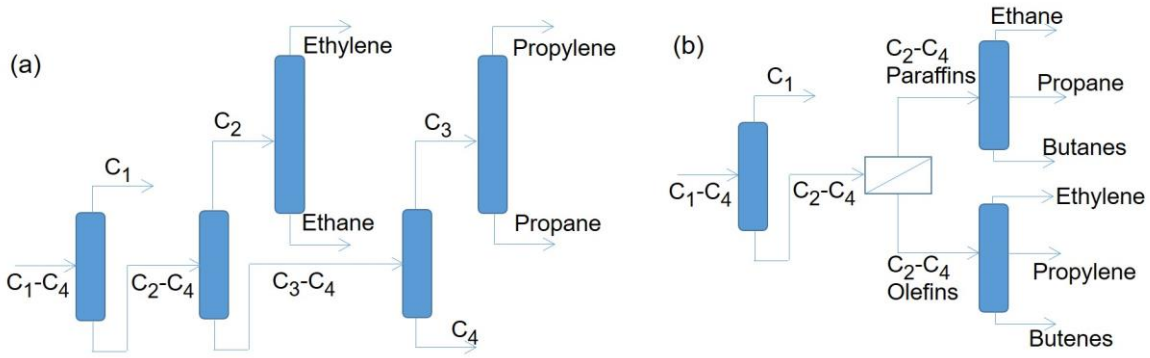

Figure 5.9 Olefin purification system from C_2-C_4 hydrocarbon mixture. (a) conventional process and (b) novel process including olefin concentration membrane.

In polymerization plant, unreacted monomers such as ethylene and propylene are removed from polymers by purge gas, nitrogen. The vent gas contains around 10-20 vol% of monomer in nitrogen. The value of unrecovered monomers reached a million dollar annually at a typical polymerization plant [21]. Although some recovery process using rubbery polymeric membrane have been proposed, separation performances of silicone rubbery membranes ($C_2^=/N_2$ = 6.3, $C_3^=/N_2$ = 16.2) were not sufficient [22].

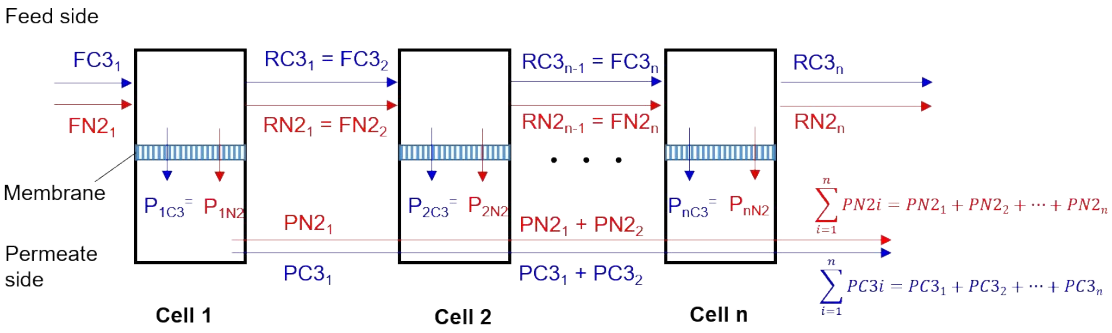

Figure 5.10 A model of calculation for $C_3^=/N_2$ mixture separation using Ag-*BEA membrane.

Here I estimate that how much propylene can be recovered by using this Ag-*BEA membrane from the purged gas. Figure 5.10 shows a model of calculation for $C_3^=/N_2$ mixture separation using Ag-*BEA membrane. Membrane unit was divided as series of micro cell. At first, feed stream ($C_3^=/N_2$ = 15/85 mol%) was inlet to the first cell. Permeation flow rates of $C_3^=$

and N_2 in the first cell were calculated according to equation (6). And then, retentate flow rates of $C_3^=$ and N_2 in the first cell were calculated according to equation (7). The retentate flow rate became the feed flow rate of the second cell.

$$P_X \text{ (mol s}^{-1}) = \Pi_X A \Delta C_X \quad (6)$$

$$F_X \text{ (mol s}^{-1}) = P_X + R_X \quad (7)$$

Here, F_X, P_X, R_X, Π_X are feed flow rate (mol s^{-1}), permeate flow rate (mol s^{-1}), retentate flow rate (mol s^{-1}), and permeance of component X (mol m^{-2} s^{-1} Pa^{-1}), respectively. A is membrane area (m^2). ΔC_X is a partial pressure difference of component X between permeate and retentate side (Pa). Table 5.2 shows the feed and membrane conditions used in this calculation.

Figure 5.11 shows the purity of propylene permeated as a function of the propylene recovery ratio. The purity of propylene permeated decreased with increasing recovery ratio. For example, the propylene purity at the propylene recovery ratios of 0.50, 0.70, and 0.90 were 0.96, 0.95, and 0.92, respectively. In our elementary calculation, about seven-tenths of propylene purged could be recovered with 95 % of purity by using Ag-*BEA membrane with separation factor of 180. Olefin recoveries from purge gas in olefin polymerization processes would also be the targets to apply Ag-*BEA membrane to.

Table 5.2 Feed and membrane conditions used in this calculation

Feed flow rate / mol s^{-1}	$C_3^=$ = 15, N_2 = 85
Feed side pressure / kPa	100
Permeate side pressure / kPa	0.1
C3= permeance / mol m^{-2} s^{-1} Pa^{-1}	1.0×10^{-7}
N2 permeance / mol m^{-2} s^{-1} Pa^{-1}	5.6×10^{-10}
Permeance ratio / -	180
Membrane temperature / K	393
Number of cell / -	5300

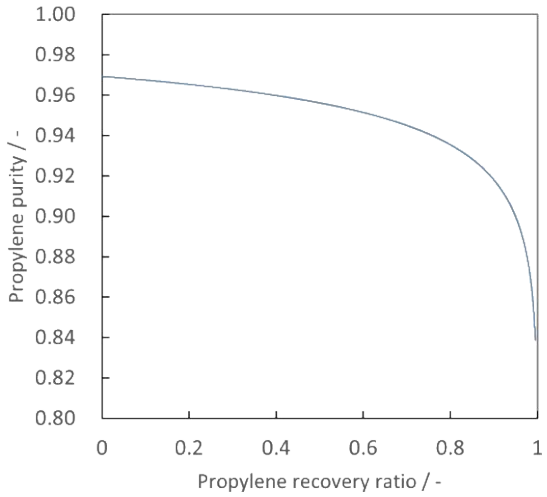

Figure 5.11 The purity of propylene permeated as a function of the propylene recovery ratio in propylene/nitrogen separation by Ag-*BEA membrane.

5.4. Conclusions

To enhance olefin selectivity, Ag cation was introduced by an ion-exchange method into *BEA-type zeolite membrane which was synthesized under OSDA-free conditions had a specific feature, large ion-exchange capacity. As I expected, Ag-*BEA membrane exhibited high olefin/paraffin separation as in the case of Ag-X membrane. In addition, the principle of affinity-based separation can apply to wide separation targets. Ag-*BEA membrane is a prospective material for olefin recovery from various gas mixture irrespective of each molecular size.

References

[1] Ma, X.; Kumar, P.; Mittal, N.; Khlyustova, A.; Daoutidis, P.; Mkhoyan, K.A.; Tsapatsis, M. Zeolitic imidazolate framework membranes made by ligand-induced permselectivation. *Science* **2018**, *361*, 1008-1011.

[2] James, J.B.; Wang, J.; Meng, L.; Lin, Y.S. ZIF‐8 Membrane Ethylene/Ethane Transport Characteristics in Single and Binary Gas Mixtures. *Ind. Eng. Chem. Res.* **2017**, *56*, 7567-7575.

[3] Kanezashi, M.; Shazwani, W.N.; Yoshioka, T.; Tsuru, T. Separation of propylene/propane binary mixtures by bis(triethoxysilyl) methane (BTESM)-derived silica membranes fabricated at different calcination temperatures. *J. Membr. Sci.* **2012**, *415-416*, 478-485.

[4] Hayashi, J.; Mizuta, H.; Yamamoto, M.; Kusakabe, K.; Morooka, S.; Suh, S.-H. Separation of Ethane/Ethylene and Propane/Propylene Systems with a Carbonized BPDA−pp‘ODA

Polyimide Membrane. *Ind. Eng. Chem. Res.* **1996**, *35*, 4176-4181.

[5] Pan, Y.; Li, T.; Lestari, G.; Lai, Z. Effective separation of propylene/propane binary mixtures by ZIF-8 membranes. *J. Membr. Sci.* **2012**, *390-391*, 93-98.

[6] Kwon, H.T.; Jeong, H.-K. *In Situ* Synthesis of Thin Zeolitic–Imidazolate Framework ZIF-8 Membranes Exhibiting Exceptionally High Propylene/Propane Separation. *J. Am. Chem. Soc.* **2013**, *135*, 10763-10768.

[7] Xu, L.; Rungta, M.; Brayden, M.K.; Martinez, M.V.; Stears, B.A.; Barbay, G.A.; Koros, W.J. Olefins-selective asymmetric carbon molecular sieve hollow fiber membranes for hybrid membrane-distillation processes for olefin/paraffin separations. *J. Membr. Sci.* **2012**, *423-424*, 314-323.

[8] Das, M.; Koros, W.J. Performance of 6FDA–6FpDA polyimide for propylene/propane separations. *J. Membr. Sci.* **2010**, *365*, 399-408.

[9] Ma, X.; Lin, B.K.; Wei, X.; Kniep, J.; Lin, Y.S. Gamma-Alumina Supported Carbon Molecular Sieve Membrane for Propylene/Propane Separation. *Ind. Eng. Chem. Res.* **2013**, *52*, 4297-4305.

[10] Sun, H.; Ma, C.; Wang, T.; Xu, Y.; Yuan, B.; Li, P.; Kong, Y. Preparation and Characterization of C_{60}-Filled Ethyl Cellulose Mixed-Matrix Membranes for Gas Separation of Propylene/Propane. *Chem. Eng. Technol.* **2014**, *37*, 611-619.

[11] Askari, M.; Chung, T.-S. Natural gas purification and olefin/paraffin separation using thermal cross-linkable co-polyimide/ZIF-8 mixed matrix membranes. *J. Membr. Sci.* **2013**, *444*, 173-183.

[12] Xu, L.; Rungta, M.; Koros, W.J. Matrimid derived carbon molecular sieve hollow fiber membranes for ethylene/ethane separation. *J. Membr. Sci.* **2011**, *380*, 138-147.

[13] Liao, K.-S.; Japip, S.; Lai, J.-Y.; Chung, T.-S. Boron-embedded hydrolyzed PIM-1 carbon membranes for synergistic ethylene/ethane purification. *J. Membr. Sci.* **2017**, *534*, 92-99.

[14] Salinas, O.; Ma, X.; Wang, Y.; Han, Y.; Pinnau, I. Carbon molecular sieve membrane from a microporous spirobisindane-based polyimide precursor with enhanced ethylene/ethane mixed gas selectivity. *RSC Adv.* **2017**, *7*, 3265-3272.

[15] Chu, Y.-H.; Yancey, D.; Xu, L.; Martinez, M.; Brayden, M.; Koros, W. Iron-containing carbon molecular sieve membranes for advanced olefin/paraffin separations. *J. Membr. Sci.* **2018**, *548*, 609-620.

[16] Lin, Y.S.; Ji, W.; Wang, Y.; Higgins, R.J. Cuprous-Chloride-Modified Nanoporous Alumina Membranes for Ethylene−Ethane Separation. *Ind. Eng. Chem. Res.* **1999**, *38*, 2292-2298.

[17] Ploegmakers, J.; Japip, S.; Nijmeijer, K. Mixed matrix membranes containing MOFs for ethylene/ethane separation Part A: Membrane preparation and characterization. *J. Membr. Sci.*

2013, *428*, 445-453.

[18] Ilinich, O.M.; Zamaraev, K.I. Separation of ethylene and ethane over polyphenyleneoxides membranes: transient increase of selectivity. *J. Membr. Sci.* **1993**, *82*, 149-155.

[19] Karimi, S.; Korelskiy, D.; Yu, L.; Mouzon, J.; Khodadadi, A.A.; Mortazavi, Y.; Esmaeili M.; Hedlund, J. A simple method for blocking defects in zeolite membranes. *J. Membr. Sci.* **2015**, *489*, 270-274.

[20] Takane, K.; Suzuki, K.; Matsuda, K.; Yamaki, T.; Endo, A. Design and Economic Evaluation of the Separation Processes using Inorganic Membrane Technology. *MEMBRANE* **2019**, *44*, 163-168.

[21] Baker, R.W.; Wijmans, J.G.; Kaschemekat, J.H. The design of membrane vapor-gas separation systems. *J. Membr. Sci.* **1998**, *151*, 55-62.

[22] Jiang, X.; Kumar, A. Performance of silicone-coated polymeric membrane in separation of hydrocarbons and nitrogen mixtures. *J. Membr. Sci.* **2005**, *254*, 179-188.

Chapter 6 General Conclusions

In this thesis, Ag-exchanged zeolite membranes were synthesized and their olefin separation performance were investigated. Adsorption properties of olefins on Ag-exchanged zeolite membranes were evaluated to shed light on the mechanism of olefin separation. Both Ag-X and Ag-*BEA membranes exhibited superior olefin permeation and separation properties by an affinity-based separation.

In Chapter 2, I found Ag-X membrane exhibited a superior propylene/propane and ethylene/ethane separation performance for the first time. Effect of ion exchange ratio on separation performance was studied. Olefin selectivity improved by ion exchange from Na to Ag cation in X-type zeolite membrane. Almost fully exchanged Ag-X membrane exhibited superior propylene selectivity which was 55.4 with its permeance of 4.13×10^{-8} mol m^{-2} s^{-1} Pa^{-1} at 353 K in a propylene/propane (50:50) binary system. This permselectivity is one of the highest values compared with various inorganic membranes. In addition, obvious deterioration of membrane performance was not observed during 10000 h for propylene/propane separation.

For Chapter 3, I explore the adsorption properties of propylene and propane on Ag-X membrane to understand the separation mechanism through the membrane. The isotherms of propylene and propane on Ag-X membrane were carefully measured by a non-destructive volumetric adsorption method. Thus, I can discuss quantitatively the relationship between adsorption properties and separation performance.

The molar fractions of propylene in the adsorbed phase in propylene/propane mixture was calculated. The calculated adsorbed amount in the binary system was in good agreement with the propylene purity on the permeation side of the Ag-X membrane. Thus, I concluded that the superior separation performance of the Ag-X membrane is mainly governed by adsorption selectivity in a binary system. This permeation mechanism is totally different from previous reports of diffusion selective membranes such as silica and ZIF-8 membranes.

As explained in Chapter 4, *BEA-type zeolite membrane was prepared by a hydrothermal secondary growth method in the absence of an organic structure directing agent. Because *BEA-type zeolite which is a kind of large pore zeolites similar to X-type zeolite and is often used as catalyst, I expect that *BEA membrane having large ion-exchange capacity is suitable membrane material for olefin separation.

Membrane formation process was carefully observed by using FE-SEM, XRD, and N_2 adsorption, and the role of seed crystals on the support surface was discussed. Seed crystals loaded on the outer surface of a tubular porous alumina support partially dissolved and a small amount of seeds remained in an amorphous layer formed on the support surface in the early

stage of secondary growth step. Subsequently, crystal growth of remaining crystals occurred, and a continuous *BEA layer was obtained following crystallization for 7 days at 393 K. In the secondary growth step, the supported seed layer played an important role in inducing the formation of a high local concentration in the vicinity of the support surface. The prepared OSDA-free *BEA membrane had very few defects and high ion-exchange capacity.

As presented in Chapter 5, to study possibility of olefin recovery by using Ag-exchanged zeolite membrane other than X-type zeolite, I prepared Ag-*BEA membrane and investigated its olefin separation and permeation performance. Ag-*BEA membrane exhibited superior olefin separation performance for both ethylene/ethane and propylene/propane mixtures. Particularly, the separation factor for ethylene at 373 K reached 57 with the ethylene permeance of 1.6×10^{-7} mol m^{-2} s^{-1} Pa^{-1}. Obtained Ag-*BEA is one of the promising membrane materials for ethylene separation; the separation factor for ethylene/ethane mixture was about 30-times greater than that through membranes having similar permeance such as metal organic framework membranes. Adsorption properties of olefin and paraffin were evaluated to discuss contribution of Ag^+ to separation performance enhancement. A strong interaction between olefin and Ag^+ in the membrane caused preferential adsorption of olefin against paraffin, leading to selective permeation of olefin. Ag-*BEA membrane also exhibited high olefin selectivities from olefin/N_2 mixtures. The affinity-based separation through Ag-*BEA membrane showed a high potential for olefin recovery and purification from various gas mixtures.

Finally, Ag-exchanged zeolite membranes for olefin separation from gaseous mixtures are summarized as follows.

Molecular sieving membranes certainly exhibit selectivity to smaller molecules, and then a molecular sieving membrane shows the selectivity for either ethylene or propylene. Obviously, the suitable pore sizes for ethylene/ethane and propylene/propane separation by molecular sieving are different. In contrast, Ag-exchanged zeolite membrane are able to recover olefins from various gas mixtures by the strong affinity between olefins and Ag^+. Ag-zeolite membranes exhibited high olefin selectivities from olefin/N_2 mixtures, whereas N_2 is smaller than both ethylene and propylene. This affinity-based separation found in this study would have a pottential to innovate the purification processes in olefin production and recovery as described above.

Acknowledgement

First of all, I would like to show my gratitude to my supervisor, Prof. Masahiko Matsukata. I cannot complete this thesis without his kind advices and fuirtful discussion.

I am also very grateful to all of the sub-chief examiners, Prof. Suguru Noda, Prof. Mikihiro Nomura, Prof. Yasushi Sekine and Prof. Atsushi Shimojima for giving me significant advice in my thesis defense. In addition, I would also give special thanks to collaborators, Prof. Hideki Tanaka in Shinshu University, Dr. Yukichi Sasaki and Dr. Kaname Yoshida in Japan Fine Ceramics Center for their investigations about membrane structure. I wish to express my sincere thanks to Prof. Tatsuya Okubo, Prof. Toru Wakihara, and Dr. Kenta Iyoki in the University of Tokyo, for fruitful discussion on the OSDA-free synthesis of *BEA zeolite.

I also deeply appriciate my co-authors, Mr. Naoyuki Fujimaki, Mr. Genki Kobayashi, Mr. Yasuhito Sasaki, Dr. Masahiko Seshimo, Mr. Yuto Tsuzuki, Mr. Taisuke Tomono, Mr. Yoshikazu Oshima and Mr. Noriyuki Yasuda for their efforts.

I give thanks to financial support by JST CREST (Japan Science and Technology agency, Create Revolutionary technological seeds for Science and Technology innovation program), Grant Number JPMJCR1324, Japan.

December 2021

List of research achievements for application of Doctor of Engineering, Waseda University

Full Name: Motomu SAKAI seal or signature

Date Submitted(yyyy/mm/dd): 2021/10/06

種類別 (By Type)	題名、 発表・発行掲載誌名、 発表・発行年月、 連名者（申請者含む） (theme, journal name, date & year of publication, name of authors inc. yourself)
○Article	Motomu Sakai, Yuto Tsuzuki, Naoyuki Fujimaki, Masahiko Matsukata, Olefin recovery by *BEA-type zeolite membrane: Affinity-based separation with olefin-Ag+ interaction, Chemistry An Asian Journal, 16 (2021) 1101-1105.
○Article	Motomu Sakai, Naoyuki Fujimaki, Yasuhito Sasaki, Noriyuki Yasuda, Masahiro Seshimo, Masahiko Matsukata, Preferential Adsorption of Propylene over Propane on Ag-exchanged X-type Zeolite Membrane, ACS Applied Materials & Interfaces, 12 (2020) 24086-24092.
○Article	Motomu Sakai, Naoyuki Fujimaki, Genki Kobayashi, Noriyuki Yasuda, Yoshikazu Oshima, Masahiro Seshimo, Masahiko Matsukata, Formation process of *BEA-type zeolite membrane under OSDA-free conditions and its separation property, Microporous and Mesoporous Materials, 284 (2019) 360-365.
○Article	Motomu Sakai, Yasuhito Sasaki, Taisuke Tomono, Masahiro Seshimo, Masahiko Matsukata, Olefin Selective Ag-exchanged X-type Zeolite Membrane for Propylene/Propane and Ethylene/Ethane Separation, ACS Applied Materials & Interfaces 11 (2019) 4145-4151.
Article	Motomu Sakai, Takuya Kaneko, Yukichi Sasaki, Masahiko Matsukata, Contribution of pore-connectivity to permeation performance of silicalite-1 membrane; Part II, Diffusivity of C6 hydrocarbon in micropore, Membranes, 11 (2021) 399.
Article	Motomu Sakai, Takuya Kaneko, Yukichi Sasaki, Masahiko Matsukata, Contribution of pore-connectivity to permeation performance of silicalite-1 membrane; Part I, Pore volume and effective pore size, Membranes, 11 (2021) 382.
Article	Masahiko Matsukata, Yasushi Sekine, Eiichi Kikuchi, Motomu Sakai, Bharathi Subramanian, Makoto Toyoda, Taisuke Furuhata, Synthesis of FAU-Zeolite Membrane by Secondary Growth Method: Influence of seeding on Membrane Growth and its Performance in the dehydration of Isopropyl Alcohol-Water Mixture, ACS Omega, 6 (2021) 9834-9842.
Article	Motomu Sakai, Hayata, Hori, Masahiko Matsukata, Self-defect-healing of silicalite-1 membrane for hydrocarbon separation in alkaline aqueous solution with surfactant, Materials Advances, 2 (2021) 3892.
Article	酒井求、松方正彦、銀カチオン交換X型ゼオライト膜によるオレフィン分離精製、膜誌、45（2020）262-267.
Article	Sanjeev Kumar Ujjain, Abhishek Bagusetty, Yuki Matsuda, Hideki Tanaka, Preety Ahuja, Carla de Tomas, Motomu Sakai, Fernando Vallejos-Burgos, Ryusuke Futamura, Irene Suarez-Martinez, Masahiko Matsukata, Akio Kodama, Giovanni Garberoglio, Yury Gogotsi, J. Karl Johnson, Katsumi Kaneko, Adsorption Separation of Heavier Isotope Gases in Subnanometer Carbon Pores, Nature communications, 12 (2021) 546.
Article	Motomu Sakai, Takuya Kaneko, Yukichi Sasaki, Miyuki Sekigawa, Masahiko Matsukata, Formation process of columnar grown (101)-oriented silicalite-1 membrane and its separation property for xylene isomer, Crystals 10 (2020) 949.
Article	Motomu Sakai, Noriyuki Yasuda, Yuto Tsuzuki, Masahiko Matsukata, Organic Structure-directing Agent-free Synthesis for *BEA-type zeolite membrane, Journal of Visualized Experiments, (156), e60500.
Article	Motomu Sakai, Masahiro Seshimo, Masahiko Matsukata, Hydrophilic ZSM-5 membrane for forward osmosis operation, Journal of Water Engineering, 32 (2019) 100864.
Book	酒井求、松方正彦、水処理分離膜の開発最前線、3章-5 親水性ゼオライト膜によるアルコールや有機酸からの脱水、シーエムシー出版、118-127、2020.

List of research achievements for application of Doctor of Engineering, Waseda University

Full Name: Motomu SAKAI seal or signature

Date Submitted(yyyy/mm/dd): 2021/10/06

種類別 (By Type)	題名、 発表・発行掲載誌名、 発表・発行年月、 連名者（申請者含む） (theme, journal name, date & year of publication, name of authors inc. yourself)
Book	酒井求、松方正彦、ホージャサイト型ゼオライト膜によるオレフィンの分離精製、化学工業、71 、137-141、2020.
Book	松方正彦、酒井求、2020年版薄膜作製応用ハンドブック、6章8節ゼオライト分離膜、2020
Book	Motomu Sakai, Masahiko Matsukata, Zeolite membranes for chemical separation, Research Outreach, 108, 114-117, 2019.
Book	松方正彦、酒井求、化学工学83巻12号（2019)、ゼオライト分離膜を用いた新規分離技術の開拓、公益社団法人化学工学会、83、740-742、2019.
Book	酒井求、松方正彦、セラミックデータブック 2019/20【工業と製品：vol.47, No.101】；超空間制御に基づく高度な特性を有する革新的機能素材の創製－ゼオライト系分離膜開発－、株式会社テクノプラザ、47 、62-65、2019.
Book	Motomu SAKAI, Kei, YOSHIHARA, Masahiro SESHIMO, Masahiko MATSUKATA, Advanced Materials for Membrane Fabrication and Modification; chapter 7 Zeolite Membrane for Gas Separation, CRC Press Taylor & Francis, 213-230, 2019.
Book	Motomu SAKAI, Masahiro SESHIMO, Masahiko MATSUKATA, Zeolites and Metal-Organic Frameworks – From lab to industry; chapter 8. Membranes with zeolites and MOFs: how, where, and why, Atlantis Press-Amsterdam University Press, 209-233, 2018.
Book	酒井求、松方正彦、先進無機高分子材料の開発；2章-2　無機膜による炭化水素分離、シーエムシー出版、2016
Invited lecture	酒井求、ゼオライト膜の透過分離特性の理解と膜設計、膜学会若手討論会MAC2019春、2019.
Invited lecture	酒井求、ゼオライト膜を用いた膜反応器開発とその課題、第18回反好会講演会、2019.
Invited lecture	酒井求、親和性の違いに基づくゼオライト膜による炭化水素分離、化学工学会第83年会、2018.
Invited lecture	酒井求、エチレン・プロピレン分離用ゼオライト膜の開発、化学工学会第82年会、2017.
Oral presentation	Motomu Sakai, Yuto Tsuzuki, Masahiko Matsukata, Contribution of adsorption property to separation property of propylene through Ag-exchanged X-type zeolite membrane, ICOM2020, 902, Dec. 2020.
Oral presentation	Motomu Sakai, Naoyuki Fujimaki, Masahiko Matsukata, Adsorption Properties of Propylene and Propane on Olefin Selective Ag-exchanged X-type Zeolite Membrane, IZMM, O-30, June 2019.
Oral presentation	Motomu Sakai, Masahiko Matsukata, Tubular Silicalite-1 membrane for n-alkane separation from light cycle oil, IMPRESS2019, B307, Oct. 2019.
Oral presentation	Motomu Sakai, Naoyuki Fujimaki, Masahiko Matsukata, Contribution of adsorption selectivity for permeation selectivity through olefin selective Ag-X membrane, Japan Adsorption 2019, May 2019.
Oral presentation	Motomu Sakai, Masahiko Matsukata, Preparation of Ag-*BEA membrane for olefin/paraffin separation, ICIM2018, June 2018.
Oral presentation	Motomu Sakai, Kei Yoshihara, Masahiko Matsukata, Development of zeolite membranes for high temperature hydrogen separation, 11th AMS, July 2018.
Oral presentation	Motomu Sakai, Noriyuki Yasuda, Masahiko Matsukata, Ethylene/ethane and propylene/propane separation through Ag-*BEA membrane, 11th ICMM, July 2017.
Poster presentation	Motomu Sakai, Yuki Nonaka, Masahiko Matsukata, Flow membrane reactor for the esterification of acetic acid using MOR-type zeolite membrane, FEZA21, PO-155, July 2021.
Poster presentation	Motomu Sakai, Yuki Nonaka, Masahiko Matsukata, Plug flow membrane reactor for esterification of acetic acid using zeolite membrane, ICCMR-14, July, 2019.

List of research achievements for application of Doctor of Engineering, Waseda University

Full Name: Motomu SAKAI seal or signature

Date Submitted(yyyy/mm/dd): 2021/10/06

種類別 (By Type)	題名、 発表・発行掲載誌名、 発表・発行年月、 連名者（申請者含む） (theme, journal name, date & year of publication, name of authors inc. yourself)
Poster presentation	Motomu Sakai, Masahiko Matsukata, Performance evaluation for forward osmosis of ZSM-5 zeolite membrane, AMS12, P1-65, July 2019.
Poster presentation	Motomu Sakai, Keisuke Tomaki, Masahiko Matsukata, Permeation properties of carbon-deposited silicalite-1 membranes, 2017ICNM, Aug. 2018.
Patent	松方正彦、酒井求、牛木涼友、岡村淳史、特開2020-186177、イソブチレンの製造方法
Patent	酒井求、松方正彦、摩庭篤、内田雅人、特開2020-157275、エチレンの分離方法
Patent	松方正彦、瀬下雅博、酒井求、金子拓矢、濱松辰雄、木村信啓、特許第6270685号、ノルマルパラフィンの分離方法
Patent	松方正彦、瀬下雅博、酒井求、金子拓矢、木村信啓、荒木泰博、足立倫明、特許第6211481号、ノルマルパラフィンまたはパラキシレンの分離方法およびゼオライト膜複合体
Patent	松方正彦、酒井求、佐々木康人、濱松辰雄、木村信啓、WO2016-098417、直鎖状共役ジエンの分離方法
Patent	松方正彦、酒井求、金子拓矢、荒木泰博、濱松辰雄、木村信啓、特開2016-098205、パラキシレンの製造方法
Patent	松方正彦、瀬下雅博、酒井求、木村信啓、足立倫明、和久俊雄、特開2015-174081、オレフィンの分離方法およびゼオライト膜複合体
Award	Motomu Sakai, Best Poster award, Flow membrane reactor for the esterification of acetic acid using MOR-type zeolite membrane, Federation of European Zeolite Associations, 2021
Award	酒井求、若手奨励研究奨励賞、CO_2吸着分離用MOF構造体のワンポット合成、ENEOS株式会社－早稲田大学 、2020
Award	酒井求、GSCポスター賞、silicalite-1膜を用いたC_6炭化水素蒸気透過分離、公益社団法人新化学技術推進協会、2013
Award	酒井求、JXエネルギー優秀研究賞、ゼオライト膜を用いた炭化水素分離、JX日鉱日石エネルギー株式会社、2013
Award	酒井求、化学工学会横浜大会2012奨励賞、管状silicalite-1膜によるヘキサン異性体分離挙動の検討、公益社団法人化学工学会、2012
Award	酒井求、日本膜学会第34年会学生賞、a-アルミナ管状支持体上へのランダム配向silicalite-1膜の調製法の検討、日本膜学会、2012